

OVERDUE FINES: 25¢ per day per item

RETURNING LIBRARY MATERIALS:

Place in book return to remove charge from circulation records

LIBRARY
Michigan State
University

# SPECTROSCOPIC STUDIES OF CHROMATIUM FLAVOCYTOCHROME c552

Ву

Mark R. Ondrias

## A DISSERTATION

Submitted to

Michigan State University
in partial fulfillment of the requirements
for the degree of

DOCTOR OF PHILOSOPHY

Department of Chemistry

## ABSTRACT

SPECTROSCOPIC STUDIES OF CHROMATIUM FLAVOCYTOCHROME c552

Ву

## Mark R. Ondrias

Various spectroscopic techniques were employed to examine Chromatium flavocytochrome  $\underline{c}_{552}$  in an effort to elucidate the structural and functional aspects of this multicenter electron transport protein. The primary techniques used in this study were absorption, fluorescence, magnetic circular dicroic (MCD), electron paramagnetic resonance (EPR) and resonance Raman spectroscopies.

Absorption and fluorescence spectroscopies yielded information concerning the binding of exogenous ligands to heme and flavin prothestic groups of the protein and showed a difference in the binding mechanisms between sulfur containing ligands ( $S_2O_3^=$  and  $SO_3^=$ ) and the cyanide ion. The relative midpoint reduction potential of the hemes in  $\underline{c}_{552}$  was determined to be  $\sim 40$  mV higher than the flavin by monitoring the absorption spectrum of the protein during reductive titrations.

The two hemes in  $\underline{c}_{552}$  were demonstrated to exist as magnetically isolated centers by their MCD and EPR spectra. Their protein environments, however, were found to be quite different. The EPR spectra of the protein indicate that one heme is maintained in a single, invariant protein environment, whereas the other can experience at least two different environments. Both techniques showed that at physiological pH only one of the hemes binds carbon monoxide. Only a small amount of flavin semiquinone was detected with EPR during the course of a reductive titration of  $\underline{c}_{552}$ , indicating that the major pathway for flavin oxidation and reduction is a concerted two electron process.

Resonance Raman spectra with both Soret and visible excitation have been obtained for Chromatium flavocytochrome  $\underline{c}_{552}$  and its isolated diheme subunit under varying conditions of pH and inhibitor binding. The spectra are generally consistent with previously established classification schemes for porphyrin ring vibrations. The presence of covalently bound flavin in the protein was apparent in the fluorescent background it produced and the ease with which heme photoreduction took place. No flavin modes were present in the Raman spectra nor was any evidence of direct heme-flavin interaction found using this technique; however, a systematic perturbation of heme  $B_{lg}$  vibrational frequencies was found in the oxidized holoprotein. The heme vibrational frequencies of  $\underline{c}_{552}$  are compared to those

of the diheme peptide and of other c-type cytochromes.

The results of these investigations are discussed in the context of the mechanism of intramolecular electron transfer in  $\underline{c}_{552}$ . They are consistent with an interpretation that involves pH-dependent changes in heme axial ligation and treats the hemes and flavin as isolated chromophores communicating via protein-mediated interactions.

To my parents

## ACKNOWLEDGMENTS

I would like to acknowledge the contributions of Professors George Leroi and Gerald Babcock to my graduate education. They each, in their own way, provided the support. advice and direction necessary for this undertaking.

The efforts of Peri-Anne Warstler and Kathryn Nyland in the preparation of this manuscript are greatly appreciated. Eric Findsen's aid with the growth of the <u>Chromatium</u> cultures and  $\underline{c}_{552}$  preparation is gratefully acknowledged.

I would also like to express my gratitude to all my compatriots who made the basement of the Chemistry Building a warm and human place. So to, Bill B., Chris Y., Dave R., Dan T., Katie N., Eric F., Dan O. Sunil K., Pat C., Tom C., Tom P. and all the others, I extend a heartfelt thanks. I couldn't have done it without you.

Finally, a special thanks to Bea Botch who, more than anyone else, endured with me the trials and tribulations associated with my research. The weight seems much lighter when shared by two.

## TABLE OF CONTENTS

Chapter	F	age
LIST OF	TABLES	vi
LIST OF	FIGURES	vii
CHAPTER	1 INTRODUCTION	1
CHAPTER	2 MATERIALS AND METHODS	15
Α.	Chromatium Growth and Protein Preparation	15
В.	Experimental	20
CHAPTER	3 ABSORPTION AND FLUORESCENCE SPECTROSCOPY OF FLAVOCYTO-CHROME 6552 · · · · · · · · · · · · · · · · · ·	24
Α.	Theory of Heme Absorption	25
В.	Results	32
c.	Binding Studies	39
D.	Reductive Titration	49
Ε.	Fluorescence Results	60
CHAPTER	4 MAGNETIC TECHNIQUES APPLIED	
OHAI IBR	TO FLAVOCYTOCHROME c <sub>552</sub>	67
I.	Magnetic Circular Dichroism	68
	A. MCD Theory	68
	B. MCD Results	72
II.	Electron Paramagnetic Resonance Spectroscopy	80
	A Theory	80

Chapter	P	age
	B. MCD Results	85
	C. Reductive Titration	92
	D. Flavin Semiquinone	97
	E. Exogenous Ligand Binding	100
CHAPTER		106
Α.	Raman Theory	107
В.	Raman Results and Discussion	118
CHAPTER	6 CONCLUSION	146
Α.	Heme/Heme Interactions	147
В.	Heme/Flavin Interactions	148
C.	Flavin Environment	150
D.	Heme Environments	151
E.	Exogenous Ligand Binding	152
F.	Protein Mediated Communication Between Redox Centers	153
APPENDI	x	159
REFEREN	CES	163

## LIST OF TABLES

Tables		Page
1	Extinction Coefficients of 695 nm	
	Absorption Bands	38
2	Cyanide Binding to Flavocyto-	
	chrome <u>c</u> 552	42
3	Ligand Field Parameters for	
	Various Hemes <u>c</u>	91
4	Raman Modes for Flavocytochrome	
	$c_{552}$ Obtained with 441.6 nm	
	Excitation	. 123
5	High Frequency Raman Modes for	
	Flavocytochrome $c_{552}$ Species	
	Obtained with 514.5 nm Excitation	. 127
Al	Calculated Values of $\Delta E$ From a	
	c <sub>552</sub> Reductive Titration	. 162

## LIST OF FIGURES

Figure	P	'age
1	The structure of heme $\underline{c}$	3
2	The structure of the flavin	
	moiety and its various reduction	
	products	5
3	Postulated electron transport	
	chain for Chromatium non-cyclic	
	photosynthesis. Components are	
	arranged vertically in order of	
	decreasing reduction potential.	
	Abbreviations: Bchl., bacterial	
	chlorophyll; <u>c<sub>555</sub></u> , cytochrome <u>c<sub>555</sub></u> ;	
	NADP, nicotinamide adenine dinucleo-	
	tide phosphate	10
4	Gel electrophoresis of flavotyco-	
	chrome $c_{552}$ preparations. Gels	
	are non-denaturing type in 5%	
	acrylanide-N,N'-methylene-bis-	
	acrylanide. Electrophoresis was	
	conducted with a constant 2 mA	
	current and gels were stained	
	with Coumassie blue. Protein:	
	Soret ratios for the various	

Figure		Page
4	samples were A (1.13), B (1.00),	
	C (0.76), D (1.50), E (0.69) and	
	F (1.24)	19
5	Schematic diagram of laser Raman	
	experimental arrangement	22
6	Spatial and nodal characteristics	
	of the lowest unfilled $(e_g)$ and	
	highest filled (a <sub>lu</sub> , a <sub>2u</sub> ) por-	
	phyrin orbitals (from Reference	
	40)	27
7	Relative energy levels of por-	
	phyrin () and iron () or-	
	bitals for ferric porphyrin	
	complexes (from Reference 42)	31
8	Absorption spectra of $\sim$ 6 $\mu M$ oxidized	
	() and reduced () flavo-	
	cytochrome $c_{552}$ in 0.1 M Tris	
	buffer, pH 7.5. Insert: ~6	
	$\mu M$ oxidized $c_{552}$ in 0.1 M MES	
	buffer, pH 6.1 before () and	
	after () addition of 2 mM	
	Na <sub>2</sub> S <sub>2</sub> O <sub>3</sub>	33
9	Transition axes giving rise to	
	the $\sim$ 450 nm and $\sim$ 360 nm flavin	
	absorption bands	35

Figure	•	Page
10	Absorption spectra of oxidized	
	() and reduced () diheme	
	peptide of flavocytochrome $c_{552}$	
	in 0.1 M Tris, pH 7.5	 37
11	Absorption spectra of reduced	
	<u>c<sub>552</sub> under Ar () in 0.1 M</u>	
	Tris, pH 7.5, reduced $c_{552}$ under	
	6 psi of CO (···) in O.1 M Tris,	
	pH 7.5 and reduced $c_{552}$ under 6	
	psi of CO in O.1 M CAPS, pH 10.0	 40
12	Absorption spectra of ∿30 µM	
	$c_{552}$ in 0.1 M MES, pH 6.1 (),	
	5 minutes after the addition	
	of 5 mM $CN^-$ (-··-), 25 minutes	
	after the CN addition (),	
	and 180 minutes after the CN-	
	addition ()	 44
13	Absorption spectra of $\sim 30~\mu M$	
	$c_{552}$ in 0.1 M MES pH 6.1 (),	
	15 minutes after the addition of	
	5 mM S <sub>2</sub> 0 <sub>3</sub>	 46
14	Absorption spectra obtained from	
	a reductive titration of flavocyto-	
	chrome $\underline{c}_{552}$ in 0.1 M Tris, pH 7.5	
	under an Ar atmosphere	 52

Figure	Page
15	The anaerobic titrator used in
	the reductive titrations of $c_{552}$ 53
16	Standardization plot for di-
	thionite reductant used in
	reductive titrations 54
17	A plot of $\Delta A_{475}$ vs. $\Delta A_{552}$
	during a reductive titration of
	flavocytochrome $c_{552}$ ( ) and horse
	heart cytochrome $\underline{c}$ (x), (type II
	obtained from Sigma Chemical),
	both in 0.1 M Tris, pH 7.5
18	The extent of heme (x) and flavin
	(o) reduction as a function of
	electrons per molecule added
	during a reductive titration
	of $c_{552}$ . Open squares and tri-
	angles denote the theoretical
	curves for two-two-electron couples
	with $\Delta E = 42$ mV and 32 mV, respec-
	tively
19	The extent of heme reduction as
	a function of electrons per
	molecule added during a re-
	ductive titration of thiosulfate
	bound $c_{552}$ in 0.1 M MES, pH 6.1
	under an Ar atmosphere 59

다	Ø1	1	n	۵	
	$\sim$		1 -	_	

## Page

20	Left panel: Fluorescence emission
	intensities of: (a) 0.1 $\mu M$ ribo-
	flavin (); (b) 2 $\mu$ M glucose oxi-
	dase () and (c) 6 $\mu M$ flavocyto-
	chrome $c_{552}$ () all in 0.1 M
	Tris buffer, pH 7.5. Right panel:
	Fluorescence emission intensities of:
	(a) 6 $\mu$ M $c_{552}$ in 0.1 M MES, pH 6.1
	one-half hour after addition of 2 mM
	KCN (); (b) 6 $\mu$ M $c_{552}$ in 0.1 M MES
	pH 6.1 one-half hour after addition
	of 2 mM $Na_2S_2O_3$ (-··-). The excita-
	tion wavelength was 442 nm for both
	sets of spectra. Concentrated solu-
	tions of KCN and $Na_2S_2O_3$ were prepared
	in 0.1 M MES and adjusted to pH 6.1
	prior to addition to the protein
	sample
21	Fluorescence excitation spectrum
	of flavocytochrome $c_{552}$ in 0.1 M
	Tris, pH 7.5 with emission intensity
	monitored at 523 nm 64
22	A schematic representation of the
	physical processes giving rise to
	MCD A, B, and C terms (lower) and

Figure		Page
22	the respective bandshapes of these	
	terms (upper). In the upper panel	
	dotted lines denote the absorption	
	of left and right circularly polarized	
	light while the solid trace is their	•
	difference (from Reference 59)	71
23	The MCD spectra of the reduced,	
	oxidized, and reduced +CO forms	
	of $c_{552}$ in 0.1 M Tris, pH 7.5 in	
	the Soret region are pictured above	
	the absorption spectra of those	
	species	73
24	The MCD spectra of reduced and	
	oxidized $c_{552}$ in 0.1 M Tris, pH	
	7.5 in the visible region are	
	pictured above the absorption	
	spectra of those species	75
25	The MCD spectra obtained in the	
	Soret region from a reductive titra-	
	tion of $\underline{c}_{552}$ under 6 psi of CO in	
	0.1 M Tris, pH 7.5. Traces of	
	the peak from left to right (or	
	through from right to left) are:	
	(), 0% reduced (), 10% re-	
	duced, (••••), 25% reduced, (),	

Figure		Page
25	35% reduced, (), 45% reduced,	
	( •••• ), 100% reduced protein	78
26	The effect of successive symmetry	
	reductions upon the energy levels	
	of the iron d-orbitals	. 81
27	An EPR spectrum of 100 µM oxidized	
	$c_{552}$ in 0.1 M Tris, pH 7.5 obtained	
	at 6.2°K with 2 mW of 9.132 GHz	
	radiation and 10 G modulation	87
28	Microwave power saturation curve	
	for the $g_z = 2.88 (\Delta), g_z = 3.02$	
	$(x)$ , $g_y = 2.35$ ( ) and $g_v = 2.25$	
	(o) resonances of $c_{552}$ under the	
	same conditions as Figure 27	88
29	A plot of rhombicity vs. tetro-	
	gonality for the hemes in flavo-	
	cytochrome $c_{552}$ ( ) and various	
	monoheme <u>c</u> proteins (o)	90
30	The EPR/Absorption anaerobic	
	titrator	93
31	The decay of the $g = 3.02$ reson-	
	ance vs. electrons per molecule	
	added during the course of a	
	reductive titration of $\sim \! 100~\mu M$	
	$c_{552}$ in 0.1 M Tris, pH 7.5 with	

Figure			Page
31	the same instrumental parameters		
	as Figure 27		95
32	Flavin semiquinone signal obtained		
	from 100 M c <sub>552</sub> in 0.1 M Tris, pH 7.5		
	at 143°K after the introduction of		
	3 electrons per molecule. Microwave		
	power was .5 mW at 9.122 GHz with		
	5 G modulation	•	.99
33	EPR spectra obtained during a		
	reductive titration of $\sim 100~\mu M$		
	c <sub>552</sub> under 6 psi of carbon mon-		
	oxide. Temperature and instrumental		
	parameters are the same as Figure		
	27		101
34	EPR spectra of $\sim 100  \mu M  c_{552}$ with		
	flavin:heme ratio ∿1.0 in 0.1 M		
	Tris, pH 7.5, after the addition		
	of 5 mM CN <sup>-</sup>	•	104
35	Raman scattering processes		109
36	Tensor symmetries for the reson-		
	ance Raman active vibrational		
	groups of hemes $\underline{c}$		116
37	Resonance Raman spectra of flavo-		
	cytochrome $c_{552}$ obtained with 441.6		
	nm excitation. The power was		

Figure		Page
37	10 mW and the $c_{552}$ concentration	
	was 75 $\mu$ M in 0.1 M Tris, pH 7.5	. 120
38	Resonance Raman spectra obtained	
	with 514.5 nm excitation of (a)	
	70 μM ferrous flavocytochrome	
	$c_{552}$ diheme peptide in 0.1 M Tris	
	pH 7.5 with 350 mW of laser power;	
	(b) 100 $\mu M$ ferrous flavocytochrome	
	$c_{552}$ in 0.1 M CAPS, pH 10.0 with 180	
	mW of laser power; (c) 80 $\mu$ M ferrous	
	flavocytochrome $\frac{c}{552}$ in 0.1 M Tris,	
	pH 7.5 with 250 mW of laser power;	
	(d) 100 μM ferrous flavocytochrome	
	$c_{552}$ in 0.1 M MES, pH 6.05 with .	
	250 mW of laser power; (e) 200 μM	
	ferrous horse heart cytochrome $\underline{c}$ in	
	0.1 M Tris, pH 7.5 with laser power	
	equal to 250 mW. Frequency positions	
	of the principal bands are given in	
	Table 5. The fluorescence background	
	of the diheme peptide spectrum arises	
	from a small amount of residual flavin	
	peptide which could not be separated	
	from the sample	. 126

39	Resonance Raman spectra obtained with
	514.5 nm excitation of (a) 70 $\mu M$ ferric
	$c_{552}$ diheme peptide in 0.1 M Tris, pH 7.5
	with 250 mW of laser power; (b) 100 $\mu M$
	ferric flavocytochrome $c_{552}$ in 0.1 M MES,
	pH 6.05 2 mM $Na_2S_2O_3$ with 200 mW of laser
	power; (c) 80 $\mu M$ ferric flavocytochrome
	$c_{552}$ in 0.1 M Tris, pH 7.5 with 95 mW
	of laser power; (d) 200 $\mu M$ ferric horse
	heart cytochrome c in 0.1 M Tris, pH 7.5
	with 250 mW of laser power. Frequency
	positions of the principal bands are
	given in Table 5
40	Resonance Raman spectrum of 80 µM
	ferric flavocytochrome $c_{552}$ in 0.1 M
	Tris, pH 7.5 obtained with 315 mW of
	514.5 nm laser light incident upon the
	sample. Insert: The position and
	intensity dependence of the oxidation
	state marker band in ferric $c_{552}$ as a
	function of 514.5 nm intensity upon the
	sample

#### CHAPTER 1

## INTRODUCTION

Biological systems depend upon the production of highenergy chemical intermediates such as adenosine triphosphate (ATP) as a source of stored energy that is available for cellular anabolic processes. The elaborate mechanisms evolved for ATP synthesis range from the photosynthetic systems of plants and some bacteria (1) to the oxidative respiration of higher animals (2). However, virtually all of these processes are ultimately dependent upon the energy generated by the transport of electrons down a potential gradient in a chain of electron transport proteins. ATP production is coupled to this electron transport (3), and conserves the potential energy lost by the electrons in a form convenient to the organism. Electron transport proteins, therefore, are fundamental to the life processes of organisms and stand at the center of a living cell's ability to construct a complex biological order from the entropic chaos of the inorganic world.

Protein electron carriers have been isolated from a large number of cellular systems, but the precise nature of the mechanisms by which these enzymes function remains

an unsolved problem of fundamental importance. In order to participate in electron transfer, a protein must possess an active center that can undergo reversible oxidation and reduction at a potential within the biologically viable range of -500 to +800 mV. Two such active centers in electron transport proteins are heme and flavin moieities.

Perhaps the most extensively characterized of any of the electron transport proteins are the high potential cytochromes c. These proteins contain heme c as the active redox center and are ubiquitously distributed among both eukaryotic and prokaryotic organisms (4). The heme redox center itself consists of an iron ion chelated within a porphyrin macrocycle which is trapped within the protein polypeptide matrix. Variations in peripheral substituents to the porphyrin ring system lead to differentiation between types of heme centers designated as heme a, b, c, etc. (5). The structure of heme c is shown in Figure 1. In cytochromes c the heme is bound to the polypeptide matrix of the protein by two covalent thioether linkages between the heme c vinyl substituents and the sulfhydryl group of cysteine amino acid residues of the matrix. Additionally, other protein amino acid residues (most commonly histidine, methionine or lysine) form coordinate bonds with the heme iron, placing it in a five or six-coordinate octahedral ligand field. The iron ion serves as the vehicle for storage and release of electrons by alternating its valence

Figure 1. The structure of heme  $\underline{c}$ .

state between +2 and +3. The exact mechanism of electron transport to and from the iron in heme proteins remains a subject of controversy (see, for example, Moore and Williams, 1976 (6)) and evidence exists for multiple pathways for electron transfer within mitochondrial cytochrome c (7). Extensive amino acid sequence studies (8) suggest that several dissimilar subclasses of cytochromes c exist, while high resolution NMR (9) and crystallographic studies (10-12) indicate that there is a large degree of protein structural homology within given subclasses.

Flavin redox centers are found in a wide variety of electron transport proteins. They are crucial to the functioning of photosynthetic systems in both plants and bacteria and play a primary role in eukaryotic oxidative metabolism (13). The flavin moiety itself is a modified isoalloxazine ring system that is stable in a number of oxidation states (See Figure 2). Flavins can exist in stable one electron reduced states (called semi-quinones) in either neutral or anionic forms (14) or in a fully reduced state formed by the addition of two electrons. Thus flavins can participate in electron transfer with either one or two electron redox centers. This makes them obvious choices as crossover points in an electron transfer chain that requires a change from concerted 2 electron transfers early in the chain to sequential one electron transfers at its terminus (15). Such a crossover is

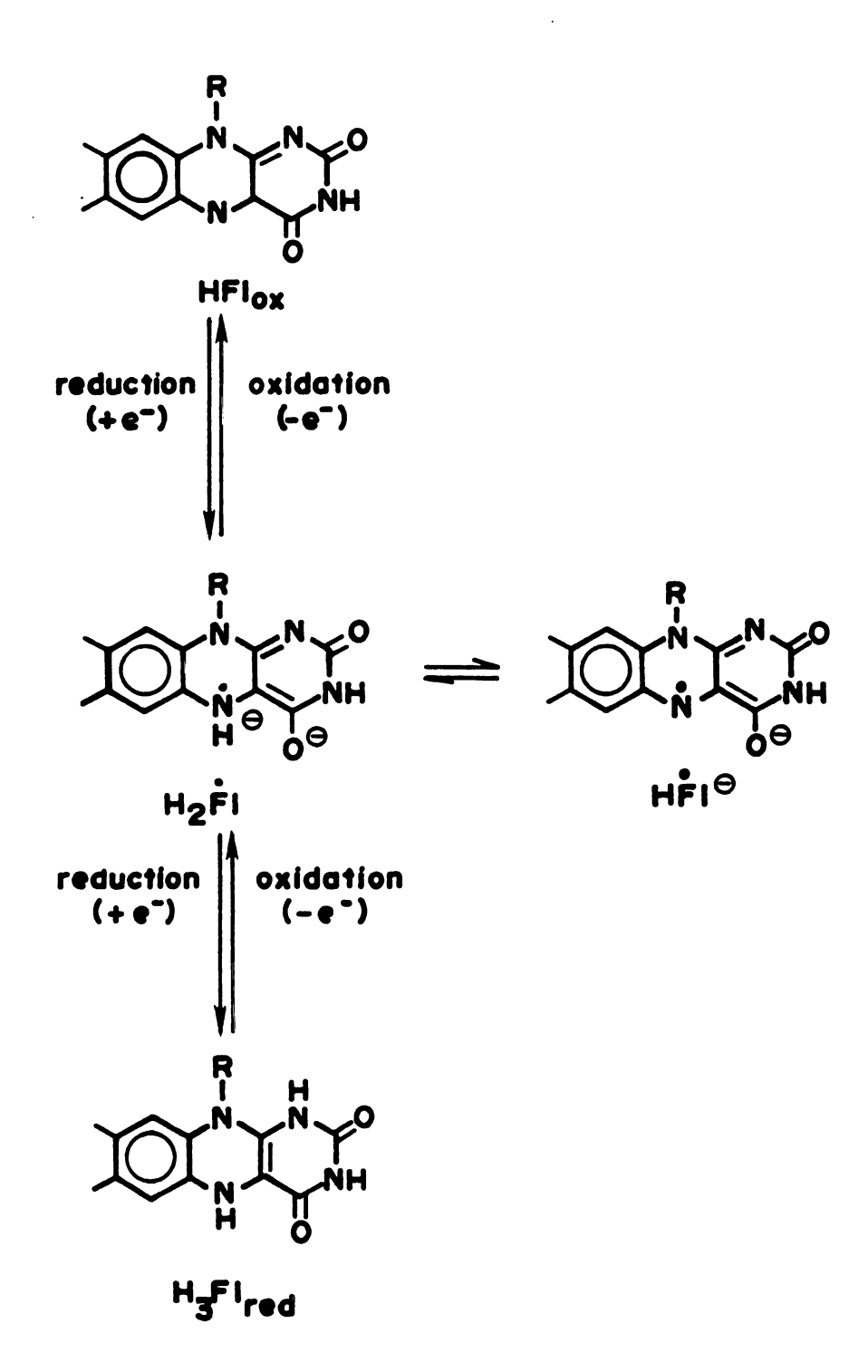


Figure 2. The structure of the flavin moiety and its various reduction products.

critical to respiratory electron transport in mammals (16). Flavins generally serve as non-covalently bound cofactors in flavoproteins, although several instances of covalent protein-flavin binding have been found (17). Considerations of the mechanisms of flavoprotein electron transport have largely been limited to elucidation of the oxidation/reduction kinetics of the isolated flavin chromophore (15). However, recent studies (18) have focussed upon the kinetics of the intramolecular flow of electrons in flavocytochromes  $\underline{b}_2$  which contains both heme and flavin centers.

Electron transport in biology is not limited to small single redox center proteins. Numerous multicenter electron transport proteins exist and are necessary for the proper function of a variety of biological systems. The importance of this class of proteins is underscored by the fact that often there are unusually severe kinetic or thermodynamic barriers to rapid and efficient progress in the reactions they catalyze. Examples include the role of nitrogenase in nitrogen fixation, cytochrome oxidase in mitochondrial oxygen reduction and the manganese-containing protein involved in photosynthetic water oxidation. Recently these proteins have attracted considerable interest both because of the complex nature of the reactions in which they are involved and because of the likely occurrence of electronic and protein mediated interaction between

the various intramolecular redox centers.

It is my intention in this thesis to examine in some detail the spectroscopic properties of an electron transport protein that contains both heme c and flavin redox centers. The enzyme chosen for this study is Chromatium flavocytochrome  $c_{552}$ . It is a soluble component in the photosynthetic system of Chromatium vinosum, a purple sulfur Flavocytochrome  $c_{552}$  was first reported by Newton and Kamen (1955) and subsequently purified and characterized (19). Further studies established the molecular weight (√72,000), oxidation-reduction potential  $(E_m^o = 10 \text{ mV})$  and isoelectric point (5.1) of the protein (20). The multicomponent nature of  $c_{552}$  is evidenced by the fact that it contains two heme and one flavin moieties per molecule. The flavin prosthetic group has been identified as a substituted  $8-\alpha$ -flavin adenine dinucleatide (FAD) linked to the protein via a thiohemiacetal bond to a protein cysteine moiety (21) while the hemes in  $c_{552}$  have been demonstrated to be the mesoheme typical of c-type cytochromes (20) and thus are bound to cysteine protein residues through thioether linkages. The structure of the protein moiety of  $c_{552}$  has been the subject of several investigations. Kennel and Kamen (22) found that treatment with mild denaturants such as 8M urea dissociated  $c_{552}$  into two subunits. One subunit contains the flavin prothestic group in a single polypeptide having a molecular

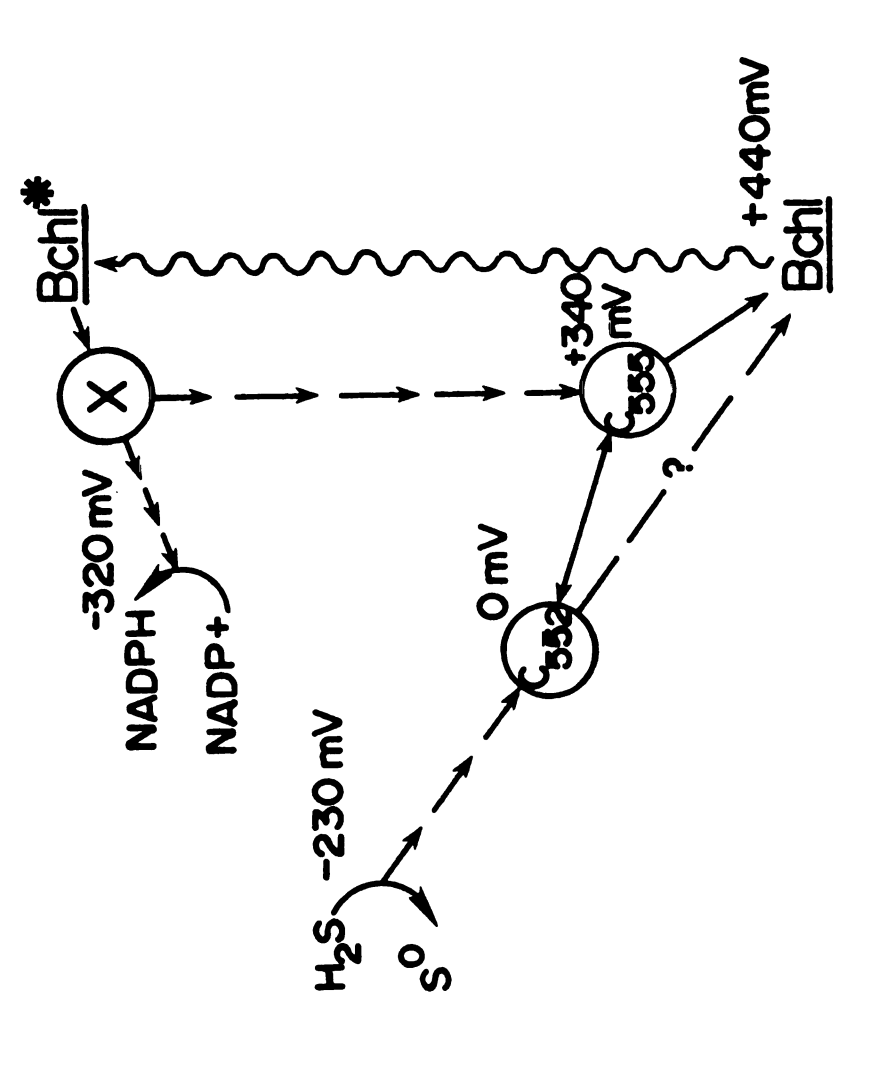
weight of  $\sim 50,000$  daltons, the other contains both hemes in a single polypeptide weighing  $\sim 21,000$  daltons (23). Attempts to reconstitute the protein from its subunits by Fukumori et al. (23) were unsuccessful.

The subunit structure and prosthetic groups of  $\underline{c}_{552}$  are representative of a broader class of enzymes found in bacteria utilizing non-cyclic photophosphorylation as an energy source. Soluble proteins have been isolated from Alcaligenes Eutrophus (24), a hydrogen metabolizing bacterium, the green sulfur bacterium Chlorobium thiosulfatophilum (20), and Pseudomonas putida (25), that contain both flavin and heme redox centers. The flavocytochrome derived from Chlorobium, in particular, appears to be analogous to  $\underline{c}_{552}$  in both structure and function. It is dissociable into flavin and heme containing subunits, although only one heme c is present in the heme subunits (25).

The biological function of flavocytochrome  $\underline{c}_{552}$  has been the subject of numerous investigations that monitored light induced oxidations within whole cells (26,27), subcellular chromatophores (28) and  $\underline{in}$  vivo preparations (29). These investigations have indicated that  $\underline{c}_{552}$  mediates the noncyclic transfer of electrons from soluble reduced sulfur compounds (S<sup>=</sup>,  $S_2O_4^{2-}$ ) to the membranebound constituents of the photosynthetic centers. It is postulated to function as the initial electron transport intermediate between the reduced sulfur substrates and

the other chain components. In this role, its function is analogous to that of the water-oxidizing manganese-containing complexes of green plants. The less demanding requirements of sulfide oxidation ( $E_{\rm m}^{\rm o}$  = -230 mV), however, apparently allow the organism to employ a more conventional set of biological redox centers. A generalized scheme for electron transfer in Chromatium is shown in Figure (3). Flavocytochrome  $\underline{c}_{552}$  has been shown to exhibit an  $\underline{\text{in}}$   $\underline{\text{vivo}}$ sulfide-cytochrome c reductase activity and also catalyzes the reduction of elementary sulfur to sulfide with reduced benzylviologen as the electron source (23). Neither flavin nor heme subunits of  $\underline{c}_{552}$  display any sulfide-cytochrome  $\underline{c}$  reductase activity. Thus  $\underline{c}_{552}$  may function as a multicenter electron transport vehicle intermediate in complexity between the relatively well characterized monocenter electron transport proteins such as mammalian cytochrome c and the highly complex, membrane-bound multi-protein electron transport chains found in higher animals. The characterization of intramolecular electron flow in flavocytochrome  $\underline{c}_{552}$  would lend valuable insight into the general problem of electron transport in more complex systems.

While a multiplicity of biochemically oriented investigations of  $\underline{c}_{552}$  have been undertaken, there have been only a limited number of studies focussing on the physical and spectroscopic properties of the protein. The optical absorption spectra of the purified holoprotein (20) and its



Postulated electron transport chain for Chromatium non-cyclic photosynthesis. Components are arranged vertically in order of decreasing reduction potential. Abbreviations: Bchl., bacterial chlorophyll; 2555, cytochrome 2555; NADP, nicotinamide adenine dinucleotide phosphate. Figure 3.

diheme peptide (30) have been characterized. The oxidized and reduced spectra of both holo- and apo-protein largely resemble those of cytochrome c except for a pronounced flavin absorption in the holoprotein. However,  $c_{552}$  displays an ability to bind exogenous ligands that cytochrome The protein binds CO (19) to its heme moieties and  $CN^-$ ,  $SO_3^-$ , and  $S_2O_3^-$  (30) to its flavin moiety. The optical rotation properties of  $c_{552}$  absorption have been investigated by Bartsch et al. (20) and Vorkink (30). Derivative shaped bands with centers at the Soret absorption maxima were found in ferric, ferro and ferro-CO forms of the protein. These were interpreted to indicate heme-heme or heme-flavin interaction. In particular, the increased magnitude and decreased bandwidth of the Soret transition in ferro-CO  $c_{552}$  circular dichroism spectra led to the speculation that the CO molecule was intercalated between the closely spaced hemes. On the other hand, optical rotatory dispersion spectra of ferro-CO  $c_{552}$  obtained by Yong and King (31) were interpreted by them as involving CO binding to only one of the two interacting hemes. Some ambiguity concerning the extent of heme-heme interaction is raised by the observations of Moss et al. (32) that the Mössbauer spectra of ferric and ferrous  $\underline{c}_{552}$  show no indication of heme-heme magnetic coupling, although a dramatic alteration of the Mössbauer spectral behavior occurs upon CO-binding. The absence of any discernable heme-heme magnetic coupling

was further substantiated by an investigation of  $\underline{c}_{552}$ 's magnetic susceptibility and EPR properties of  $\underline{c}_{552}$  by Strekas (33). The magnetic susceptibility of  $\underline{c}_{552}$  was found to be indicative of low spin heme  $\underline{c}$ . The protein exhibits two sets of EPR resonances arising from uncoupled low spin (S = 1/2) hemes  $\underline{c}$ , showing no indication of spin-spin interactions. One set of EPR resonances displays a marked pH dependence, whereas the other set is insensitive to environmental pH. Moreover,  $CN^-$  binding to the protein was found to convert the pH-labile resonances exclusively to their low pH form. This was interpreted as an indication of heme-flavin interaction.

Finally, several investigations into the energetics of  $\underline{c}_{552}$  oxidation and reduction have been made. Vorkink (30) expanded on earlier investigations (20) of the enzyme's mid-point reduction potential and determined the potentials of both the flavin and heme prosthetic groups to be approximately 0 mV. This potential is anomalously low relative to that of other heme  $\underline{c}$  containing proteins and much higher than the  $\underline{E}_{m}^{o}$  of -187 mV measured for the flavin containing peptide of  $\underline{c}_{552}$  produced by peptic digestion of the protein (34). Stopped flow techniques were used to monitor the  $\underline{in}$   $\underline{vivo}$  kinetics of  $\underline{c}_{552}$  oxidation and reduction by a variety of donors and acceptors (30). Although  $\underline{c}_{552}$  does auto-oxidize in aerobic solutions, its rate of oxidation by ferricyanide is about seven orders of magnitude faster

than with molecular oxygen. Rates of reduction of  $\underline{c}_{552}$  by sulfur-containing compounds (S<sup>=</sup>, S<sub>2</sub>0<sub>4</sub>) were measured and are 1-2 orders of magnitude slower than rates measured using non-biological reductants of comparable  $E_m^o$ . This strongly implies the existence of a multiplicity of oxidation-reduction pathways in the protein. The value of  $E_m^o$  varies widely with pH but is largely invariant to changes in ionic strength (29), indicating the probable uptake of a proton to keep the net charge of the cytochrome constant upon reduction.

The body of research done to date concerning flavocytochrome  $\underline{c}_{552}$  is sufficient to expose the complexity of the protein. It provides a foundation for the further application of physical techniques to the elucidation of the intramolecular structure and function of this protein and other multicenter enzymes of its general class. thesis will pursue that application by extending the use of some of the methods already mentioned and bringing new techniques to bear on this problem. Absorption, magnetic circular dicroic (MCD), fluorescence, electron paramagnetic resonance (EPR) and resonance Raman spectroscopies were utilized during the course of this study. Absorption spectroscopy was useful in the characterization of the protein's purity and binding behavior. The magnetic techniques (MCD, EPR) were employed to define the extent and nature of the heme magnetic environment in the protein and thus served as a complement to the heme vibrational information obtained via resonance Raman scattering. Flavin fluorescence proved to be a sensitive indicator of the intramolecular interactions of that chromophore. Applied to a molecule as complex as  $\mathbf{c}_{552}$  each of these techniques alone provides information that is too specific to admit an unambiguous interpretation. However, when multiple techniques are employed a synergistic effect is realized and a consistent picture of the structure-function relationships within  $\mathbf{c}_{552}$  can be obtained.

#### CHAPTER 2

#### MATERIALS AND METHODS

## A. Chromatium Growth and Protein Preparation

Flavocytochrome  $c_{552}$  was isolated from heterotrophically grown Chromatium vinosum st. D obtained from the American Type Culture Collection (culture E-17899). The nutrient medium of Cusanovich (35) was used to grow the photosynthetic bacteria in 10 & carboys. The yield of wet cells was 6-8 g/liter and displayed little dependence on the incident light intensity on the carboys. Light levels between 100 and 800 ft. candles produced nearly equivalent  $\mathrm{Na}_{2}\mathrm{S}$  was used as the source of reduced sulfur substrate for the organism. Concentrations of S = exceeding ∿0.150 g/l led to an accumulation of elemental sulfur particles within the bacterial cells (a distinguishing characteristic of purple sulfur bacteria) and a subsequent depression of cellular growth rate evidenced by decreased yields and a pronounced change in culture color from deep purple to pink. Maintenance of the Chromatium culture was accomplished by continuous growth of the organism in 1 & bottles using an autotrophic medium of Cusanovich (35).

Heterotrophic growth was initiated by introducing a ~1% innoculum of late log phase autotrophs into the anaerobic heterotrophic medium. Heterotrophs reached stationary phase in 3-10 days (depending on light level and size of innoculum) and were subsequently harvested by centrifugation. The cells were resuspended in two volumes of buffer (.1M Tris pH 7.5) and broken by 1 to 2 passes through an Aminco 50 ml French Pressure Cell at 16,000 psi.

Purification of  $\underline{c}_{552}$  from the crude cellular extract generally followed a procedure detailed elsewhere (30) and is briefly summarized as follows:

- 1. Crude cellular extract was centrifuged on a Beckman ultracentrifuge at 90,000 g for ∿5 hrs to remove
  particulate matter. (The pellets from centrifugation could be resuspended and recentrifuged resulting in a ∿15% increase in protein yield.)
- 2. The supernatant from above was next chromatographed on a DEAE cellulose column. High potential ironsulfur protein was eluted with .05 M NaCl in .02 M Tris, cytochrome  $\underline{c}$ ' with .10 M NaCl in buffer and cytochrome  $\underline{c}_{552}$  with .15-.18 M NaCl in buffer.
- 3. The <u>c</u><sub>552</sub> fraction could be subsequently purified by gel filtration carried out on Sephadex G-150 in 0.02 M Tris, 0.05 M NaCl, pH 7.5 an ammonium sulfate precipitation (a5 95% saturation) filtration

or a combination of both filtration and precipitation.

4. The yield of purified protein from the above procedure was  $8-12\,\mu$  moles per kilogram wet weight of cells.

Criteria for  $c_{552}$  purity have been established by Barstch et al. (20) using the protein's optical properties. Ratios of  $A_{475}/A_{525} = 1.25$  (flavin:heme) and  $A_{280}/A_{410}$ = 0.58 (protein: Soret) indicate purified  $c_{552}$ . All samples used in this study had  $A_{475}/A_{525} \ge 1.15$  and  $A_{280}/A_{410} \le 0.75$ unless otherwise noted. Two other measures of protein integrity were also used. The ability of  $c_{552}$  to bind CNand  $S0_3^{-}$  (accompanied by a decrease in  $A_{475}/A_{525}$ ) was found to be a sensitive criterion of protein integrity. Assays of the protein by gel electrophoresis were also conducted by Eric Findsen. The effect of increased protein:Soret ratio on the number of subunits seen with gel electrophoresis is demonstrated in Figure (4), from which it is apparent that the increased protein: Soret ratio reflects the presence of several additional protein subunits. By far the most mutable of the parameters mentioned above was the flavin: heme ratio. Some preps yielded protein with a flavin:heme ratio as low as 0.95. The  $A_{475}/A_{525}$ value could be "restored" by treatment with mild oxidants such as ferricyanide but this resulted in a loss of the proteins CN binding ability. Minor deviations in either

various samples were A (1.13), B (1.00), C (0.76), D (1.50), E (0.69) Gel electrophoresis of flavocytochrome  $\frac{c_{552}}{1000}$  preparations. Gels are non-denaturing type in 5% acrylanide-N,N'-methylene-bis-acrylanide. Electrophoresis was conducted with a constant 2 mA current and gels were stained with Coumassie blue. Protein: Soret ratios for the and F (1.24). Figure 4.

Figure 4

flavin:heme or protein:Soret ratios had no apparent effect on the spectral or chemical binding properties of the protein.

The diheme peptide of  $\underline{c}_{552}$  was prepared by overnight incubation of the holoprotein in either 0.10 M CAPS buffer at pH = 11.0 or an 8 M Urea solution (22) and purified using gel chromatography (Sephadex G-100) to eliminate the dissociated flavin-containing subunits. Urea treatment resulted in significantly higher yields and was the method of choice.

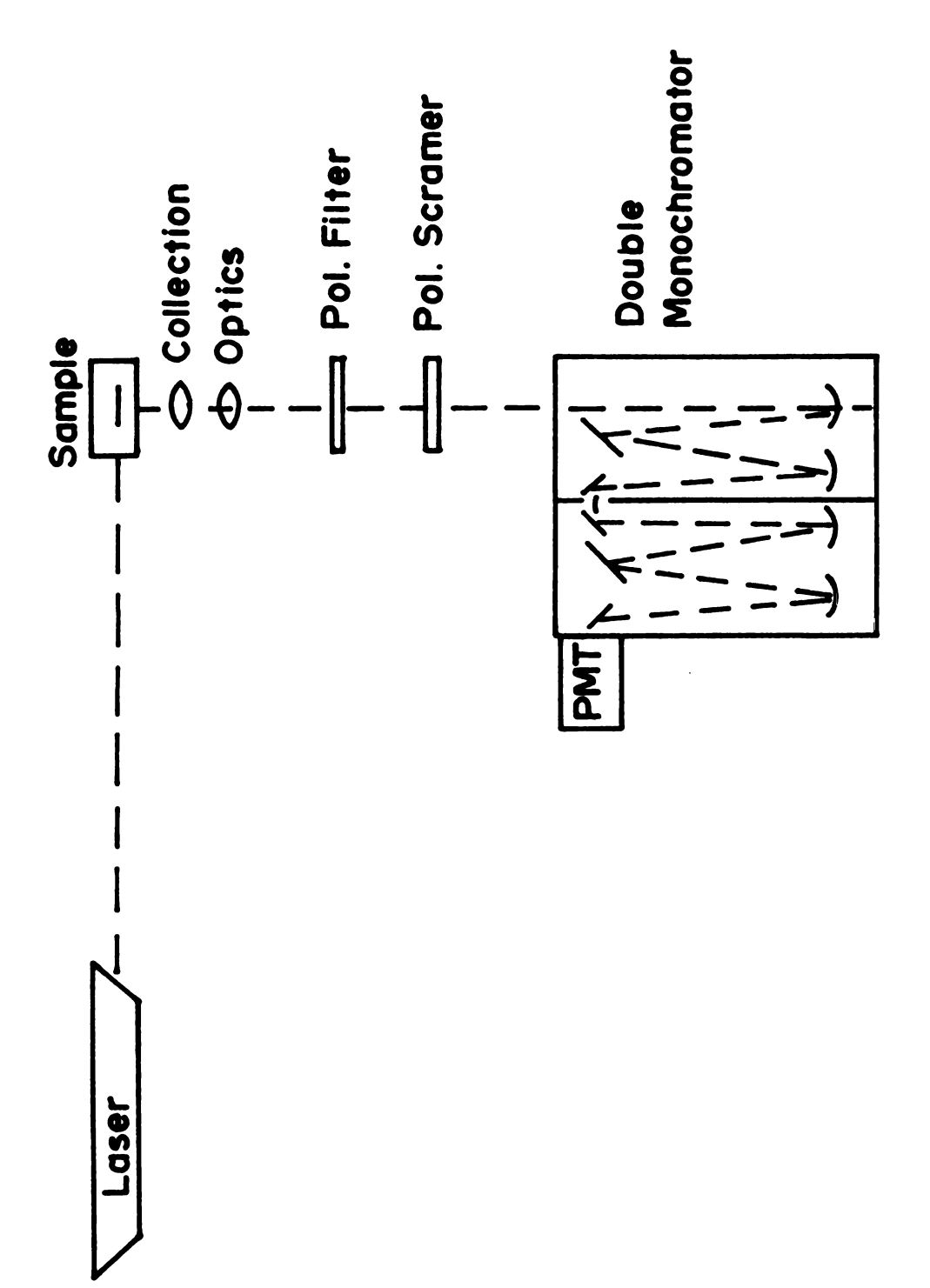
## B. Experimental

Resonance Raman spectra were obtained with two similar spectrometers utilizing different laser light sources. Investigations at  $\lambda_{\rm ex}$  = 441.6 nm were conducted on an instrument previously described (36) utilizing an RCA LD 2186 helium-cadmium laser. Spectra with 514.5 nm excitation were obtained with a Spectra-Physics 164 argon-ion laser and a spectrometer consisting of a Jarrel-Ash Model 25-100 double Czerny-Turner monochromator equipped with a thermoelectrically cooled RCA C31034 photomultiplier tube. Baird-Atomic spike filters were employed to help eliminate laser-plasma lines. Since resonance Raman requires introducing relatively high powers of radiation into an absorption band of the sample, local heating of the sample can

The state of the s

be a problem, particularly when biological molecules are involved. In order to circumvent this problem, the protein samples were cooled during Raman spectroscopy by passing cold dry nitrogen gas through a copper housing which held either 5 mm or 10 mm optical cuvettes. The sample temperature was controlled at  $5^{\circ}\text{C} \pm 2^{\circ}$  by regulation of the cooling gas flow rate. Bottom illumination geometry was employed in both spectrometers. A photon counting detection mode was used with the helium-cadmium instrument while the argon ion instrument employed direct current detection. In both cases slit widths which provided a spectral bandpass  $\leq 8 \text{ cm}^{-1}$  were used. A schematic diagram detailing the above instrumental arrangement is given in Figure (5).

Optical spectra were obtained with Cary 17 or McPherson EU-707D recording spectrophotometers. Protein fluorescence was monitored with a Perkin Elmer MPF-2 dual-scanning fluorimeter. A Varian E4 spectrometer equipped with an Oxford Instruments ESR-9 liquid helium cryostat was utilized to obtain EPR spectra at low ( $T \leq 50^{\circ}$ K) temperature. For EPR measurements at  $-145^{\circ}$ C a Varian Cryostat was used. MCD spectra were taken with a computer-interfaced spectrometer previously described (37). Reductive titrations were accomplished utilizing anaerobic titrators described later in the text. Samples for titration were gently but extensively degassed by exposure to alternate cycles of vacuum and either argon or carbon monoxide gas. Fully



Schematic diagram of laser Raman experimental arrangement. Figure 5.

reduced samples were obtained by the introduction of excess sodium dithionite into sealed cuvettes under an argon gas atmosphere.

#### CHAPTER 3

# ABSORPTION AND FLUORESCENCE SPECTROSCOPY OF FLAVOCYTOCHROME $c_{552}$

The optical absorption spectrum of  $c_{552}$  is dominated by the heme prosthetic groups of the protein. Thus, knowledge of the phenomena contributing to heme absorption is a necessary prerequisite for the appreciation of the protein's absorption characteristics. The absorption spectra of porphyrins in general (and hemes in particular) have long been the focus of extensive inquiry both theoretical and experimental. In this chapter a brief explanation of the theoretical interpretation of heme optical properties will be It will be followed by an examination of those properties as they pertain to  $c_{552}$ . Absorption spectroscopy is useful in the characterization of the mechanism of exogenous ligand binding to heme and flavin centers in the molecule and can be employed for the determination of relative reduction potentials of the hemes and flavin. application of fluorescence spectroscopy to  $c_{552}$  yields additional information concerning the protein environment of the flavin chromophore.

## A. Theory of Heme Absorption

The absorption spectra of porphyrins and porphyrin metal complexes are, in general, characterized by two strong transitions (38). These are the intense Soret (or B) transition in the near uv spectral region of the spectrum and a less intense visible (or Q) absorption in the 500 to 600 nm region. The Q transition is usually accompanied by a vibronic sideband and may or may not be split depending on the symmetry of the specific porphyrin. As a first approximation, the absorption spectra of porphyrins may be treated as arising from a conjugated 16-member cyclic polyene. The effects of peripheral substituents and the central metal ion (if present) are then viewed as perturbations upon the polyene spectra.

The earliest attempt to explain porphyrin spectra that met with qualitative success was the free electron model advanced by Simpson (39). This model assumes that the  $\pi$ -electrons of porphine are essentially free particles on a ring composed of the 16 lattice points (atoms) in the conjugated pathway of the molecule. The  $18-\pi$  electrons of the molecule are then paired in orbitals of increasing angular momentum, filling the system to the  $\ell=\pm 4$  level. Transitions then occur from that level to the  $\ell=\pm 5$  orbitals resulting in transitions with  $\Delta \ell=\pm 1$  or  $\pm 9$ . The former transitions are allowed by angular momentum

selection rules whereas the latter are not. Moreover, Hund's rule predicts that the  $\Delta\ell$  = ±9 transition will be lowest in energy. Thus, this model achieves qualitative agreement with both the relative positions and intensities of the porphyrin visible and Soret transitions. However, it is too simplistic to be useful in appreciating the more esoteric aspects of porphyrin spectra, such as coupling between  $\pi^-\pi^*$  transitions or the interaction of metal orbitals with the  $\pi$  system.

The formulation of a model based on the configuration interaction (CI) of cyclic polyene molecular orbitals (MOs) by Gouterman (40) provided a more detailed picture of porphyrin spectra. The model considers only the two highest filled and the two lowest unfilled cyclic polyene orbitals and is frequently referred to as the four orbital model. The MO procedure when applied to cyclic polyenes results in the prediction that the lowest unfilled states are a degenerate orbital of  $e_g$  symmetry, with the highest filled states being orbitals of  $a_{1u}$  and  $a_{2u}$  symmetry. In the cyclic polyene the highest filled states are energetically degenerate. This is not the case for hemes, but the generality of the argument still obtains. The energetic relationships and the nodal characteristics of the four orbitals involved in the Gouterman model are shown in Figure 6. Simple MO theory would ascribe the observed Q and B transitions individually to  $e_g + a_{2u}$  and  $e_g + a_{1u}$ 

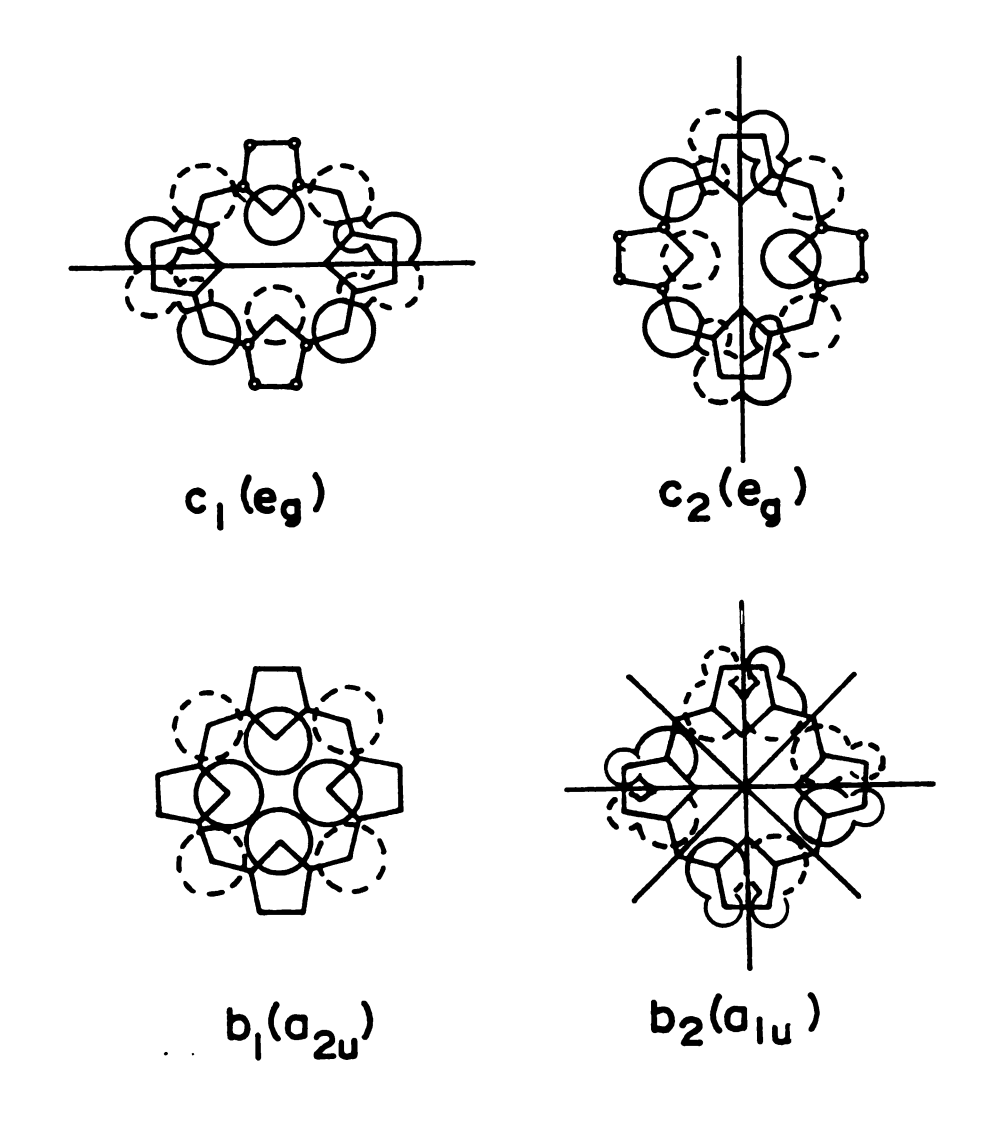


Figure 6. Spatial and nodal characteristics of the lowest unfilled ( $e_g$ ) and highest filled ( $a_{1u}$ ,  $a_{2u}$ ) porphyrin orbitals (from Reference 40).

transitions. However, at this level the Q and B transitions are degenerate. Since both transitions possess the same symmetry ( $E_u$ , in the  $D_{4h}$  symmetry group) configuration interaction between them is allowed and the observed transitions must be mixtures of such configurations. Configuration interaction occurs because the states  $a_{2u}e_g$  and  $a_{1u}e_g$  are solutions to the unperturbed eigenproblem for one-electron orbitals,

$$\hat{H}_{eff}(a_{2u}e_g) = E(a_{2u}e_g)$$

whereas the full Hamiltonian is,

$$\hat{H} = \hat{H}_{eff} + \hat{H}'$$

Electron repulsion terms,  $e^2/r_{ij}$ , provide the principal contributions to  $\hat{H}$ ' and cause states of the same symmetry to be mixed and driven apart in energy. The new states  $(\underline{i.e.}$ , eigenvectors of  $\hat{H}$  instead of  $\hat{H}_{eff}$ ) are now,

$$B_{x}^{\circ} = \sqrt{2}/2 \ (a_{2u}e_{gx} - a_{1u}e_{gy})$$
 $B_{y}^{\circ} = \sqrt{2}/2 \ (a_{2u}e_{gy} + a_{1u}e_{gx})$ 
 $Q_{x}^{\circ} = \sqrt{2}/2 \ (a_{2u}e_{gx} + a_{1u}e_{gy})$ 
 $Q_{y}^{\circ} = \sqrt{2}/2 \ (a_{2u}e_{gy} - a_{1u}e_{gx})$ 

and are referred to as 50-50 mixtures of the configurations for obvious reasons. Further mixing of states is required between the above states in order to obtain a model consistent with experimental data. The reason for this is that the dipole intensity of the  $Q^O$  states (in the above model) would be zero. This is easily demonstrated as follows: Let

$$R_{ly} = \langle a_{lu} e_{gx} | y | \psi_o \rangle$$

$$R_{2y} = \langle a_{2u} e_{gy} | y | \psi_o \rangle$$

now the dipole strength, q^2, of a transition is computed as the square of its transition moment. Thus for  $Q_y^0$ 

$$q^2 = \langle (a_{2u}e_{gy} - a_{1u}e_{gx})|y|\psi_0 \rangle^2 = \frac{1}{2}(R_{1y} - R_{2y})^2$$

for 
$$B_y^0$$
:

$$q^2 = \langle (a_{2u}e_{gy} + a_{1u}e_{gx}) | y | \psi_o \rangle^2 = \frac{1}{2} (R_{1y} + R_{2y})^2$$

with the same results for  $B_{\mathbf{X}}^{\mathsf{O}}$ ,  $Q_{\mathbf{X}}^{\mathsf{O}}$  dipole strengths. It can be shown that in rigorous  $D_{\mathsf{4h}}$  symmetry  $R_1 = R_2$ , and  $q^2(Q_{\mathbf{X},\mathbf{y}}^{\mathsf{O}}) = 0$ . The observed dipole intensity of the Q state in porphyrin spectra derives from a coupling of the Q<sup>o</sup> and B<sup>o</sup> transitions. If it is assumed that no

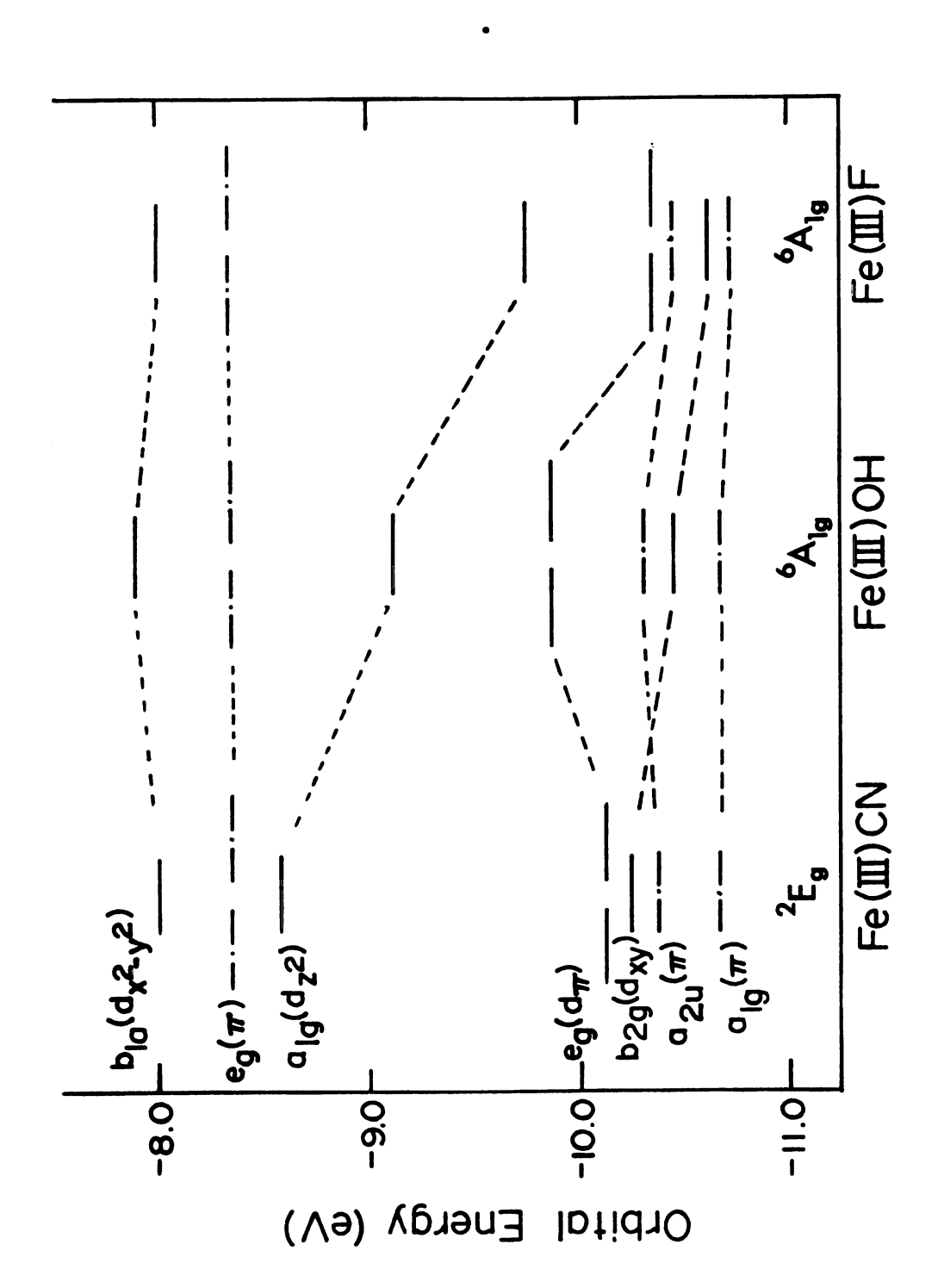
mixing occurs between states of different polarization, then the application of perturbation theory yields the Q states of an arbitrary porphyrin as,

$$Q_{x} = Q_{x}^{O} + \lambda_{x}B_{x}^{O}$$

$$Q_y = Q_y^0 + \lambda_y B_y^0$$

Where  $\lambda$  is a coupling parameter dependent on the form of the perturbation operator used. The perturbation operator can be a simple electronic coupling (40) arising from a splitting in the orbital degeneracy of the  $a_{lu}$  and  $a_{2u}$  states or one involving vibronic coupling introduced by the breakdown of the Born-Oppenheimer approximation (41). The former is a strong function of the electronic effects of porphyrin substituents upon the molecule's  $\pi$ -system, whereas the latter arises from the parametric dependence of the electronic energy of the molecule upon its vibrational motions. This will be discussed in some detail in Chapter 5.

The situation found in heme  $\underline{c}$  is complicated by the possibility of interaction between iron d orbitals and the porphyrin system. Inclusion of iron d orbitals in extended Hückel calculations (42) results in the energy levels depicted in Figure 7. It can be seen that the effect of strong field axial ligands (such as  $CN^-$ ) is to

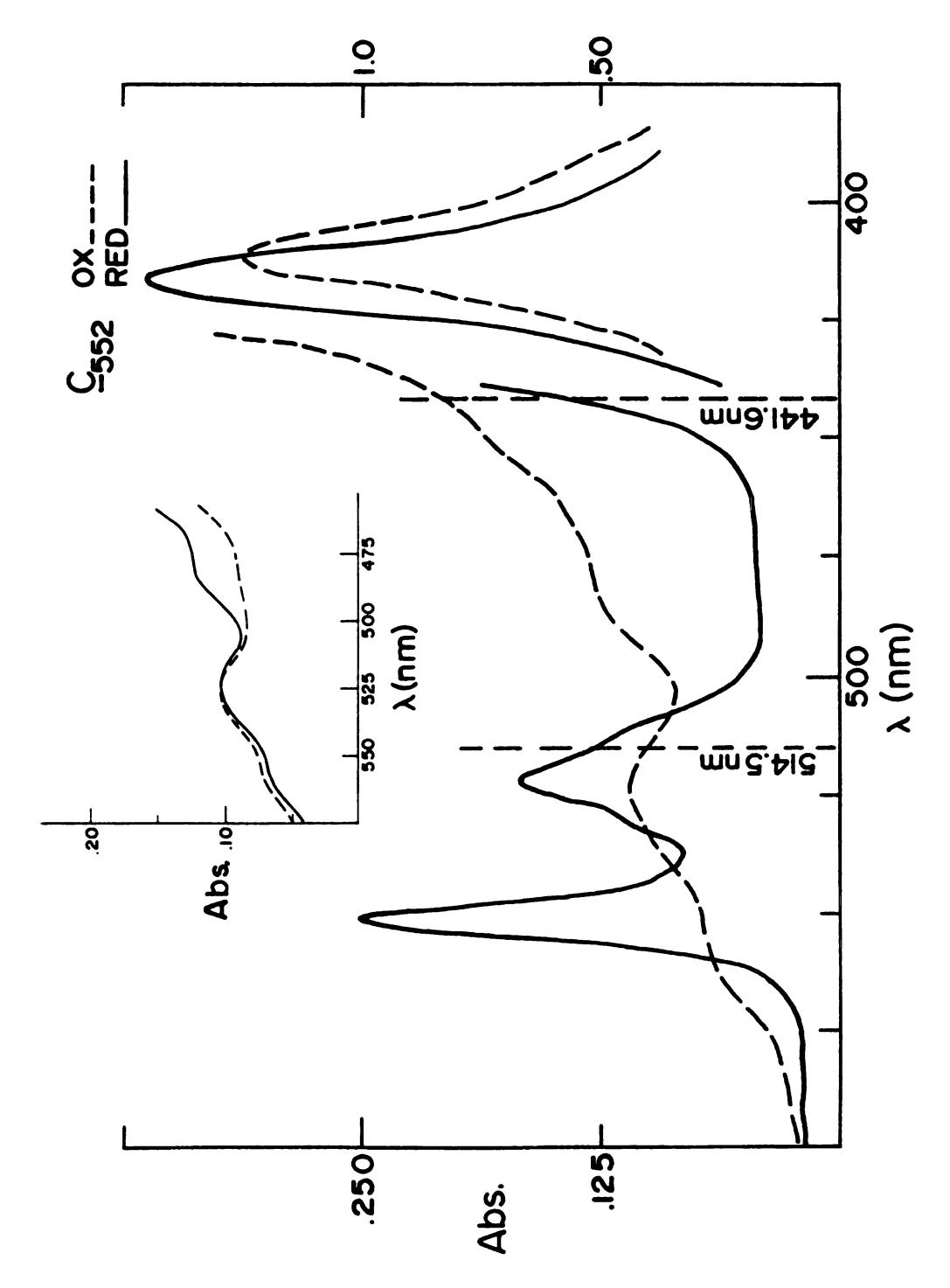


Relative energy levels of porphyrin  $(-\cdot-)$  and iron (---) orbitals for ferric porphyrin complexes (from Reference 42). Figure 7.

drive  $d_{z^2}$  and  $d_{x^2-y^2}$  up in energy, forcing the iron into a low spin (S = 1/2) configuration. The charge transfer transitions  $a_{1u}$ ,  $a_{2u} \rightarrow d_{z^2}$ ,  $d_{x^2-v^2}$  would occur at energies comparable to the porphyrin  $a_{1u}$ ,  $a_{2u} + e_{g}$  transitions; however, mixing of the states involved in these transitions is symmetry-forbidden. The only other unfilled iron orbital in ferric low-spin hemes  $(d_{\pi} = d_{xz}, d_{yz})$  is of  $e_{\varphi}$ symmetry, and since  $\mathbf{a}_{1u}$ ,  $\mathbf{a}_{2u}$  and  $\mathbf{d}_{\pi}$  are nearly isoenergetic the transition would occur in the near IR spectral region. In ferrous low-spin hemes, the  ${\rm d}_{\pi}$  orbitals are filled and the possibility of this transition is eliminated. in either the ferric or the ferrous case the effect of the iron d orbitals on the heme visible spectrum is small. If the iron is complexed to weak-field ligands the decreased splitting between  $d_{x^2-y^2}$ ,  $d_{z^2}$  and  $d_{\pi}$  orbitals forces the iron into a high-spin (S = 5/2) configuration. The  $d_{\pi}$  orbitals are now unfilled and charge transfer transitions are expected in the visible region of the These transitions have been observed in a variety of high-spin metalloporphyrin complexes (43).

#### B. Results

The heme moieties in flavocytochrome  $\underline{c}_{552}$  display optical absorption spectra (shown in Figures 8,12) consistent with their assignment as low-spin heme  $\underline{c}$ . The oxidized protein has a Soret maximum of 410 nm and a



Absorption spectra of  $\sim 6 \, \mu M$  oxidized (---) and reduced (---) flavocytochrome  $c_{552}$  in 0.1 M Tris buffer, pH 7.5. Insert:  $\sim\!\!6~\mu M$  oxidized  $c_{552}$  in 0.1 M MES buffer, pH 6.1 before (——) and after (---) addition of 2 mM Na $_2$ S $_2$ O $_3$ Figure 8.

poorly-resolved visible band that peaks at 525 nm. The addition of another electron to the iron d-orbital system results in a shift in the Soret maxima to 416 nm in the ferrous protein. The visible transitions are intensified and distinct  $Q_{00}$  (at 552 nm) and  $Q_{01}$  (at 523 nm) components become apparent. These effects are primarily due to the decrease of central ion charge and the consequent lowering of the  $a_{1u}, a_{2u} \rightarrow e_g$  energy gap and to the decrease in the spin and orbital angular momentum of the iron d-electrons, resulting in decreased  $d_{\pi}$  - porphyrin magnetic interaction and better  $Q_{00}, Q_{01}$  resolution. Such behavior is typical of all  $\underline{c}$ -type cytochromes (44).

There are, however, some noteworthy deviations from typical heme  $\underline{c}$  behavior evidenced by  $\underline{c}_{552}$ . Its covalently bound flavin moiety is apparent in the oxidized protein as pronounced shoulders on the low and high energy sides of the Soret peak. Flavin absorption arises from the long and short axis  $\pi \to \pi^*$  transition dipoles of the isoalloxazine portion of the molecule shown in Figure 9. This shoulder bleaches completely upon flavin reduction and is sensitive to  $\mathrm{CN}^-$ ,  $\mathrm{SO}_3^\pm$  and  $\mathrm{S}_2\mathrm{O}_5^\pm$  binding to oxidized  $\mathrm{c}_{552}$ . Additional structure is also apparent in the 600-700 nm region of the absorption spectrum of oxidized  $\mathrm{c}_{552}$  where weak bands at  $\mathrm{v}650$  nm and  $\mathrm{v}695$  nm are present in  $\mathrm{c}_{552}$ . The 695 nm transition is observed in horse heart cytochrome  $\mathrm{c}$  and other small molecular weight mono-heme  $\mathrm{c}$  proteins (45) and could arise from a charge transfer from porphyrin

Figure 9. Transition axes giving rise to the  $\sim\!450$  nm and  $\sim\!360$  nm flavin absorption bands.

 $\pi$  orbitals to the unfilled iron  $\textbf{d}_{\pi}$  or from iron  $\textbf{d}_{\pi}$  orbitals to distal protein sulfur orbitals. Experimental studies (46) have assigned this transition to the charge transfer interaction between the heme iron and the sulfhydryl group of a methi nineoamino acid residue acting as a heme axial ligand. The intensity of the 695 nm band in  $c_{552}$  is relatively invariant to pH changes (See Table 1) indicating that methionine remains coordinated to the heme over the pH range of 6.0 - 10.3. The 650 nm band has no analog in horse heart cytochrome c spectra. The most likely assignment of this band is to a high-spin heme chargetransfer band. The existence of a d  $\rightarrow$   $\pi$ \* charge transfer interaction in high spin hemes is well documented (43); they typically produce absorption bands in the near-infrared with extinction coefficients of  $0.050 \text{ mM}^{-1} \text{ cm}^{-1}$ . The extinction coefficients of the  $\underline{c}_{552}$   ${\sim}650~\text{nm}$  band is variable but is always less than 0.0015 mM<sup>-1</sup> cm<sup>-1</sup>. Thus, 2-3% high spin heme in the sample could account for the observed effect.

The optical absorption of the diheme peptide of  $\underline{c}_{552}$  lacks the flavin effects mentioned above and is analogous to that of small molecular weight monoheme proteins (See Figure 10). The near-infrared spectrum of ferric heme peptide offers no evidence of a methionine-iron chargetransfer band, indicating that neither heme has methionine as an axial ligand in the apoprotein.

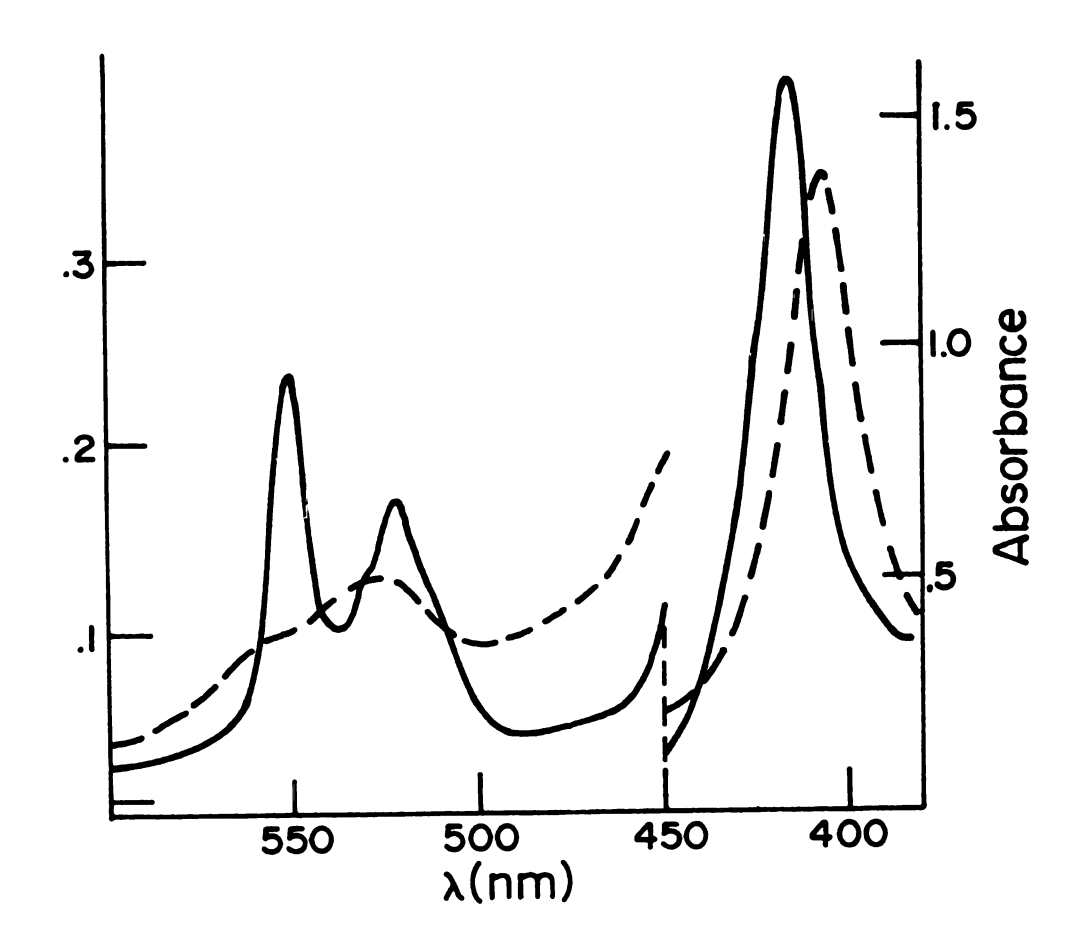


Figure 10. Absorption spectra of oxidized (---) and reduced (---) diheme peptide of flavocytochrome  $\underline{c}_{552}$  in 0.1 M Tris, pH 7.5.

Table 1. Extinction Coefficients of 695 nm Absorption Bands.

		ε (	$\varepsilon$ (mM <sup>-1</sup> cm <sup>-1</sup> )	
Horse heart cytochrome <u>c</u> , pH 7.5		.215	(Ref. 45)	
		.200	(This study)	
Flavocytochrome c <sub>552</sub>	pH 7.5	.210		
11	рН 6.05	.205		
n	pH 10.3	.220		
n	pH 6.05 + SmM CN			
	$\Delta t = 5 min$	.155		
	$\Delta t = 25 \text{ min}$	.070		
	Δt = 180 min	<.030		

Calculation of 695 extinction coefficients was based on the values of Q band extinction coefficients of Vorkink (30).

#### C. Binding Studies

Flavocytochrome  $\underline{c}_{552}$  binds a variety of exogenous ligands. The heme prosthetic groups of  $\underline{c}_{552}$  bind CO while its flavin moiety binds CN $^-$ , SO $_3^-$  and S $_2$ O $_3^-$ . These binding characteristics are well documented (30,47). It is my intention in this section to confirm such binding behavior as a necessary prelude to investigation of the effects of binding on the EPR and fluorescence spectra of  $\underline{c}_{552}$  and to examine the behavior of the near IR  $\underline{c}_{552}$  transitions with respect to binding.

Reduced  $c_{552}$  binds CO under a wide range of pH conditions. The effects of CO binding at pH 7.5 and 10.0 are shown in Figure 11. The intensification of Soret absorption and a decrease in the  $Q_{00}$  band oscillator strength resulting from CO binding are indicative of decreased coupling between heme B and Q electronic states and is much more pronounced at high pH. Binding decreases the extinction coefficient for the  $Q_{00}$  transition by  $\sim 15\%$  at pH 7.5 and by  $\sim 50\%$  at pH 10.0. An obvious explanation for the smaller effect at low pH is that only one heme is accessible to the CO whereas at high pH both hemes are able to bind CO. This binding scheme is substantiated by the MCD and EPR behavior of the  $c_{552}$ ·CO complex and will be elaborated upon later.

The effects of CN<sup>-</sup>, SO<sup>=</sup><sub>3</sub>, and S<sub>2</sub>O<sup>=</sup><sub>3</sub> binding to  $c_{552}$  are most obvious in the bleaching of flavin absorption at

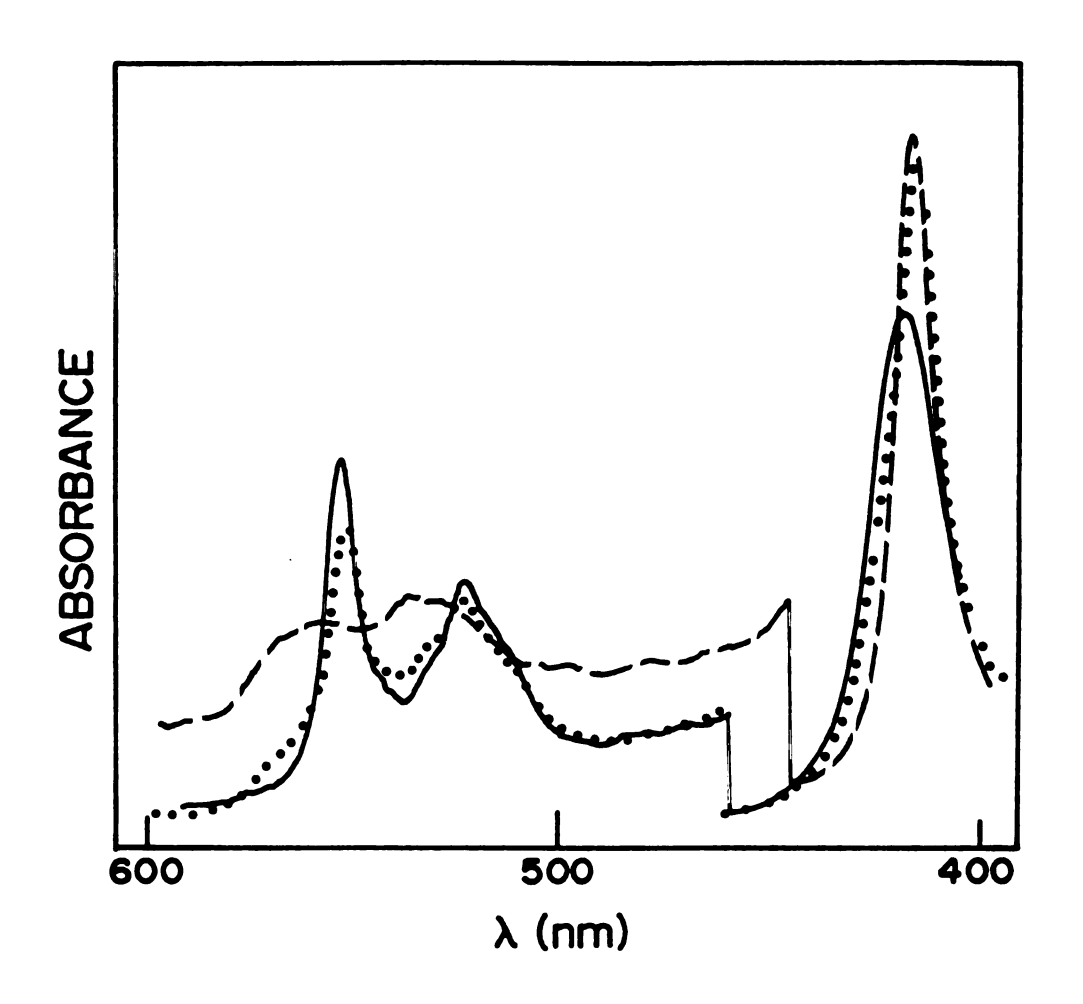


Figure 11. Absorption spectra of reduced  $\underline{c}_{552}$  under Ar (—) in 0.1 M Tris, pH 7.5, reduced  $\underline{c}_{552}$  under 6 psi of CO (…) in 0.1 M Tris, pH 7.5 and reduced  $\underline{c}_{552}$  under 6 psi of CO in 0.1 M CAPS, pH 10.0.

475 nm. All three of these exogenous ligands bind most efficiently at low pH (0.1 M MES pH = 6.0 - 6.2 was used as a buffer system for all binding experiments) and result in a lowering of  $A_{475}/A_{525}$  to 0.85. The spectral changes occasioned by CN binding are shown in Figure 12. A calculation of the dissociation constant for the binding of CN from the data shown in Table 2 yields a value of  $^{\circ}$ 1.5 x 10<sup>-5</sup> M<sup>-1</sup> which correlates well with previously measured values of  $K_d$  (30). Such bleaching marks the protein's flavin moiety as the site of binding. Indeed, extensive studies with both free and bound flavins by Massey et al. (48) have established that formation of a direct adduct between flavin and  $SO_3^{=}$  proceeds through binding at the flavin (N5) position. No such adduct formation was found using CN, however. Since thiosulfate can act as a natural electron source for Chromatium (35), its binding to the flavin group of the protein in vitro indicates that it is the likely point of protein: substrate interaction in vivo.

In vivo cytochrome c reductase activity in the presence of S has been demonstrated for  $c_{552}$  (23). CN and  $so_3^{\pm}$  can be postulated to serve as substrate analogs on the basis of their effects on flavin absorption. However, while  $s_2o_3^{\pm}$  and  $so_3^{\pm}$  apparently bind reversibly to the flavin and remain bound unless removed via dialysis, CN displays irreversible behavior. Subsequent to cyanide binding,  $A_{475}/A_{525}$  returns to its initial value and cannot

Table 2. Cyanide Binding to Flavocytochrome  $c_{552}$ .

[ <u>c</u> 552]	[CN <sup>-</sup> ]	<sup>A</sup> 475 <sup>/A</sup> 525	% Bound	K <sub>d</sub> (M <sup>-1</sup> )
4.3 μM	0	1.23	0	
11	40 µM	.965	72.8	1.5 x 10 <sup>-5</sup>
n	100 μΜ	.899	90.9	$1.0 \times 10^{-5}$
11	150 µM	.893	92.6	$1.2 \times 10^{-5}$
11	250 μM	.890	93.4	$1.8 \times 10^{-5}$
11	500 μM	.876	100	
11	1000 µM	.876	100	

Figure 12. Absorption spectra of  $^{\circ}30~\mu\text{M}~c_{552}$  in 0.1 M MES, pH 6.1 (---), 5 minutes after the addition of 5 mM CN (----), 25 minutes after the CN addition (---), and 180 minutes after the CN addition (---).

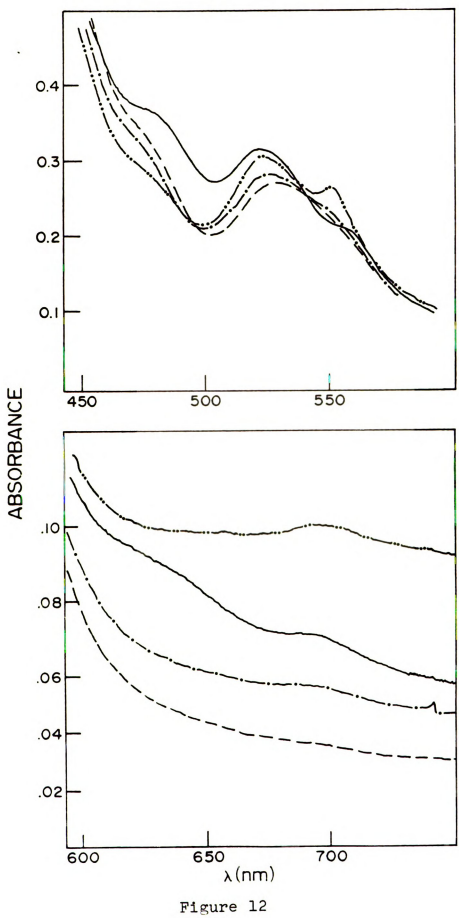


Figure 13. Absorption spectra of  $\sim 30~\mu M \ c_{552}$  in 0.1 M MES pH 6.1 (---), 15 minutes after the addition of 5 mM S<sub>2</sub>0 $\frac{=}{3}$  (----).

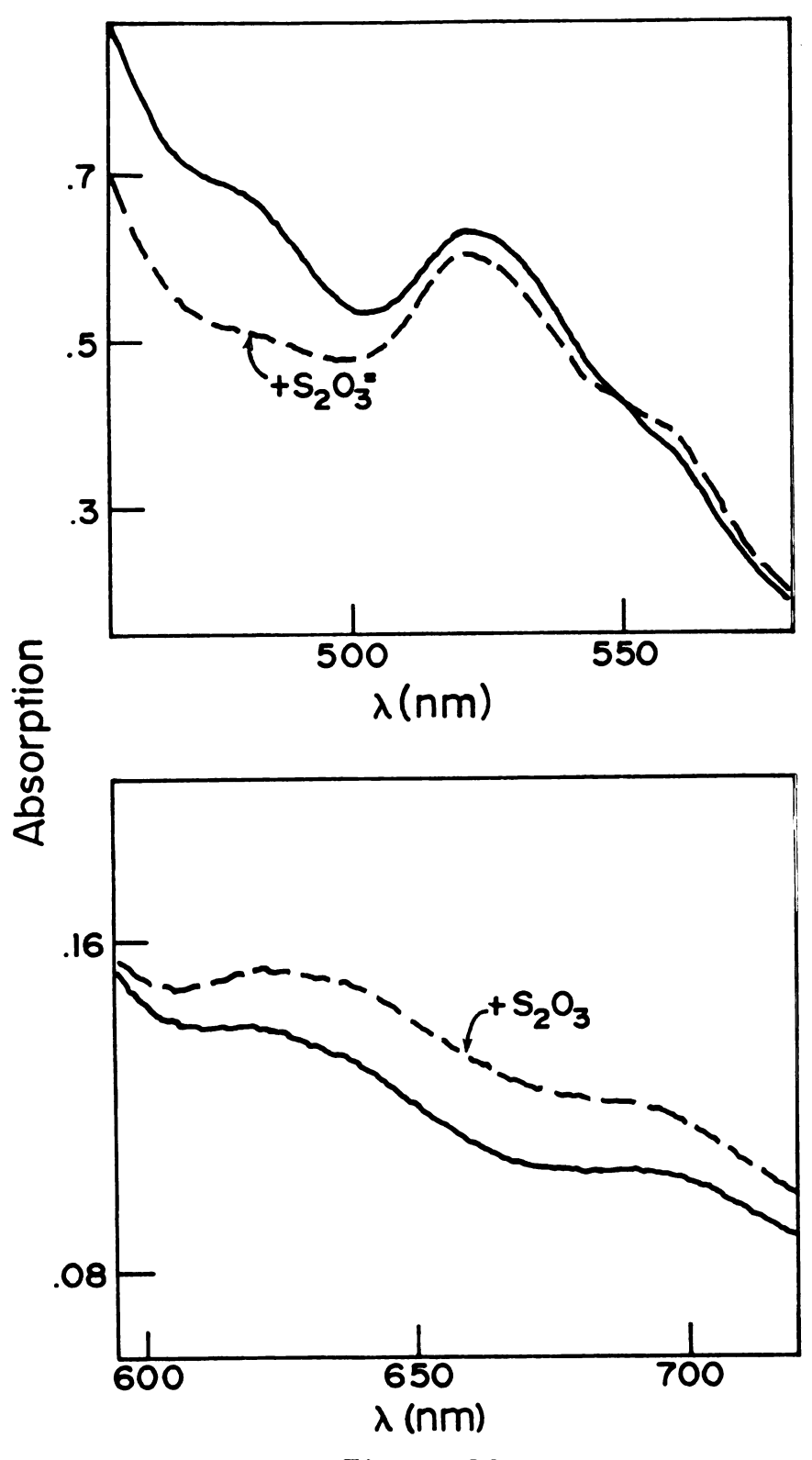


Figure 13

be re-bleached by further addition of CN<sup>-</sup>. Moreover, this was accompanied by a significant alteration of the heme Q-band absorption, which decreased in intensity and shifted to ~528 nm. Such behavior usually occurred within 1/2 hour of the initial CN<sup>-</sup> addition, but its time dependence was variable.

A distinction between the effects of  $CN^-$  and  $S_2O_3^$ binding to  $\underline{c}_{552}$  can also be seen in behavior of the near IR (750-600 nm) absorption bands. (See Figures 12,13.) On the basis of its extinction coefficient, the 695 nm band in  $\underline{c}_{552}$  can be postulated to arise from a single methionine-heme interaction in the protein (See Table 1). Neither  $N_3^-$  nor any of the sulfur-containing flavin ligands has any effect on the intensity of either the 650 or 695 bands. Upon cyanide binding the spectrum displays a rapid broad increase in absorption in the 600-750 nm region accompanied by a bleaching of the 650 band and a time dependent decrease in intensity both of the broad 600-750 nm background and of the 695 band that parallels the previously discussed time dependent increase in absorption at 475 nm. Apparently, the initial effects of CN upon the flavin are reversed by other cyanide-protein interactions. The alteration of the visible heme absorption spectrum implicates at least one of the hemes as the site of this interaction. The decrease in intensity of the 695 nm band is indicative of a disruption of methionine-heme axial

ligation. CN readily serves as a strong field ligand for hemes c (49) and could be expected to assume this role with  $c_{552}$ . The fact that the hemes in  $c_{552}$  are already 6-coordinate would require a ligand displacement reaction in order to bind CN to the hemes. Whether methionineheme ligation is disrupted by such a direct replacement or as a result of a protein conformational change induced by CN attack on the non-methionine ligated heme is unclear. The kinetic barriers encountered in the replacement of an axial amino acid residue with CN might produce the observed long time dependence of cyanide effects. tein conformational changes associated with axial ligand displacement could also induce a significant reduction in the ability of the flavin group to bind CN and result in the restoration of absorption intensity at 475 nm. dence is found in the EPR spectra of  $\underline{c}_{552}$  to substantiate this scenario and will be discussed in a later chapter. Since the sulfur containing flavin ligands do not exhibit any substantial interactions with the hemes in  $c_{552}$ , they can be postulated to react with the protein in a single-step flavin-adduct formation.

Despite the fact that the high spin heme resulting from "damaged" protein makes up a very minor component of our samples and must be considered of parenthetical interest, some insight into the heme protein environment can be gained by examination of its behavior with respect to

exogenous ligands. If the 650 nm band results from high spin heme charge transfer bands, the addition of a strong field heme ligand like CN should produce the observed bleaching. What is surprising is the lack of a similar effect with a 5 mM  $N_3$  addition, since azide is also a strong field heme ligand, although not as strong as CN. The complete lack of effect by  $N_3$  would appear to indicate that the high spin band in  $c_{552}$  is not the result of a simple unfolding of the protein upon denaturation. Such a situation would result in exposure of the hemes to the solvent and provide equal accessibility to cyanide and and azide. The high spin heme in "damaged"  $c_{552}$  is obviously still in an environment that can discriminate between ligands.

## D. Reductive Titration

Monitoring the absorption spectrum of  $\underline{c}_{552}$  during the course of a reductive titration of the protein provides a simple means of determining the relative reduction potentials of the protein's two types of chromophores. Application of the Nernst Equation to a system of two active redox couples results in:

$$E_o(Flavin) + \frac{2.303 \text{ RT}}{nF} \log [Fl]_{ox}/[Fl]_{red} = E$$

$$= E_o(Heme) + \frac{2.303 \text{ RT}}{nF} \log \frac{[H]_{ox}}{[H]_{red}}$$
(3.1)

where

n', n = number of e transferred;

F = Faraday's constant;

 $E_0$  = midpoint potential of flavin or heme;

 $[Fl]_{ox}$ ,  $[Fl]_{red}$  = concentrations of oxidized and reduced flavin; and

 $[H]_{ox}$ ,  $[H]_{red}$  = concentrations of oxidized and reduced heme

at 25°C this reduces to

$$\Delta E_0 = .059 \log [F1]_{ox}^{1/n} [H]_{red}^{1/n'} / [F1]_{red}^{1/n} [H]_{ox}^{1/n'}$$
 (3.2)

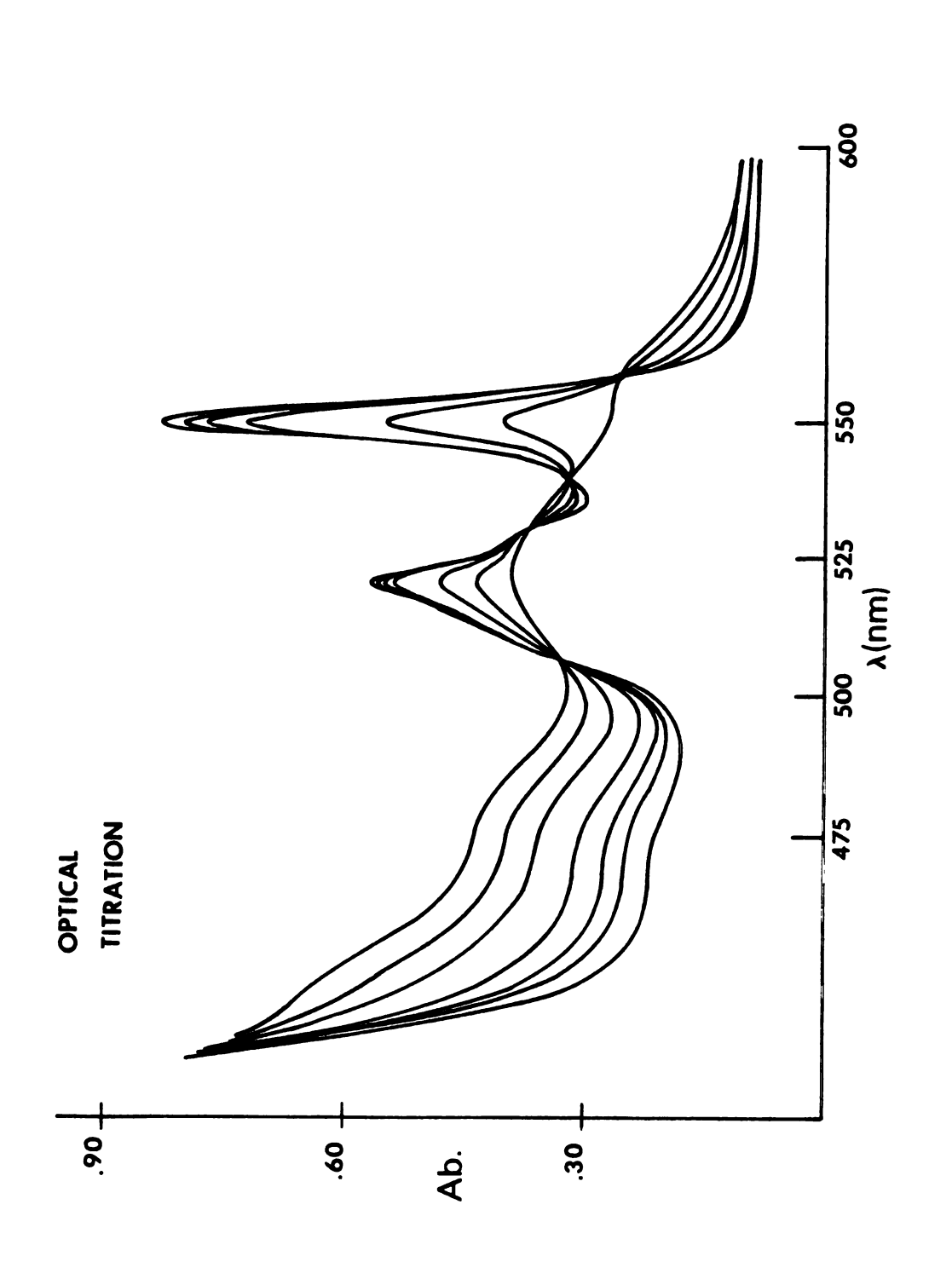
where

$$\Delta E_{o} = E_{o}(Heme) - E_{o}(Flavin)$$

Thus, determination of the relative concentrations of reduced and oxidized flavin and heme species allows for calculation of the relative potentials of the two redox couples involved. The above derivation contains the implicit assumption that the hemes in  $\underline{c}_{552}$  behave as one two-electron redox couple having an average midpoint potential of  $\underline{E}_0$  (heme) rather than acting as two independent one-electron couples. Analysis of the data from reductive

titrations indicates that such an assumption is justified. Calculation of  $\Delta E_{\rm O}$  from Equation (3.2) resulted in a relatively constant value throughout the course of the titration whereas solving the Nernst equation using three independent redox couples (one flavin and two hemes) produced widely and systematically varying values of  $\Delta E_{\rm O}$  at different points in the titration. (See Appendix.)

Figure 14 shows the spectra collected from a single reductive titration of  $\underline{\mathbf{c}}_{552}.$  The titrations were performed in a sealed anaerobic titrator shown in Figure 15. were extensively degassed by alternate exposure to vacuum and Ar gas. A sodium dithionite solution was introduced via an air-tight syringe in measured aliquots. The concentration of the sodium dithionite solution was determined by performing a reductive titration upon a solution with a known concentration of lumiflavin-3-acetate (obtained from Dr. Graham Palmer, Department of Biochemistry, Rice University), a two-electron acceptor having an absorption maximum at 446 nm with  $\Delta \varepsilon$  (oxidized-reduced) of 10.8 mM<sup>-1</sup> cm<sup>-1</sup>. A representative plot of dithionite standardization against lumiflavin-3-acetate is shown in Figure 16. Optical spectra were recorded and the procedure repeated until reduction was complete. Flavin: heme ratios of the samples used in different titrations varied from 1.25 to 1.12 with no apparent effect on the quantification of the titrations (i.e., all titrations consumed between 4.03 and 4.18 electrons per molecule).



Absorption spectra obtained from a reductive titration of flavocytochrome 2552 in 0.1 M Tris, pH 7.5 under an Ar atmosphere. Figure 14.

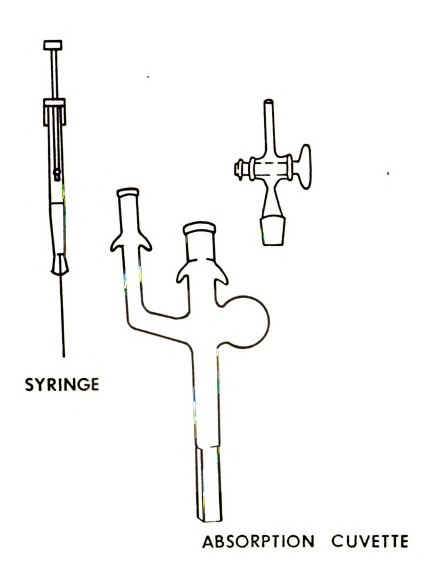
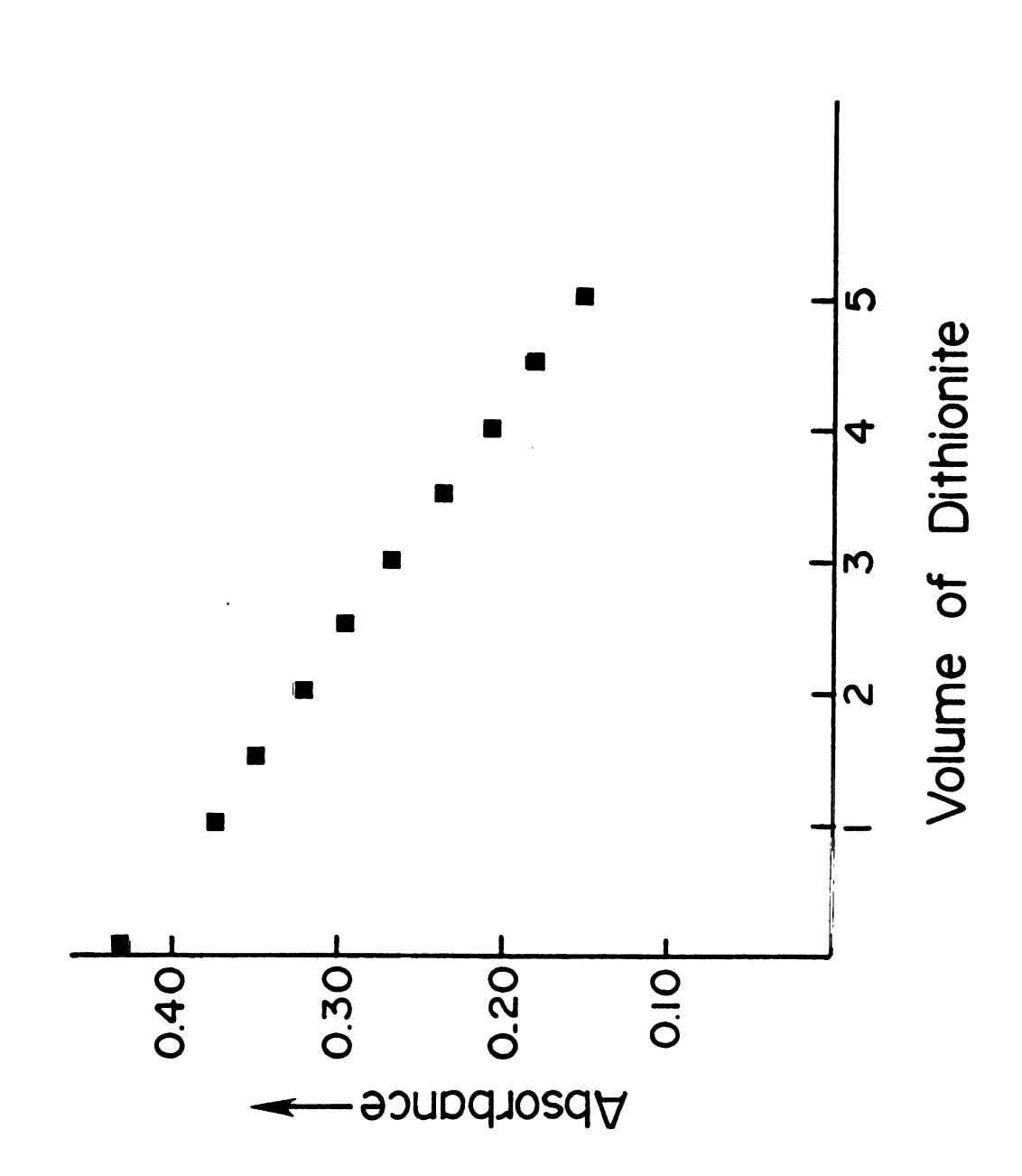


Figure 15. The anaerobic titrator used in the reductive titrations of  $\underline{\mathbf{c}}_{552}$  .

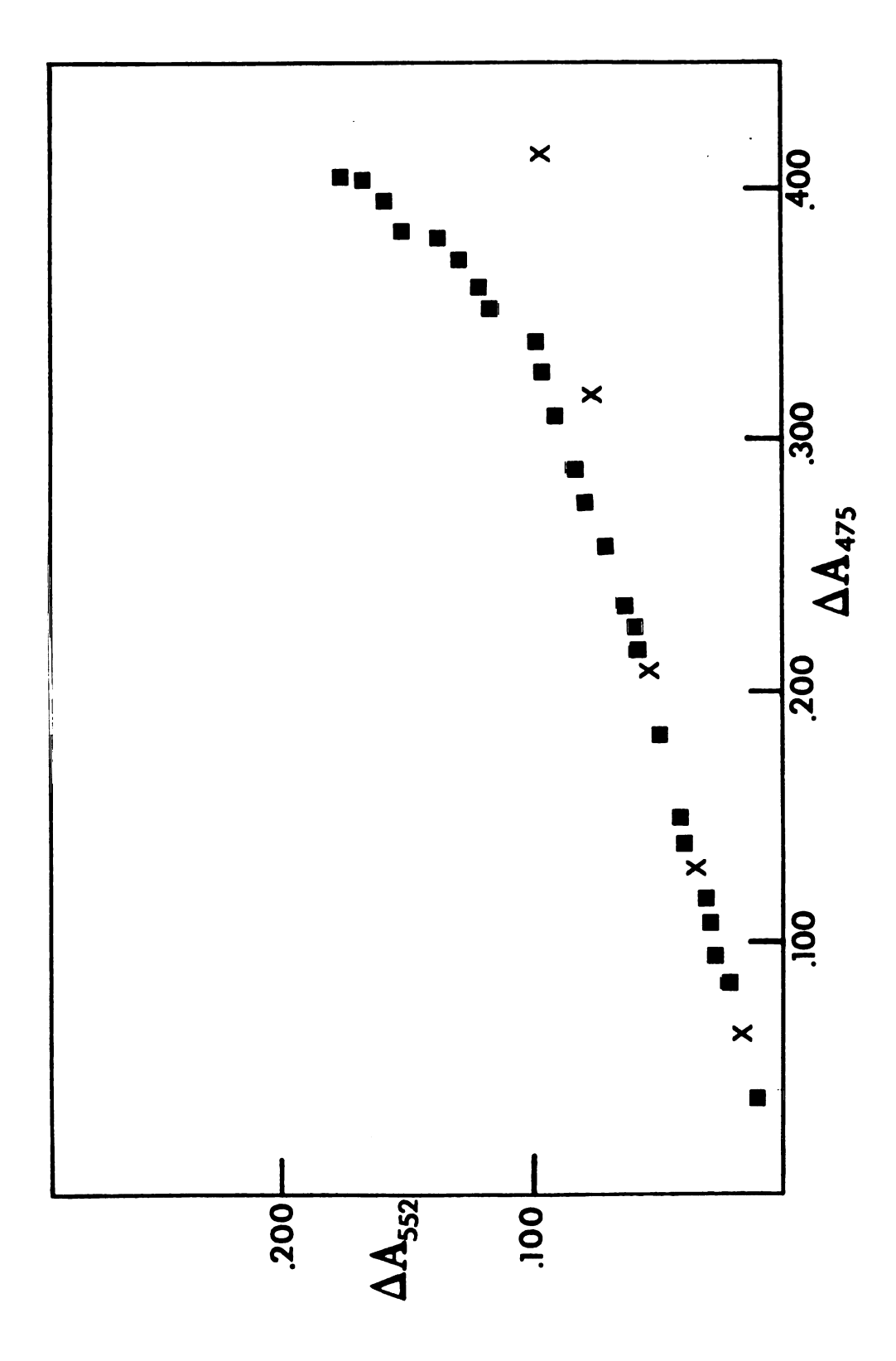


Standardization plot for dithionite reductant used in reductive titrations. Figure 16.

Determination of relative concentrations from titration data required some deconvolution of the spectral data. Relative concentrations of oxidized and reduced hemes can be obtained directly from  $\Delta A_{552}$  measurements; however, flavin concentrations can be determined from  $\Delta A_{475}$  only after heme effects at that wavelength have been accounted for. A plot of  $\Delta A_{552}$  vs  $\Delta A_{475}$  (Figure 17) clearly shows non-linear behavior. This is due to the fact that initially the hemes provide the only active redox couple leading to a slope of  $\Delta A_{475}$  (heme)  $\Delta A_{552}$  (heme)

[ $\Delta \epsilon_{475}$ (heme)+ $\Delta \epsilon_{475}$ (flavin)].  $\Delta C_{flavin}/\Delta C_{heme}/\Delta \epsilon_{552}$ (heme)>0.25 where  $\Delta C_{i}$  = change in concentration of species i

By subtracting the effect of the heme component at 475 nm an accurate determination of  $\Delta C(\text{flavin})$  can be made. Previous attempts (30) to determine  $\Delta E_m^O$  between flavin and heme did not recognize the dual contribution to  $A_{475}$  and consequently derived erroneous values for  $\Delta E_m^O$ . Determination of  $\Delta E_m^O$  by the above method yielded a value of  $E_{\text{Heme}}^O$  -  $E_{\text{Flavin}}^O$  = 37 ± 5 mV. The reduction of heme and flavin

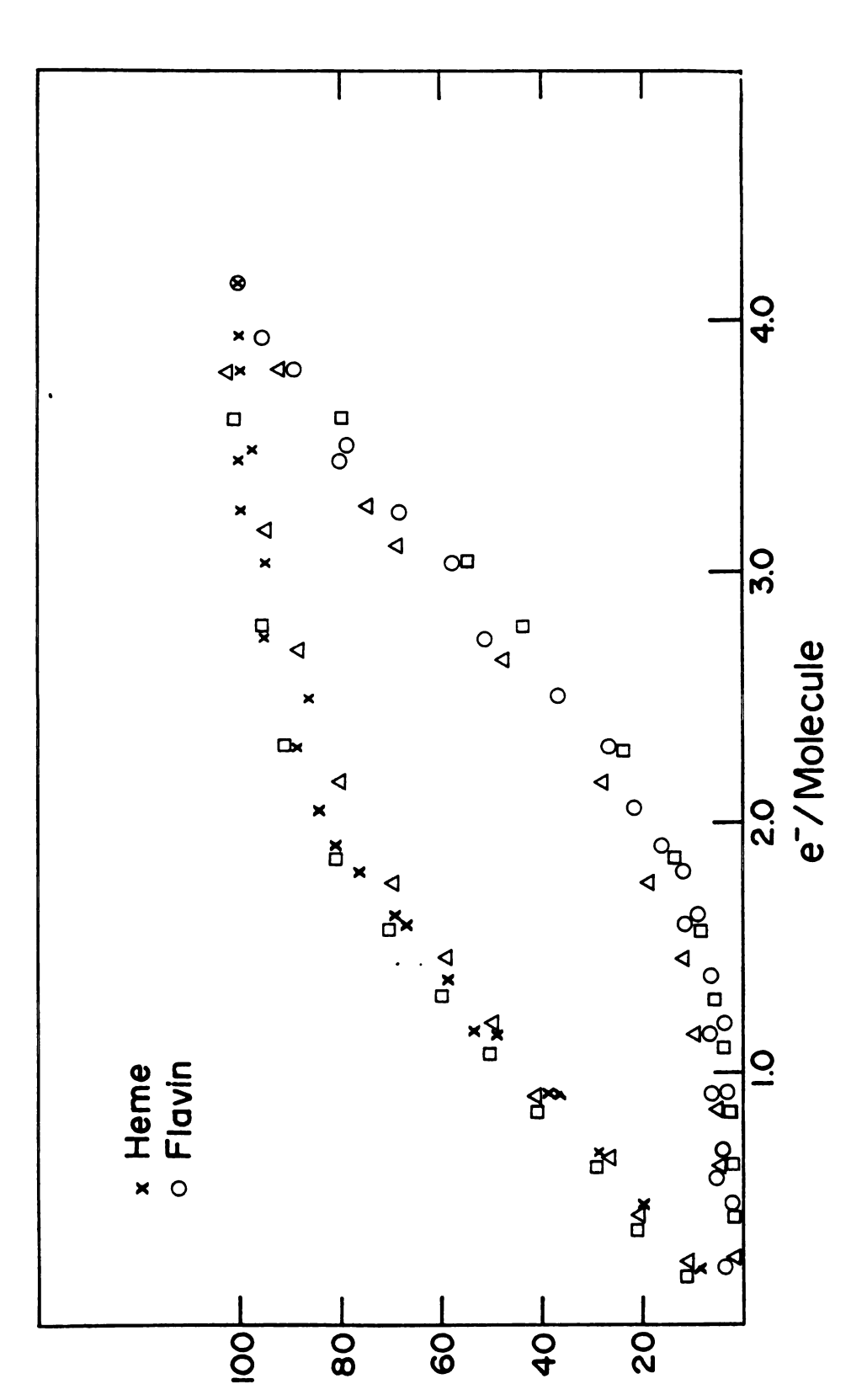


A plot of  $\Delta A_{475}$  <u>vs.</u>  $\Delta A_{552}$  during a reductive titration of flavocytochrome  $\frac{c}{2552}$  ( $\blacksquare$ ) and horse heart cytochrome  $\underline{c}$  (x), (type II obtained from Sigma Chemical), both in 0.1 M Tris, pH 7.5. Figure 17.

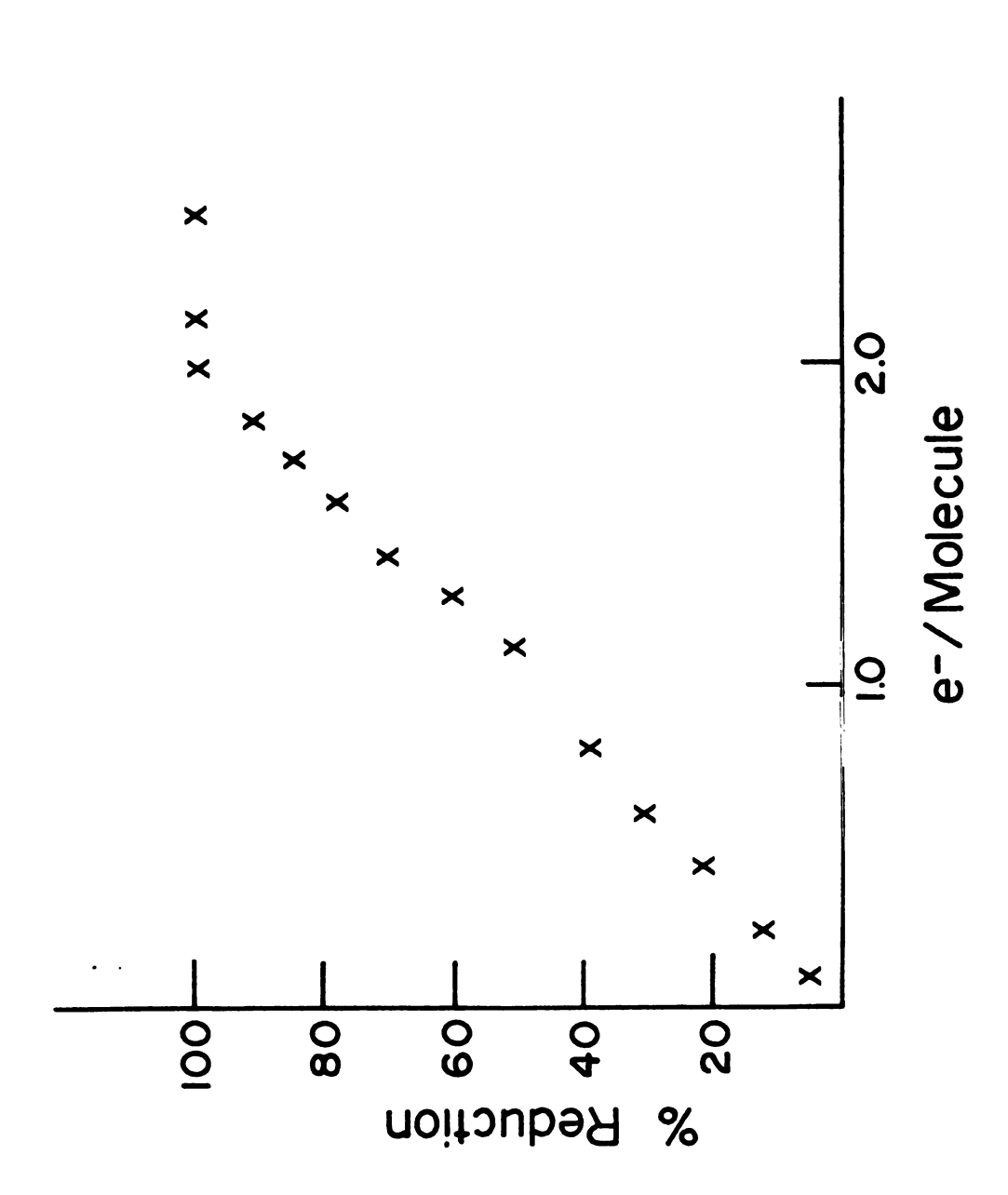
redox centers in the protein as a function of electrons/molecule added is plotted in Figure 18 along with the theoretical lines for two two-electron redox couples with  $\Delta E_m^O$  = 32 mV and  $\Delta E_m^O$  = 42 mV.

The binding of a thiosulfate ion to the oxidized flavin moiety affects its redox capabilities. This is to be expected since the coupling of the binding and reduction reactions of the flavin will result in stabilization of the oxidized form of that center. This lowers its apparent midpoint potential. Figure 19 attests to the fact that thiosulfate binding lowers the flavin potential to the extent that hemes in  $\underline{c}_{552}$  become fully reduced after the introduction of only two equivalents of electrons into the molecule.

When protein with a flavin heme ratio of less than one was used, the titrations described above yielded a biphasic behavior in flavin reduction. Quantification of the reduction remained at 4e/molecule but the flavin reduction occurred in a stepwise manner. Two components, one ~20 mV and the other ~40 mV lower than the hemes potentials, were present. A mixture of high flavin:heme (1.25) and low flavin:heme (.85) forms of the protein could be expected to produce the observed behavior. In any case, it is apparent that a low flavin:heme ratio in the protein does not arise from partial flavin reduction as the molecule still requires 4 e to become fully reduced, nor



The extent of heme (x) and flavin (o) reduction as a function of electrons per molecule added during a reductive titration of  $c_{552}$ . Open squares and triangles denote the theoretical curves for two two-electron couples with  $\Delta E = 42 \text{ mV}$  and 32 mV, respectively. Figure 18.



The extent of heme reduction as a function of electrons per molecule added during a reductive titration of thiosulfate bound  $c_{552}$  in 0.1 M MES, pH 6.1 under an Ar atmosphere. Figure 19.

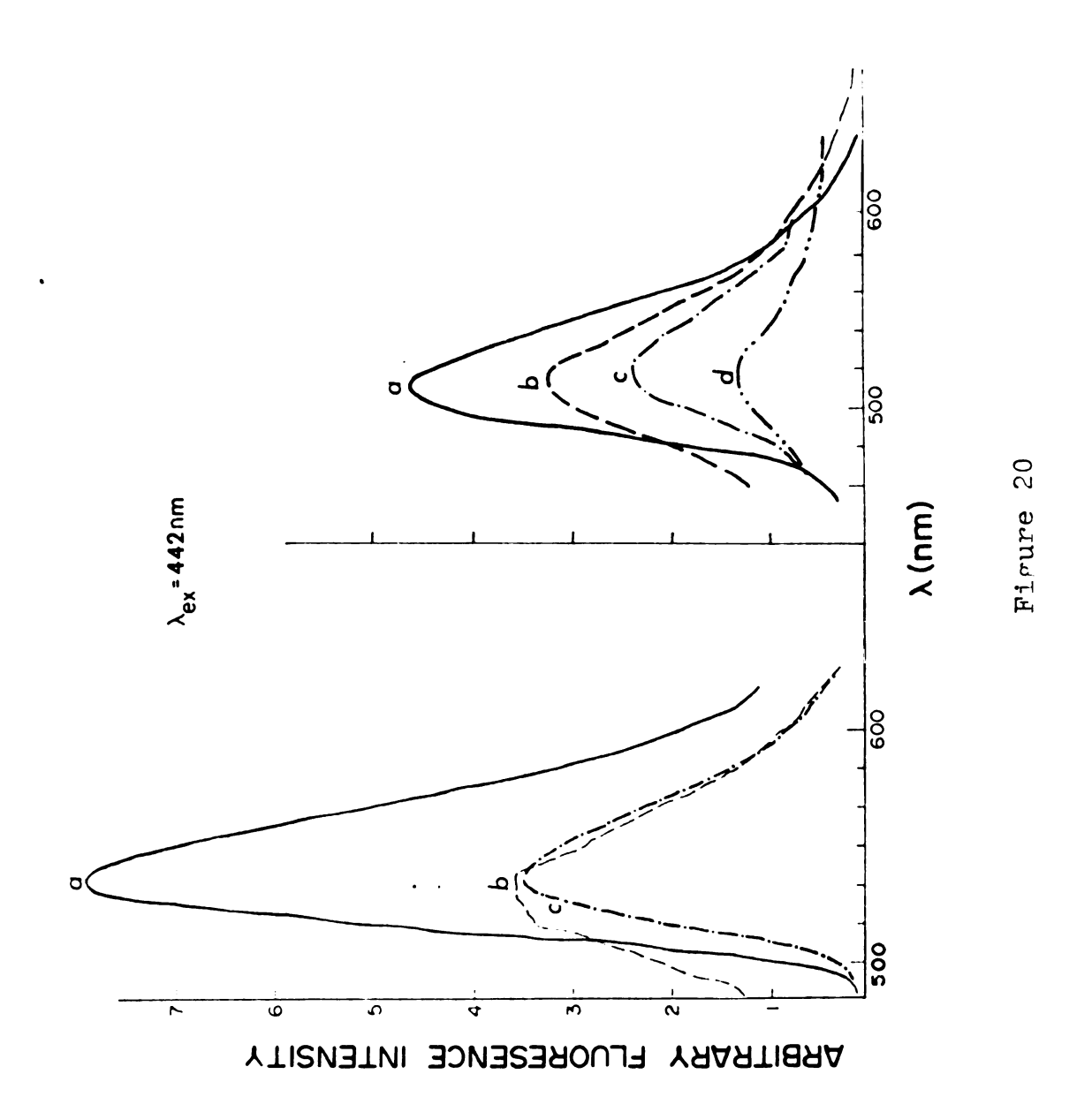
does it result from the binding of exogenous ligands to the oxidized flavin since this would serve to increase.  $\Delta E_{\rm m}^{\rm O}$  rather than diminish it. Further, there exists a correlation between the bleaching of flavin absorption and an alteration of its redox capabilities. The flavin moiety in the molecule apparently exists in an oxidized state irrespective of the absorption properties; however, its environment within the protein matrix is subject to changes which dictate its spectral and redox behavior. The mutability of the flavin's environment in  $c_{552}$  is even more graphically illustrated by the fluorescence properties of the protein.

# E. Fluorescence Results

The fluorescence properties of  $\underline{c}_{552}$  are totally dominated by the protein's flavin moiety and arise from the same isoalloxazine  $\pi \to \pi^*$  transitions seen in the absorption spectrum of the molecule. The position and shape of  $\underline{c}_{552}$  fluorescence emission strongly resemble those of free riboflavin. At room temperature, both display a featureless emission band with a maximum at 525 ± 3 nm. However, the fluorescence of  $\underline{c}_{552}$  is strongly quenched relative to both free riboflavin and glucose oxidase, a flavoprotein containing no heme groups. Figure 20 shows the fluorescence emission spectra of the oxidized form of

(-.-.) all in 0.1 M Tris buffer, pH 7.5. Right panel: Fluorescence emission intensities of: (a) 6  $\mu$ M  $c_{552}$  in 0.1 M MES, pH 6.1 one-half hour after addition of 2 mM KCN (---); (b) 6  $\mu$ M  $c_{552}$  in 0.1 M MES pH 6.1 (---); (c) 6  $\mu$ M  $c_{552}$  in 0.1 M Tris, pH 7.5 (-.--); (d) 6  $\mu$ M  $c_{552}$  in 0.1 M MES pH 6.1 one-half hour after addition of 2 mM Na<sub>2</sub>S<sub>2</sub>O<sub>3</sub> (-.--). The excitation KCN and  ${\rm Na_2S_2O_3}$  were prepared in 0.1 M MES and adjusted to pH 6.1 prior to wavelength was 442 nm for both sets of spectra. Concentrated solutions of Left panel: Fluorescence emission intensities of: (a) 0.1 µM riboflavin (---); (b) 2  $\mu M$  glucose oxidase (---) and (c) 6  $\mu M$  flavocytochrome  $c_{552}$ addition to the protein sample. 20.

Figure



those three molecules with actinic excitation at 442 nm. The position of the maxima (at  $\sim 445$  and 355 nm) in the excitation spectrum (shown in Figure 21) clearly demonstrates the participation of the flavin  $\pi \rightarrow \pi^*$  transitions in the fluorescence process. After heme reabsorption is taken into account, the fluorescence quantum efficiency of  $\underline{c}_{552}$  is approximately 1% that of free riboflavin and 33% that of glucose oxidase. This intensity is relatively invariant over the pH range 6.5 - 9.0, decreasing slightly to a minimum at pH  $\sim$ 7.5, but increasing rapidly as the high pH limit (pH √10.0) for heme:flavin subunit binding stability is reached. The extent of this quenching is quite striking in that free flavins are strongly fluorescent, some having quantum efficiencies as high as 58% The quenching of flavin fluorescence upon binding to peptides is well established. Flavin interactions with aromatic amino acid residues in both flavoproteins and model complexes have been shown to result in flavin fluorescence quantum yields as low as 3% (51). The quenching exhibited in  $\underline{c}_{552}$  results in a quantum efficiency of  $\sim 0.7\%$  that of riboflavin in the same solvent, or  $\sim 0.20\%$ absolute efficiency (based on the Kotaki et al. value of 26% for riboflavin quantum efficiency). This anomalously low fluorescence level can be attributed to two effects. The first, and more important of the two, is the quenching due to protein tyrosine residues. Sequencing and CD

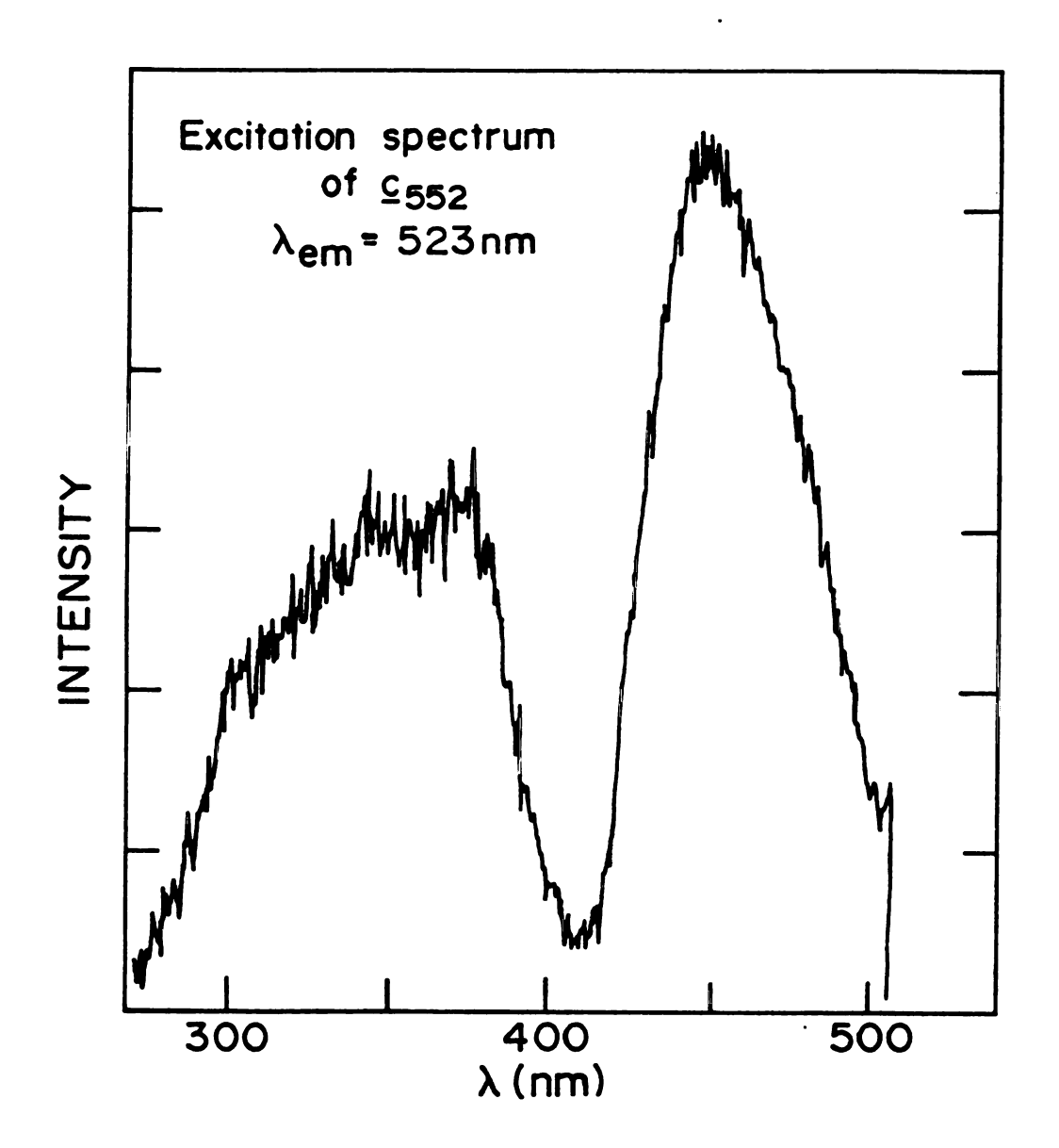


Figure 21. Fluorescence excitation spectrum of flavocytochrome  $\underline{c}_{552}$  in 0.1 M Tris, pH 7.5 with emission intensity monitored at 523 nm.

studies on  $\underline{c}_{552}$  digestive peptide fragments containing the covalently bound flavin by Kenney et al. (52) have established that the flavin is intimately associated with at least one and probably two tyrosine residues of the pro-The circular dichroism spectra of these peptide fragments were indicative of direct tyrosin-flavin interaction resembling the parallel stacking arrangement found in flavodoxin (53). They found that the fluorescence efficiency of the flavopeptides prepared by trypsin-chymotrypsin digestion to be 1% that of free riboflavin, only marginally larger than that of the holoprotein. Heme reabsorption is the second factor which influences the apparent fluorescence yield and produces a decrease of approximately 15% in apparent flavin fluorescence at 525 nm (based on a 5 mm pathlength in a 6 uM solution of  $\underline{c}_{552}$ ). These two considerations appear to be sufficient to explain the quenching of flavin fluorescence in  $\underline{\mathbf{c}}_{552}$  and obviate the necessity of evoking direct heme-flavin energy transfer of the Förster type (54).

The binding of exogenous ligands to  $\underline{c}_{552}$  has a pronounced effect on the protein's fluorescence properties. The initial results of CN and  $S_2O_3^-$  binding upon the visible absorption spectrum of  $\underline{c}_{552}$  are quite similar. Their effect on flavin fluorescence, however, is markedly different (See Figure 20). Shortly after cyanide binding the fluorescence yield of  $\underline{c}_{552}$  dramatically increases as

 $A_{475}/A_{525}$  is restored to its original value, whereas  $S_{2}O_{3}^{=}$  binding results in nearly complete quenching of flavin emission for an indefinite period of time.

Clearly, two different effects are experienced by the flavin for the two different ligands. The CN, in time, disrupts the delocalization of the flavin excited state in a manner that diminishes the effect of radiationless transfer (presumably to protein tyrosine residues). thiosulfate binding, on the other hand, contributes to the efficiency of such processes. One possible explanation for these effects is a difference in the mechanism of ligand-protein interaction between  $CN^-$  and  $S_2O_3^-$ . Thiosulfate behavior is probably due to direct adduct formation, as discussed earlier, which would be expected to increase quenching. The increase in flavin fluorescence subsequent to cyanide binding cannot be attributed to adduct formation and must reflect more pervasive protein-cyanide interactions. Manifestations of these interactions are seen in the effects of CN upon the absorption and EPR spectra of the hemes in  $c_{552}$  which indicate that CN significantly alters the protein environment of those redox centers. The fluorescence spectra of cyanide treated  $\underline{c}_{552}$  implies that these environmental changes extend to the flavin moiety as well.

#### CHAPTER 4

# MAGNETIC TECHNIQUES APPLIED TO FLAVOCYTOCHROME <u>c</u>552

The application of MCD and EPR spectroscopies to flavocytochrome  $\underline{c}_{552}$  provides probes of the heme magnetic environments in the protein. This is desirable for a number of reasons. Specific magnetic interactions between the two heme groups in  $c_{552}$  can be determined via MCD spectroscopy. MCD is a far more sensitive indicator of heme:heme interaction than simple CD since the latter technique relies on the global effects of the molecule's interaction with light whereas MCD is not directly influenced by the protein matrix. EPR spectroscopy allows discrimination between the two heme groups and thus serves as an effective complement to the absorption and resonance Raman investigations which yield information concerning the average properties of two hemes. Moreover, the data obtained with absorption, MCD and EPR spectroscopies are progressively more specific to the d-orbital electronic system of the heme iron. Absorption spectroscopy probes primarily the  $\pi$  electronic system of the heme porphyrin. The spin-orbit interactions between iron d- and porphyrin

π- electrons are evident as perturbations upon the general properties of the porphyrin absorption spectrum. These interactions are directly manifest in the MCD spectra of hemes and give rise to the character and intensities of the transitions observed. EPR spectra are characteristic of the energy level spacing of the iron d-orbitals which is dictated by the combined ligand field effects of the porphyrin macrocycle and the local protein environment of the heme.

## I. Magnetic Circular Dichroism

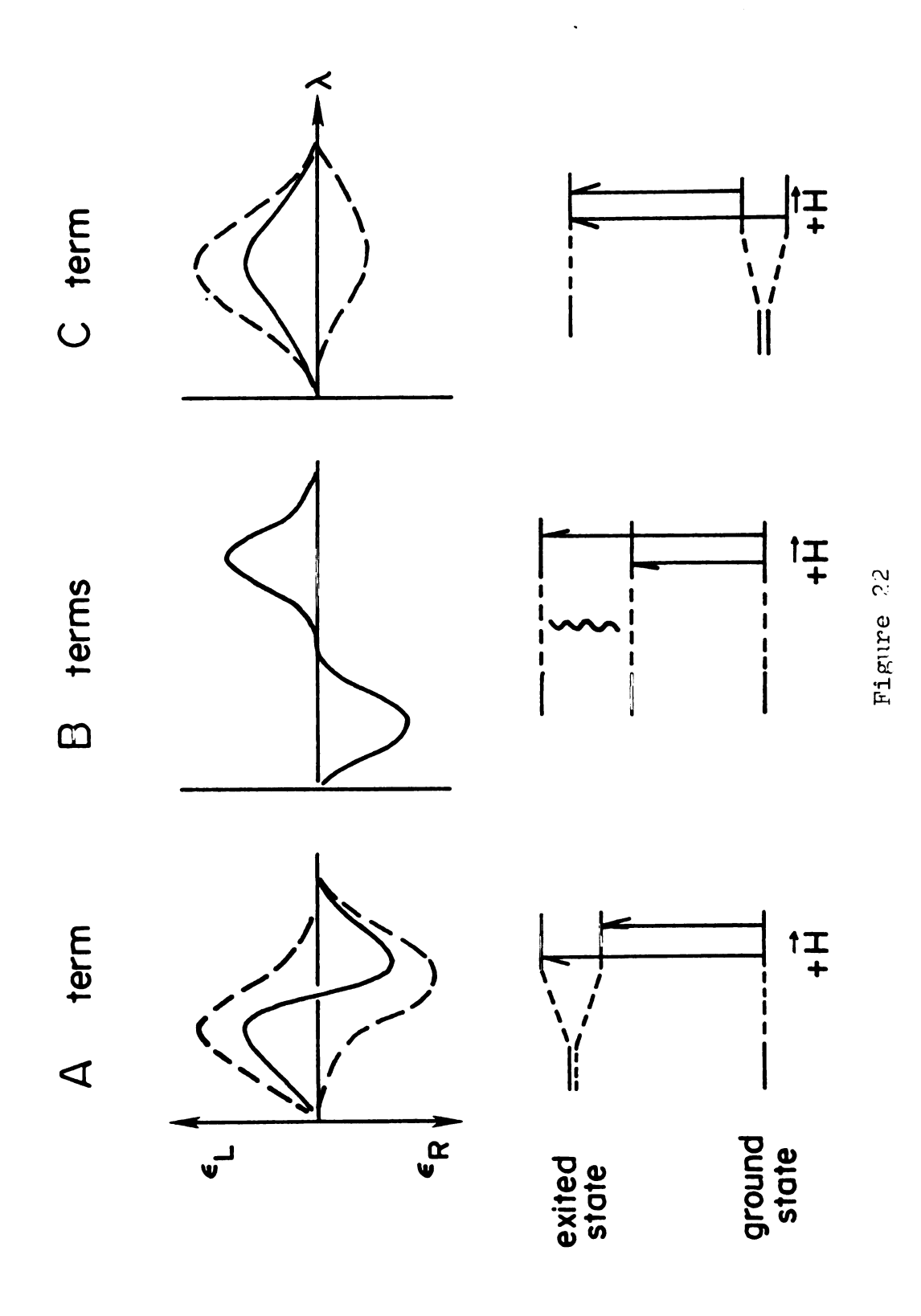
#### A. MCD Theory

The qualitative sensitivity of hemeprotein optical spectra to the spin state of the heme iron has been discussed in Chapter 3. MCD spectroscopy provides a relatively straightforward means of assessing the degree to which such iron spin state influences exist and of determining the extent of interaction between the two heme centers in  $c_{552}$ . The theory for the origin of magnetically induced dichroism in hemes, however, is still in its formative stages (55,56). In this application to  $c_{552}$  MCD is used primarily as an analytical tool and, as such, only a brief description of the basis for such effects is given here.

An MCD spectrum is simply a plot of the differential absorption of left circularly polarized and right circularly

polarized light by a molecule under the influence of a Zeeman field (measured in Tesla). It is conventionally plotted as  $\Delta \epsilon/\text{Tesla}$  (where  $\Delta \epsilon$  =  $\epsilon_R$  -  $\epsilon_L$ ) <u>vs</u> wavelength. There are three types of MCD effects arising from different origins. These are designated Faraday A, B, or C terms and each gives rise to a characteristic band shape in MCD spectra. A terms arise from transitions to orbitally degenerate excited states whose degeneracy has been split by an external magnetic field. Heme  $\pi-\pi^*$  transitions conform to this situation and, in the absence of spinorbit coupling, would be expected to yield  $\underline{A}$  terms in their MCD spectra. Their shape resembles the first derivative of the absorption band. Faraday C terms originate via transitions from Zeeman split ground states. Thus, they occur in paramagnetic materials and exhibit a difference in absorption intensities for left and right circularly polarized light due to the fact that there is a Boltzmann population distribution in the split ground states. population difference is exponentially proportional to 1/T and imparts a temperature dependence to C term intensity. C terms are thus expected in all hemes transitions that include the iron d-orbitals. Moreover, C-term behavior has been found to dominate the MCD of  $\pi-\pi^*$  transitions in a variety of heme proteins (57,58) and is indicative of iron spin-porphyrin orbit coupling. The bandshape of C-terms resembles that of the absorption peak. Faraday B terms

A schematic representation of the physical processes giving rise to MCD  $\underline{A}$ ,  $\underline{B}$ , and  $\underline{C}$  terms (lower) and the respective bandshapes of these terms (upper). In the upper panel dotted lines denote the absorption of left and right circularly polarized light while the solid trace is their difference (from Reference 59). Figure 22.



arise from a perturbative mixing of transitions by the applied magnetic field. They occur, to varying degrees, in all compounds but are generally weak in  $\underline{c}$ -type hemes (59).  $\underline{B}$  terms also resemble the bandshape of the absorption spectrum. A schematic representation of the processes giving rise to Faraday  $\underline{A}$ ,  $\underline{B}$ , and  $\underline{C}$  terms is shown in Figure 22.

#### B. MCD Results

The MCD spectra in the Soret region of oxidized, reduced and reduced +CO (at pH 7.45)  $\underline{c}_{552}$  are shown in Figure 23. The holoprotein displays MCD intensities and bandshapes that closely parallel those of other low spin mono-heme c proteins (60). The Soret MCD in oxidized  $\underline{c}_{552}$  is composed of mixed  $\underline{A}$  and  $\underline{C}$ -terms which produce a derivative shaped MCD curve with a zero crossover at 410 nm. studies (57) have established an empirical correlation between the intensity of the low energy trough and the percentage of the molecular population in a low spin con-The values obtained for  $\underline{c}_{552}$  indicate that figuration. it is exclusively low spin heme  $\underline{c}$  (i.e., no thermal equilibrium exists between low-spin and high-spin configurations). There is no indication of any magnetic coupling between the heme groups of oxidized  $\underline{c}_{552}$  seen in its MCD spectrum. Such coupling could be expected to result in a mixing of

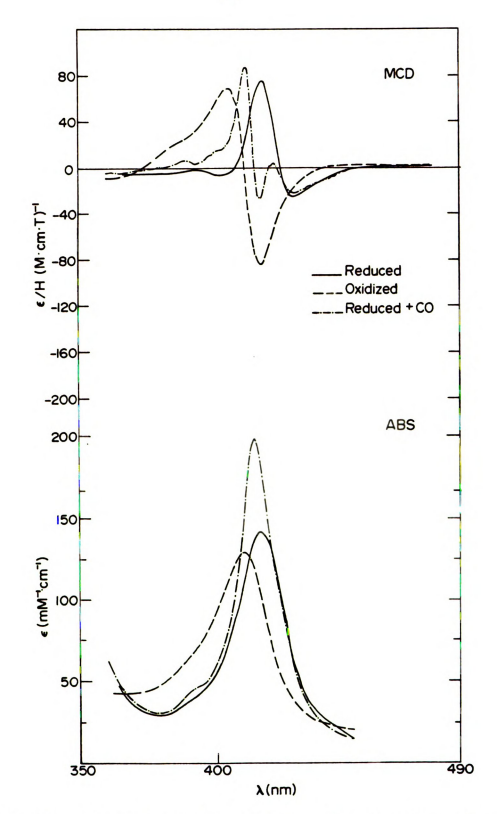


Figure 23. The MCD spectra of the reduced, oxidized, and reduced +CO forms of  $\underline{c}_{552}$  in 0.1 M Tris, pH 7.5 in the Soret region are pictured above the absorption spectra of those species.

states by magnetic dipole coupling or electron spin-spin The former effect would lead to a dramatic interactions. increase in B-term intensities introducing a severe asymmetry to the derivative MCD Soret bandshape whereas the latter would produce a quantum mechanical admixture of spins resulting in a departure from low spin behavior. The complete absence of any observable deviation from low spin mono-heme  $\underline{c}$  behavior in the MCD spectra of oxidized  $\underline{c}_{552}$ clearly rules out strong coupling such as would occur for a bridging ligand between hemes, and makes even weak direct heme-heme interaction unlikely. Upon reduction the MCD spectrum exhibits the characteristics of an S = 0 heme system. Heme spin-porphyrin orbit coupling is no longer a factor and the spectrum is composed of a mixture of A and  $\underline{B}$  terms peaking at 417 nm. The MCD behavior of  $\underline{c}_{552}$ in the visible region of  $\underline{c}_{552}$ 's absorption spectrum is qualitatively different from that in the Soret region while remaining entirely consistent with behavior exhibited by mono-heme c proteins (See Figure 24). In contrast to the Soret region, A terms form the dominant contribution to the visible MCD. The zero crossovers of these terms coincide with  $Q_{00}$  band (at 552 nm) and the various vibronic components of the  $Q_{01}$ . These are expected from porphyrin  $\pi-\pi^*$  transitions that are not spin-orbit coupled to the paramagnetic iron d-orbital system and are stronger for the reduced protein than the oxidized, reflecting the

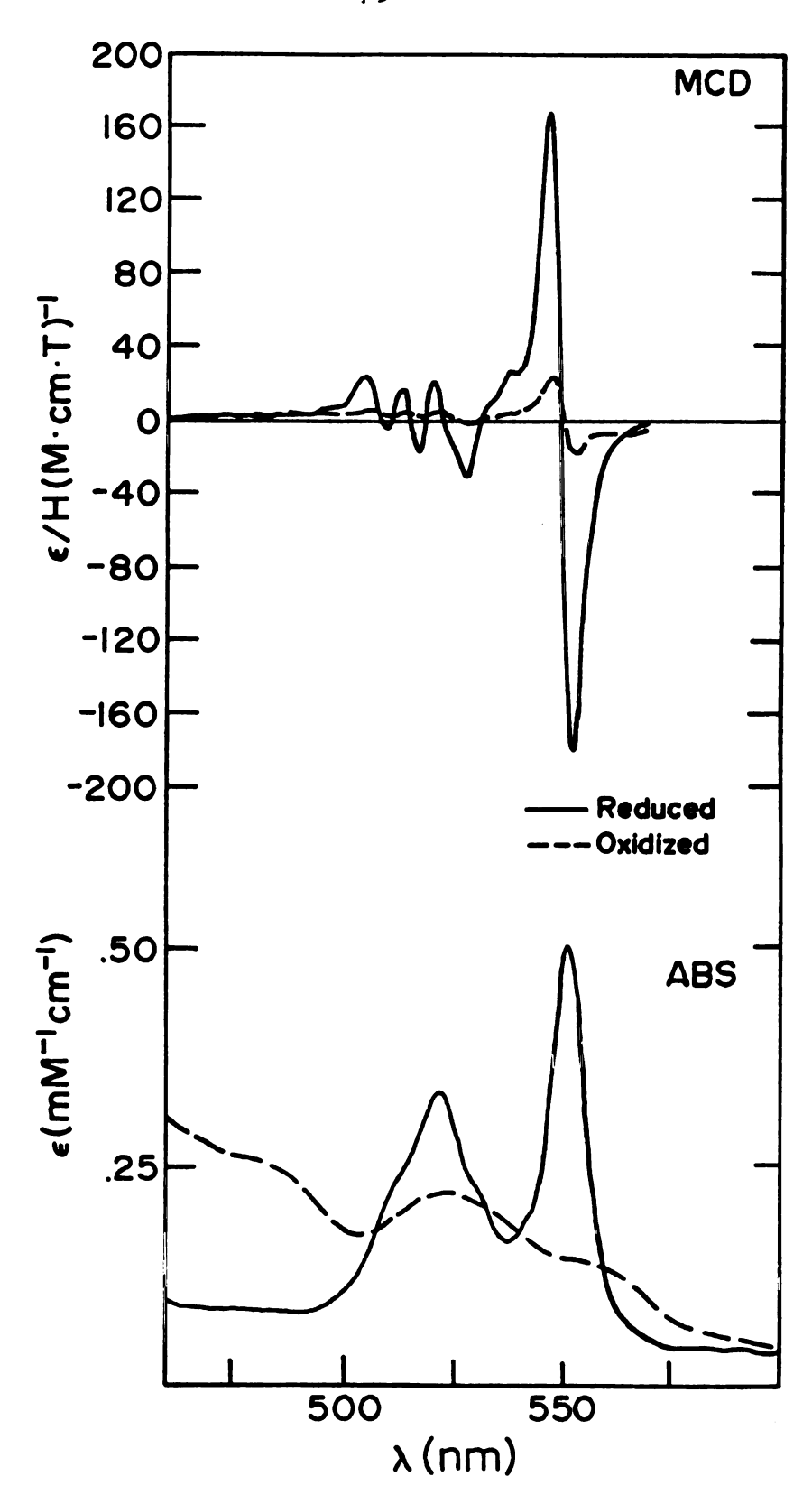


Figure 24. The MCD spectra of reduced and oxidized  $\underline{c}_{552}$  in 0.1 M Tris, pH 7.5 in the visible region are pictured above the absorption spectra of those species.

increase in  $Q_{00}$  absorption upon reduction. While the  $Q_{01}$  band of oxidized  $\underline{c}_{552}$  display a greater absorption intensity than the  $Q_{00}$  band, the MCD is much weaker. This arises from the fact that vibrational components of different symmetry can have  $\underline{A}$  terms of opposite sign and will tend to cancel each other.

A reductive titration of  $c_{552}$  under an Ar atmosphere (performed in the same manner as the absorption titration described earlier) resulted in a smooth transition between oxidized and reduced MCD bandshapes and provided no evidence of bi-phasic behavior with respect to reduction in either the Soret or visible regions. The hemes in  $c_{552}$  then, apparently either contribute equally to the observed MCD spectra or titrate with approximately the same redox potential or both.

The binding of CO to reduced  $\underline{c}_{552}$  produces a peak sharpening in the Soret MCD spectrum and a shift of the peak to 412 nm reflects the changes seen in its optical spectrum. However, the spectrum now clearly exhibits two components. It is composed of the "typical" combination of  $\underline{A}$  and  $\underline{B}$  terms seen with the unbound reduced protein with a broad peak and trough at 417 nm and 429 nm respectively, superimposed upon a sharper  $\underline{A}$  term with a zero crossover of 414 nm. The multicomponent nature of this spectrum strongly implies that CO binding occurs to only one of the two hemes in  $\underline{c}_{552}$  producing the sharp  $\underline{A}$ -term in the MCD spectrum

with the unbound heme producing the remaining MCD features. Moreover, the Soret MCD displays bi-phasic behavior during the course of a reductive titration under a CO atmosphere. This is shown in Figure 25. The growth of the sharp  $\underline{A}$  term preceds the gradual transition of the features arising from the "unbound" heme. This is to be expected since under a CO atmosphere, the reduction of the "bound" heme:

heme  $\underline{c}(\text{Fe}^{3+}) + e^{-} \not\equiv \text{heme } \underline{c}(\text{Fe}^{2+})$  is coupled to the chemical binding of CO

heme 
$$\underline{c}(Fe^{2+}) + CO \updownarrow heme \underline{c}(Fe^{2+}) \cdot CO$$

The effect of this coupling on the heme midpoint potential is

$$E_{M+CO}^{\circ} = E_{M-CO}^{\circ} + \frac{.059}{n} \log (1 + K_a[CO])$$

where  $K_a$  is the CO affinity constant for  $c_{552}$  previously measured (30) to be 7 x  $10^3$  M<sup>-1</sup>. The solubility of CO in cold buffer is 1.4 mM. Thus

$$E_{M+CO}^{O} = E_{M-CO}^{O} + 0.058/1$$

and a 58 mV difference in potential should exist between the binding and nonbinding hemes. This is sufficient to insure that nearly all of the electrons initially introduced

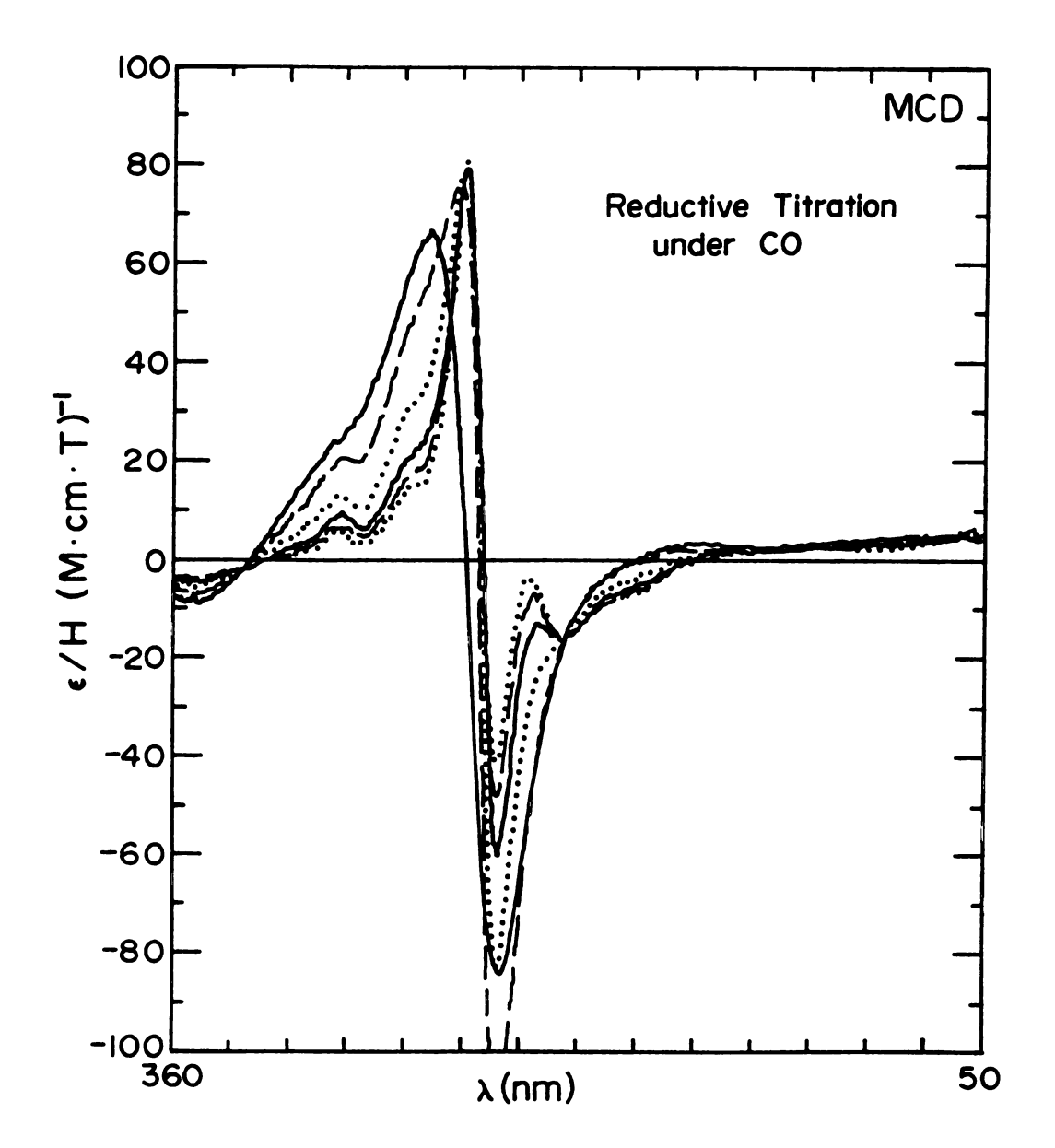


Figure 25. The MCD spectra obtained in the Soret region from a reductive titration of  $c_{552}$  under 6 psi of CO in 0.1 M Tris, pH 7.5. Traces of the peak from left to right (or trough from right to left) are: (——), 0% reduced (---), 10% reduced, (····), 25% reduced, (——), 35% reduced, (---), 45% reduced, (····), 100% reduced protein.

will produce the CO-bound species. These results clearly show that CO binding to  $\underline{c}_{552}$  occurs at only one heme and does not result in CO intercalation between hemes as has been suggested as an explanation for the molecule's CD spectra (20). A CO reductive titration performed at pH 11.1 showed no multicomponent features in the Soret MCD nor was any bi-phasic behavior with respect to heme reduction potential found. This suggests that at high pH a conformational change in  $\underline{c}_{552}$  occurs that allows CO access to both of the hemes.

The MCD spectra of oxidized  $c_{552}$  heme peptide and CNbound  $\underline{c}_{552}$  at pH 6.0 were also investigated. Neither was found to deviate substantially from the spectrum of the unbound oxidized holoprotein. Thus, the alteration or removal of the flavin prosthetic group has little or no effect on the MCD properties of the hemes in  $c_{552}$ . Flavins themselves exhibit quite weak MCD spectra. Because of the limited symmetry ( $C_s$ ) of the isoalloxazine moiety these spectra would be expected to be composed of B-terms. Recent studies (61) have determined that two weak ( $\Delta \varepsilon$ /Tesla 10) positive MCD transitions occur at ~370 nm and ~460 nm in The former transition would be completely obscured by the intense Soret heme MCD in  $c_{552}$ . Some evidence for the 460 nm transition can be found in a comparison of the oxidized heme peptide and holoprotein MCD spectra, but it is too weak to quantify with confidence.

## II. Electron Paramagnetic Resonance Spectroscopy

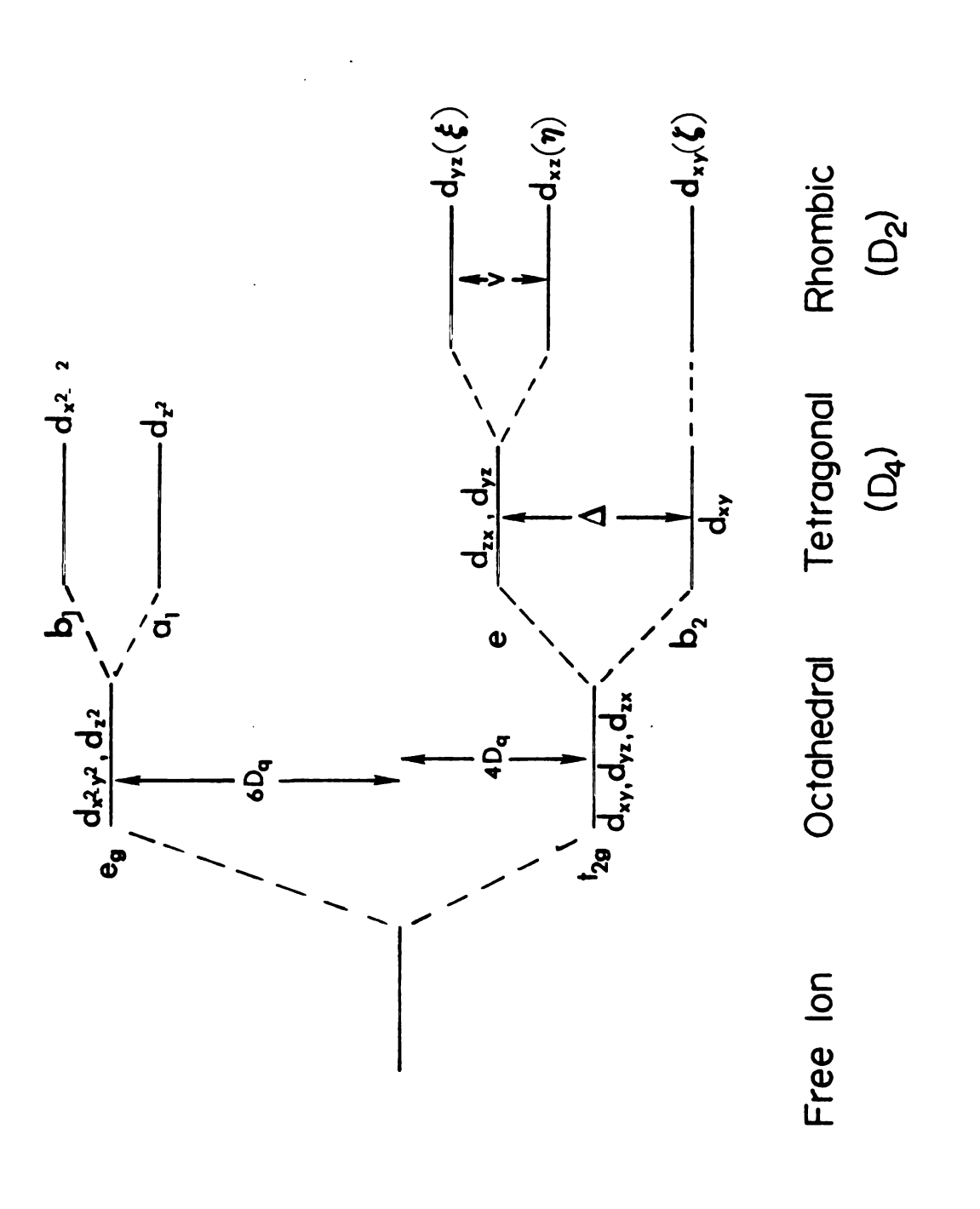
## A. Theory

EPR spectroscopy has been extensively applied to both high spin (S = 5/2) ferric hemoproteins (62). Although other valence states of iron are paramagnetic, the spectra of these states are extremely broad (presumably due to increased spin-orbit relaxation) and generally undetectable. Only a brief explanation of heme EPR specific to low spin heme  $\underline{c}$  will be given here. The model employed here was originated by Griffith (63). More detailed theoretical explanations can be found in the work of Kotani (64) or Weissbluth (65).

All low spin hemes display three distinct g-values which can be analyzed assuming that the cubic (octahedral) splitting,  $\Delta$ , is sufficient to force all five iron d electrons exclusively into the  $t_{2g}$  orbitals,  $\xi = d_{yz}$ ,  $\eta = d_{zx}$ , and  $\zeta = d_{xy}$  (See Figure 26). It is more convenient to deal with a single electron hole than five electrons, thus, a wavefunction for one of the six possible low spin configurations is:

$$|\xi^{-}\eta^{2}\zeta^{2}\rangle = |\xi^{+}\rangle$$
 (4.1)

where ± denotes unpaired electron spin and paired orbitals



The effect of successive symmetry reductions upon the energy levels of the iron d-orbitals. Figure 26.

(having no net orbital angular momentum) are supressed in the ket expression. Similar expressions are obtained for the other five configurations.

Since  $g_x \neq g_y \neq g_z$  for low spin hemes a reduction of field symmetry from octahedral to rhombic (D2) is anticipat-The energy level diagram for successive levels of dorbital symmetry reduction is shown in Figure 26. origin of the three distinct resonances displayed by lowspin hemes can be traced to this splitting of d-orbital degeneracy and subsequent spin-orbit interactions between these orbitals, as follows: Spin-orbit coupling will mix the orbitals resulting in three sets of Kramer's doublets corresponding to  $m_s$  values of  $\pm 1/2$ ,  $\pm 3/2$ , and  $\pm 5/2$ . are linear combinations of d-orbitals having nonvanishing spin-orbit matrix elements among themselves that are eigenfunctions of the total Hamiltonian including the coupling between spin  $(\overline{S})$  and orbital  $(\overline{\ell})$  angular momentum. spin-orbit operator  $\overline{l} \cdot \overline{s}$  is nonzero between  $(\xi^{\dagger}, \eta^{\dagger}, \zeta^{-})$ and  $(\xi^-, \eta^-, \zeta^+)$ , thus the resulting wavefunctions are:

$$|\psi^{+}\rangle = A\xi^{+} + iB\eta^{+} + C\zeta^{-}$$

$$|\psi^{-}\rangle = -A\xi^{-} + iB\eta^{-} + C\zeta^{+}$$
(4.2)

for the lowest lying ( $m_s = 1/2$ ) Kramer's doublet. Moreover, the eigenvalues of the orbital interaction with an external

magnetic field can be determined from the matrices of magnetic interaction operators  $l_z + 2s_z l_x + 2s_x$ , and  $l_y + 2s_y$  using  $\psi^+$  and  $\psi^-$  as the basis functions. This yields energy separation of:

$$\Delta E^{(z)} = E_{+}^{(z)} - E_{-}^{(z)} = 2\beta H_{z}[(A_{1} - B_{1})^{2} - C_{1}^{2}]$$

where

 $\beta$  = Bohr magnetron; and

Hz = applied magnetic field.

between  $|\psi^{\dagger}\rangle$  and  $|\psi^{-}\rangle$  and electron paramagnetic resonance will be observed at:

$$h\omega = g_z \beta H_z = \Delta E$$

Thus

$$g_z = 2 | (A - B)^2 - C^2 |$$

Similarly,

$$g_y = 2|(A - C)^2 - B^2|$$
 (4.3)

$$g_{x} = 2|(B + C)^{2} - A^{2}|$$

These relationships plus the normalization requirement

$$A^2 + B^2 + C^2 = 1$$

allows for determination of A, B, and C from experimental g values.

A, B, and C can be directly translated into the relative energies of the  $\xi$ ,  $\eta$ , and  $\zeta$  orbitals by determining the eigenvalues of the combined spin-orbit and crystal field Hamiltonian,

$$H_T = -\lambda \dot{\hat{l}} \cdot \dot{\hat{S}} + V_{\text{(crystal field)}}$$
.

 $\lambda$ - spin-orbit parameter = 435 cm<sup>-1</sup> for the free ferric ion

V = potential of the rhombic field.

Solving  $H\psi^{+} = E\psi^{+}$  one obtains

$$A(\varepsilon_{\xi} - E) - iB \cdot \frac{1}{2}\lambda + \frac{1}{2}\lambda C = 0$$

$$A \frac{1}{2}\lambda + iB(\varepsilon_{\eta} - E) - \frac{1}{2}\lambda C = 0$$

$$A \frac{\lambda}{2} + iB \frac{1}{2}\lambda + C(\varepsilon_{\zeta} - E) = 0$$

$$(4.4)$$

which can easily be solved for the energy differences

between  $\xi$ ,  $\eta$ , and  $\zeta$  given the values of A, B and C. These energy differences are conveniently expressed in multiples of  $\lambda$ , the spin-orbit coupling constant for the system. In the free ion  $\lambda = 435~\text{cm}^{-1}$  and is probably lower in complexes due to a ligand induced decrease in spin density at the metal (66).

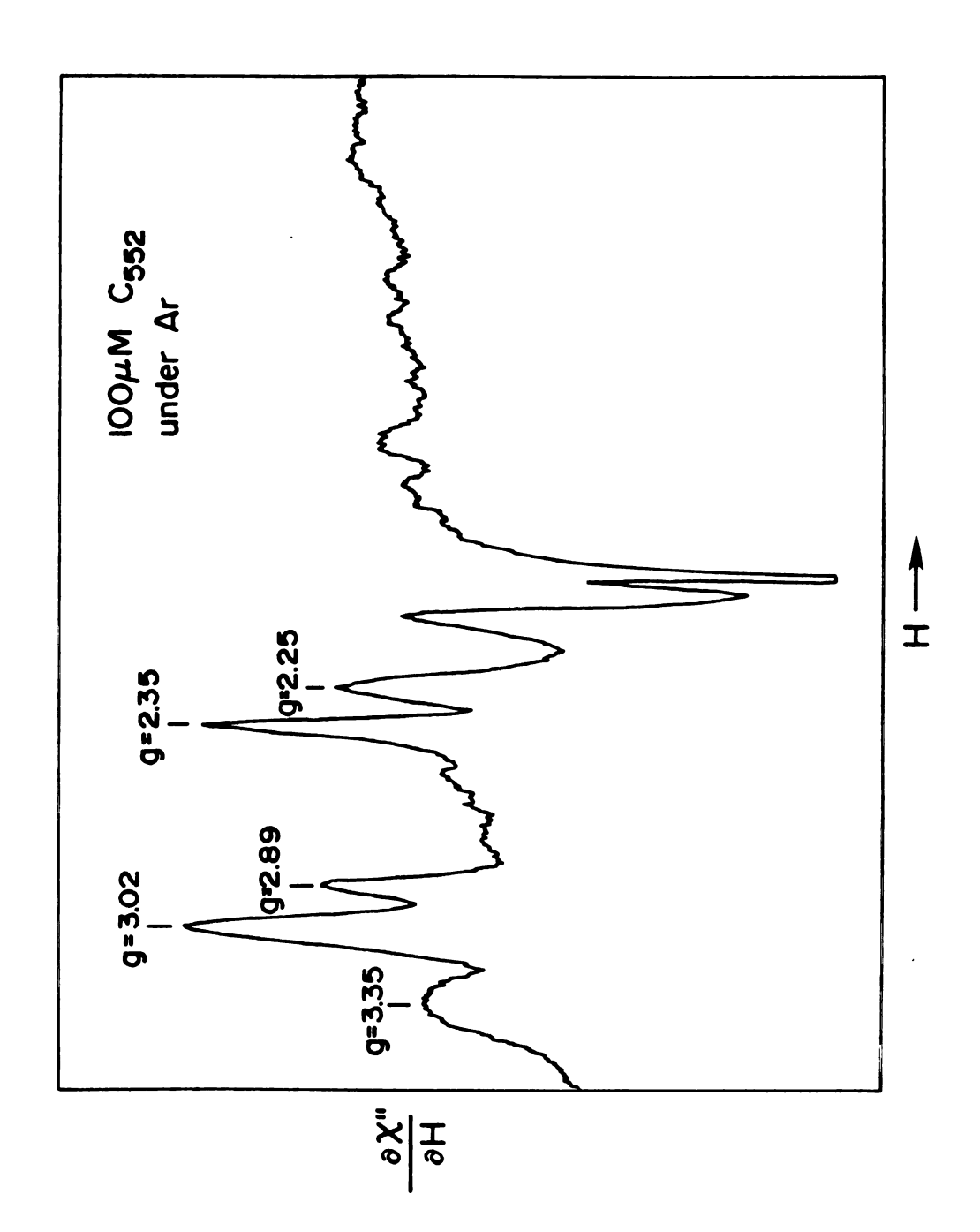
Two parameters useful for the quantification of the asymmetric ligand field experienced by the iron d-orbitals in hemes  $\underline{c}$  are the tetragonality  $(\Delta/\lambda)$  and rhombicity  $(V/\Delta)$  of the field. The tetragonality reflects the contribution of the large axial field component and thus depends largely on the charge donation ability of the z-ligands. The rhombicity, on the other hand, is a measure of the overall geometric distortion of the complex and is sensitive to distinctions between ligands in the x-y plane of the complex. A systematic classification of iron porphyrins based on their ligand field parameters was originated by Peisach and co-workers (67) and later extended to a variety of hemes  $\underline{c}$  (68,69).

## B. EPR Results

The EPR spectrum of oxidized  $\underline{c}_{552}$  is consistent with that expected of low spin heme  $\underline{c}$ , but is complicated by the fact that at least three separate heme ligand fields are evident in the holoprotein. A previous study of the

protein's EPR spectra by Strekas (33) revealed three sets of resonances whose respective low field components ( $g_z$ ) occur at g=3.35, g=3.00 and g=2.89. He interpreted the pH dependence of these signals as a pH dependent interconversion of the signals associated with  $g_z=3.35$  and  $g_z=2.89$  hemes with the  $g_z=2.89$  form being favored at high pH, while noting that  $g_z=3.00$  signal displayed no pH dependence. Cyanide binding was found by Strekas to reduce the intensity of the resonances associated with the  $g_z=2.89$  heme and he suggested that this implied heme/flavin interaction.

The EPR spectra of  $c_{552}$  obtained in our laboratory generally confirm those obtained by Strekas. Figure 27 shows the EPR spectrum of ferric  $c_{552}$  at pH 7.5 and 7°K. Three distinct sets of EPR resonances are apparent, one with  $g_z = 2.89$ ,  $g_y = 2.35$  and a very weak  $g_x = 1.55$ , a second with  $g_z = 3.02$ ,  $g_y = 2.25$  and a very weak  $g_x = 1.36$ , and the third with  $g_z = 3.35$  and both  $g_x$  and  $g_y$  too broad to detect. With these g- values it is possible to assign the heme axial ligands for each set of resonances. This can be accomplished by correlating either the  $g_z$  values or the ligand field parameters of  $c_{552}$  to those of other  $c_z$ -type hemes with known axial ligands. Actually, these two methods are largely similar since both the value of  $g_z$  and the tetragonal field are directly proportional to the electron donating ability of the axial ligand. The



An EPR spectrum of 100  $\mu M$  oxidized  $\underline{c}_{552}$  in 0.1 M Tris, pH 7.5 obtained at 6.2°K with 2 mW of 9.132 GHz radiation and 10 G modulation. Figure 27.

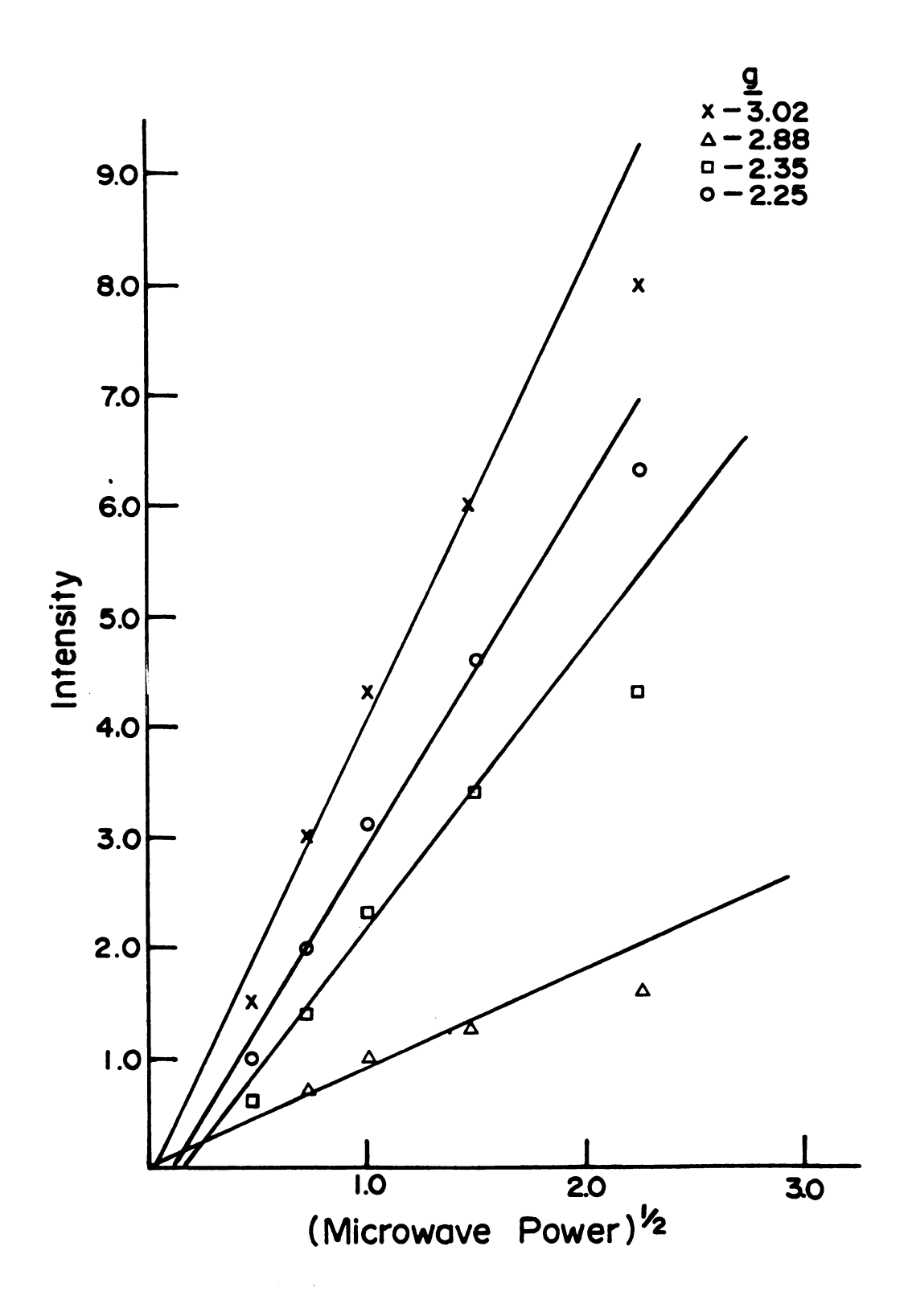
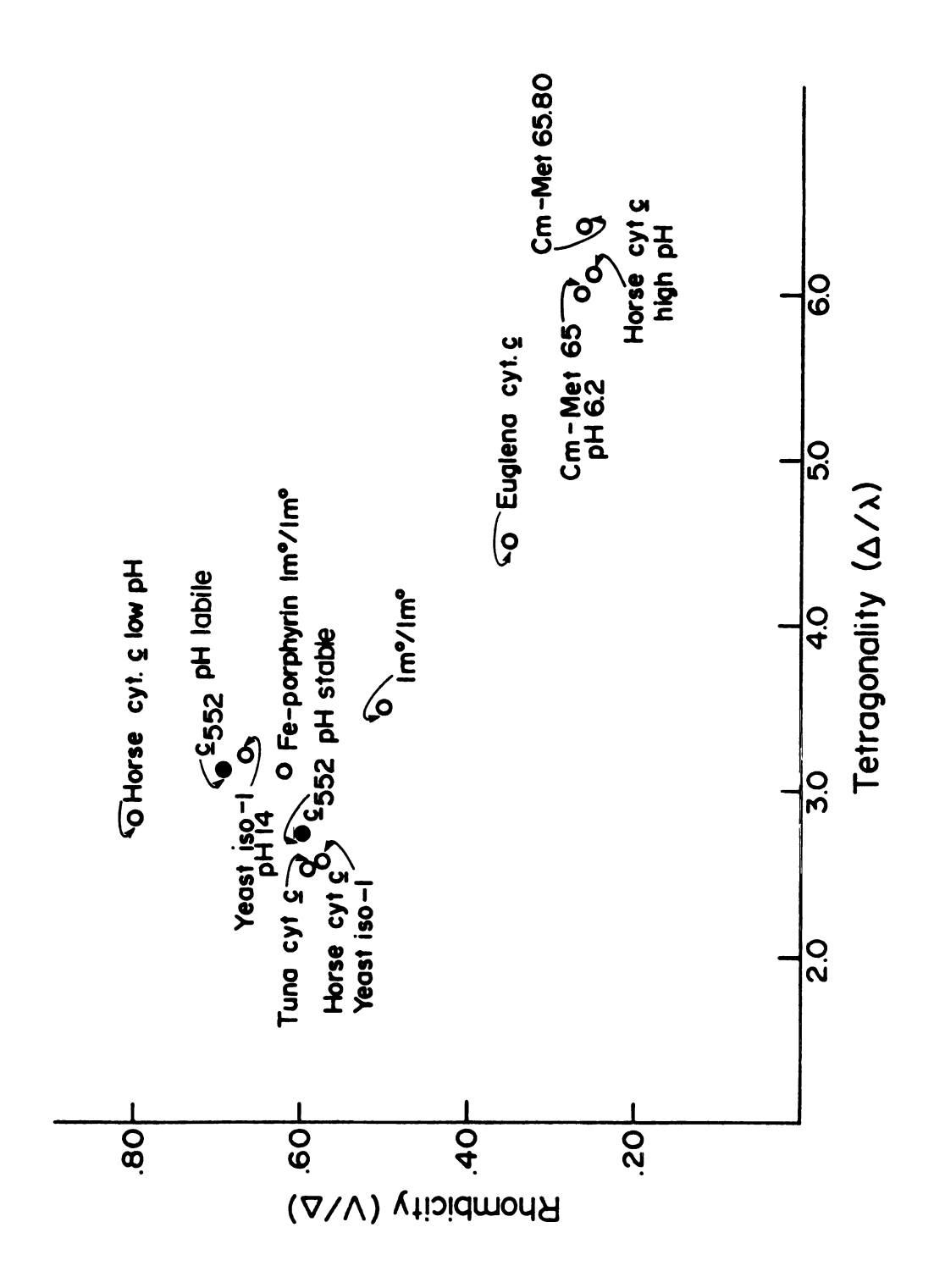


Figure 28. Microwave power saturation curve for the  $g_z = 2.88$  ( $\Delta$ ),  $g_z = 3.02$  (x),  $g_y = 2.35$  ( $\Box$ ) and  $g_y = 2.25$  (o) resonances of  $\underline{c}_{552}$  under the same conditions as Figure 27.

correlation of  $\underline{c}_{552}$   $g_z$ -values and ligand field parameters with those of other hemes c is displayed in Figure 29. Note that a general correlation between tetragonality,  $g_z$ values and the electron donating power of axial ligands exists for the species shown in the order amine > imidazole > imidazole<sup>O</sup> > methionine. The g value of the pH stable heme falls within the range expected of either bis-imidazole or imidazole /methionine ligation. The low value of its tetragonal field, however, makes the latter axial ligation scheme more likely. The  $\mathbf{g}_{\mathbf{z}}\text{-values}$  of the high and low pH forms of the pH-labile heme are those expected from amine/imidazole and bis-imidazole oo respectively, although the rhombicity of the bis-imidazole form is somewhat higher than that of heme c models (69). This is not unexpected. In fact, in the limit where all six nitrogens coordinated to the heme iron (four from the porphyrin and one from each histidine imidazole) donate electrons equally, a purely rhombic field ( $V/\Delta = .69$ ) should result. In the absence of the solvent effects found in the bis-imidazole heme  $\underline{\mathbf{c}}$  models such a situation may obtain for the pH-labile heme in  $c_{552}$ . Thus, it can be seen that the EPR spectrum of  $c_{552}$  is consistent with an axial ligation scheme of involving one pH-stable heme with methionine/histidine ligands and one pH-labile heme favoring lysine/histidine ligands at low pH and histidine/ histidine at high pH. Table 3 summarizes the g-values,



A plot of rhombicity  $\frac{vs}{vs}$ , tetrogonality for the hemes in flavocytochrome  $\frac{c}{c}_{552}$  ( $\oplus$ ) and various monoheme  $\frac{c}{c}_{000}$  proteins (0). Figure 29.

Table 3. Ligand Field Parameters for Various Hemes  $\underline{\mathbf{c}}$ .

Species	$g_{\mathbf{x}}$	gy	gz	Δ/λ	V/D	Ligands	Ref.
<u>c</u> 552							
heme 1	3.02	2.25	1.4	2.84	•57	Met/His°	
heme 2	2.89	2.35	1.6	3.10	.68	His°/His°	
	3.35					Lys/His°	
horse heart cytochrome c							
pH 7.0	3.06	2.25	1.3	2.56	.58	Met/His°	68
pH 11.0	3.37	2.10		6.2	.25	Met/Lys	69
pH 2.5	2.90	2.4	1.5	2.9	.80	His°/His°	69
CM-Met 65,80	3.40	2.08		6.4	.27	His°/Lys	69
bis-imidazole heme <u>c</u>	2.92	2.30	1.5	3.12	.62	Im°/Im°	68
yeast iso-1 (pH 14) cytochrome <u>c</u>	2.71	2.26	1.8	3.22	.67	His°/His°	69
Euglena cytochrome <u>c</u>	3.20	2.05	1.4	4.5	•35	Met/His-	69

CM-Met = carboxymethylated.

Met-methionine, Hiso-neutral histidine, Hiso-deprotonated histidine, Lys-lysine, Imo-neutral imidazole.

ligand field parameters and axial ligand assignments for the hemes shown in Figure 29.

# C. Reductive Titration

The ability of EPR spectroscopy to distinguish between the two hemes in  $\underline{c}_{552}$  allows the determination of their relative redox potentials. Since ferrous heme is diamagnetic (S = 0), it is possible to monitor the extent of reduction of a given heme by measuring the decay of its EPR signal intensity. Thus, by plotting the decrease in signal at g =  $3.02 \text{ } \underline{\text{vs}}$  the "average" extent of heme reduction obtained via absorption spectroscopy, comparison of the relative redox potentials of the two hemes in  $\underline{c}_{552}$  could be made.

Simultaneous determination of the absorption and EPR spectra of degassed  $c_{552}$  under an Ar atmosphere during a reductive titration was accomplished by modifying the anaerobic titrator shown in Chapter 3 to include a side-arm/value system for the removal of an EPR sample (See Figure 30). An EPR sample tube could be attached to the sidearm and evacuated using the two-way stopcock (#1). The titrator was turned so that the sidearm nipple was covered with sample and the desired amount ( $\sim 0.3 \text{ ml}$ ) of sample was drawn into the sidearm which was calibrated to determine sample volume to the nearest 0.05 ml. The titrator was then turned so that the nipple was no longer covered

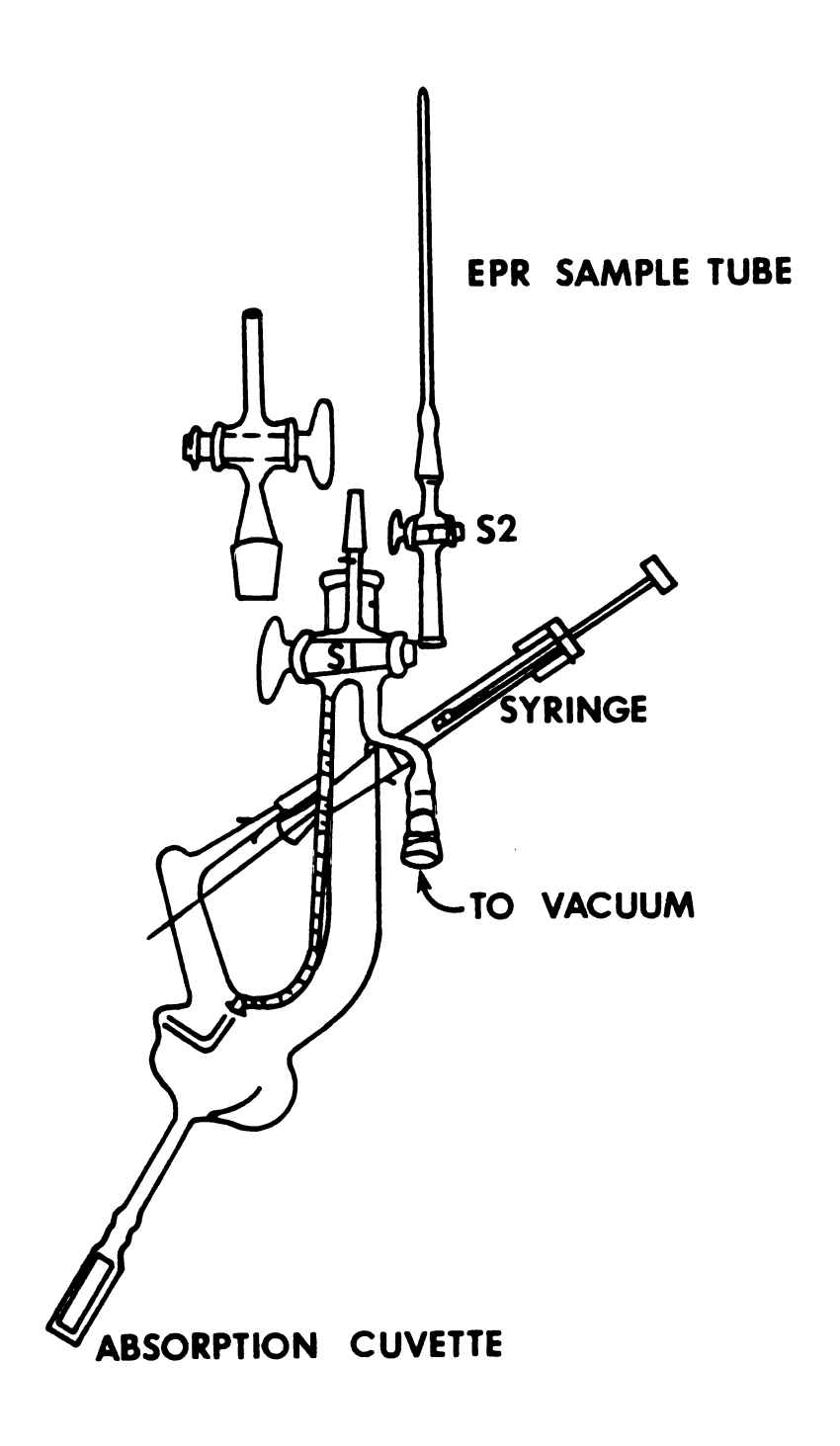
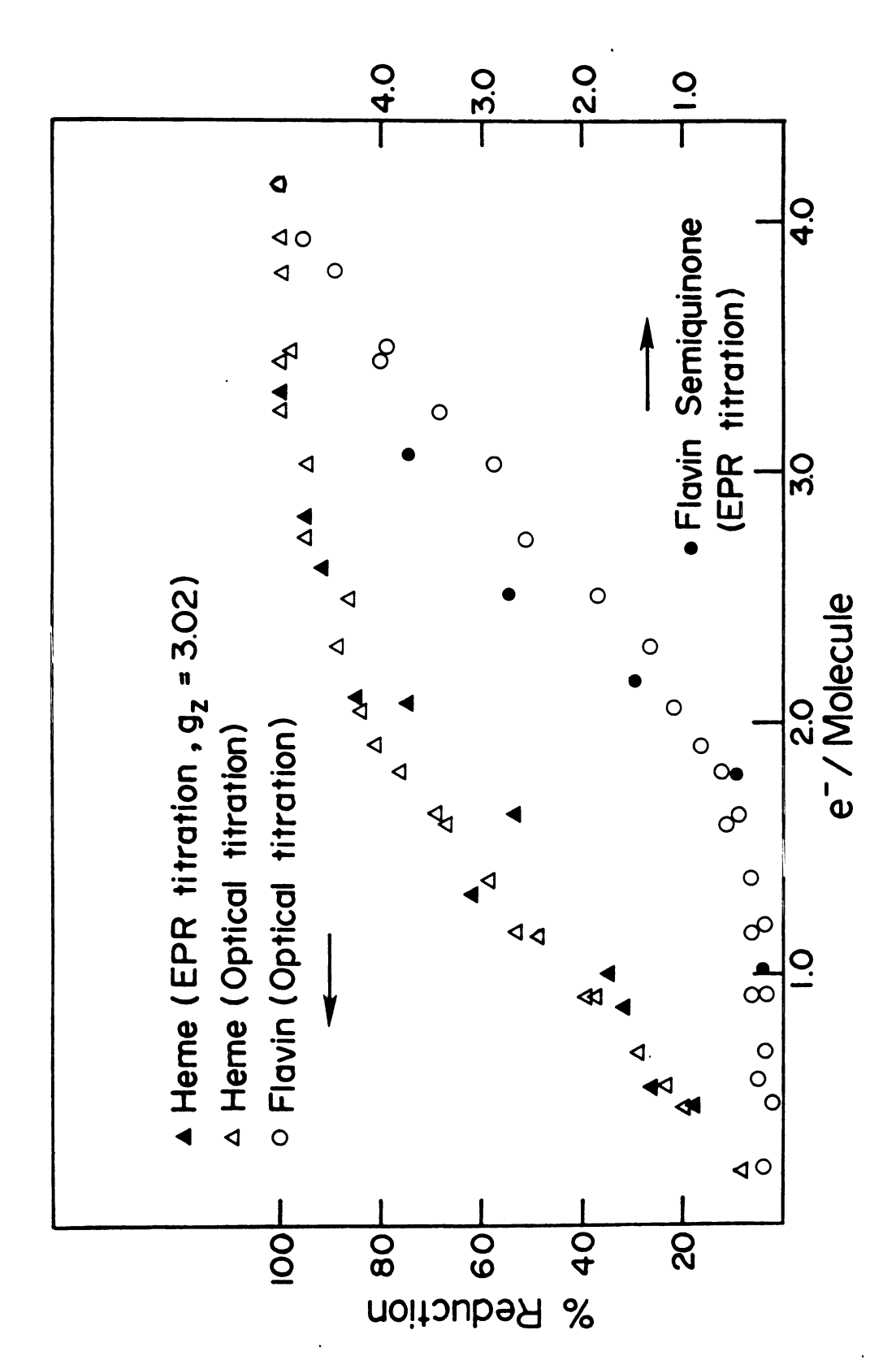


Figure 30. The EPR/Absorption anaerobic titrator.

with sample and the sample now in the sidearm was transferred to the EPR sample cell by opening both stopcocks 1 and 2. The now-filled EPR sample tube was then anaerobically removed (by closing both stopcocks) and frozen in liquid nitrogen. Stopcock 2 could now be removed from the sample tube, more reductant added, and the process repeated for the next point. A sodium dithionite solution whose concentration was previously determined as in the titrations described in Chapter 3 was used as the reductant in these titrations.

A comparison (Shown in Figure 31) of the decay of g=3.02~vs extent of total heme reduction reveals that the methionine/histidine ligated heme in  $c_{552}$  has approximately the same reduction potential as the protein's pH-labile heme. This precludes the possibility of sequential reduction of the two hemes and, in light of the previous potentiometric titrations (30), establishes both hemes as having  $E_m^0 \approx 0$  mV. This is an anomalously low potential, particularly for the heme with methionine/histidine ligation (horse heart cytochrome c which also has methionine/histidine ligands has  $c_m^0 \approx 0$  mV.

The nature of heme axial ligands has been postulated to be the dominant effect upon heme redox potential (70). All other factors being equal, the methionine/histidine ligated heme would be expected to have a much higher redox potential than either form of the pH-labile heme due to



The decay of the g = 3.02 resonance vs. electrons per molecule added during the course of a reductive titration of ^100  $\mu M$   $c_{552}$  in 0.1 M Tris, pH 7.5 with the same instrumental parameters as Figure 27. Figure 31.

the greater  $\pi$ -acceptor power of methionine over either histidine or lysine. Investigations of well characterized heme c analogs suggest that thioether/imidazole ligation is responsible for an 160 mV shift in iron redox potential relative to bis-imidazole ligation, independent of environment (71). The same trend is apparent in small heme proteins. Monoheme c proteins with methionine/histidine ligands have redox potentials of between -60 and +400 mV whereas those with histidine/histidine ligands are generally much lower (-200 to -500 mV) in potential (72). This is obviously not the case for  $c_{552}$ . Both hemes exhibit approximately the same redox potential despite the disparity in their axial ligands. There are other exceptions to the general trend in the dependence of heme potential upon axial ligand configuration, most notably spinach cytochrome f which has lysine and histidine as axial ligands but possesses a midpoint potential of +420 mV (73). This indicates that factors other than axial ligation figure strongly in the determination of heme redox potential. One such influence is the hydrophobicity of the medium surrounding the heme. Theoretical models (74) suggest that small differences in the volume and dielectric constant of the immediate heme environment can result in changes of hundreds of millivolts As the heme enin the apparent potential of the heme. vironment becomes more hydrophobic, the ferrous heme is more stabilized relative to the more highly charged ferric

state and the midpoint potential of the heme would be expected to rise. Experimentally, the potential exhibited by hemes in a homologous series of bacterial monoheme <u>c</u> proteins has been linked to the degree of hydrophobicity of the heme protein environment by Pettigrew <u>et al</u>. (75). This effect is independent of axial ligand effects.

The difference in potential between the pH stable heme in  $\underline{c}_{552}$  and horse heart cytochrome  $\underline{c}$  indicates that the former may be in a distinctly more hydrophilic environment than the latter. Moreover, in order for the pH-stable (methionine/histidine) and pH-labile (histidine/histidine or lysine/histidine) hemes of  $\underline{c}_{552}$  to have the same potential they likely exist in different protein environments, with the environment of the pH-labile heme being more hydrophobic.

## D. <u>Flavin Semiquinone</u>

Flavins can exhibit a number of oxidation states during the course of a reductive titration depending upon whether the reduction proceeds through a one- or two-electron step. Addition of one electron to the flavin results in the creation of a paramagnetic semiquinone free radical (76). The unpaired electron in the radical is extensively delocalized and appears in an EPR spectrum as a resonance at  $g \approx 2.00$ . Several flavoproteins, most notably amino acid oxidase (77) and flavocytochrome  $b_2$  (78), have been

shown to exhibit semiquinone behavior upon partial reduction. The simultaneous addition of two electrons to the flavin results in a diamagnetic species that is EPR silent.

Samples of  $\underline{c}_{552}$  obtained during a reductive titration under an Ar atmosphere were examined for the existence of flavin semiquinone. EPR spectra were obtained at ∿130°K since EPR signals from free radical systems saturate too easily to be observed at liquid helium temperatures. Recording a spectrum at the higher temperature has the added advantage of increasing the dipolar broadening of the heme systems to the point where the heme resonances are undetectable and no longer complicate the spectrum. A weak signal at g = 2.01 (See Figure 32) was observed in partially reduced  $c_{552}$ . This signal increased in intensity as the extent of reduction reached 3e molecule and thus is consistent with the relative redox potentials between flavin and heme obtained via absorption spectroscopy. However, the magnitude of the signal was quite small and could account for no more than 5% of the total flavin content of the sample. This indicates that the major pathway for flavin reduction does not involve the semiquinone form of this species and implicates a concerted two-electron transfer as the vehicle for flavin oxidation and reduction in the protein. The EPR spectrum of the flavin free radical can also be used to determine the ionization state of the semiquinone species formed.

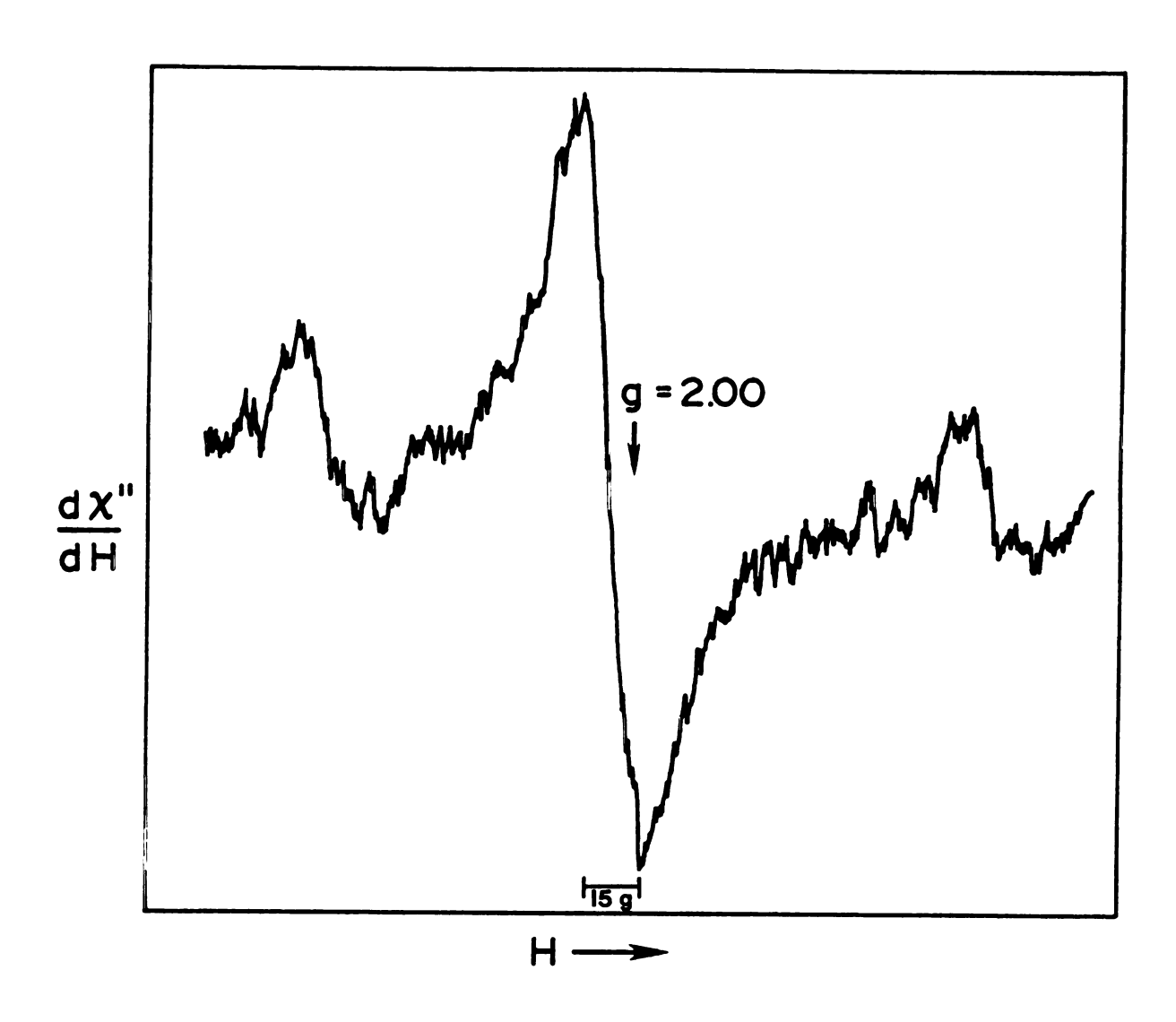


Figure 32. Flavin semiquinone signal obtained from  $\sim \! 100~\mu M$   $c_{552}$  in 0.1 M Tris, pH 7.5 at 143°K after the introduction of 3 electrons per molecule. Microwave power was .5 mW at 9.122 GHz with 5 G modulation.

According to Palmer et al. (78) the bandwidth of the neutral radical is 19G while the anionic semiquinone has a bandwidth of 15G. The bandwidth of the flavocytochrome  $\underline{c}_{552}$  radical is 14±2 G and thus it can be assumed to be anionic.

It is interesting to note that during the reduction of flavocytochrome  $\underline{b}_2$ , which contains only one heme per flavin, an initial burst of fully reduced flavin is followed by the accumulation of up to 50% of the flavin as semiquinone (18). This has been interpreted as resulting from the rapid distribution of one electron from reduced flavin to the heme followed by a slower addition of a third electron to the flavin semiquinone. For flavocytochrome  $\underline{c}_{552}$  it is possible that the two hemes in the protein act cooperatively to allow the simultaneous transfer of two electrons from the reduced flavin, thus obviating the necessity of the flavin semiquinone in the reduction mechanism of that molecule.

## E. Exogenous Ligand Binding

EPR spectroscopy also allows for the unambiguous assignment of the CO binding site in  $\underline{c}_{552}$ . At neutral pH absorption and MCD spectroscopy indicate that only one heme in  $\underline{c}_{552}$  binds CO. Since CO-binding serves to increase the apparent heme redox potential by  $\sim 58$  mV, an EPR reductive titration performed under a CO atmosphere can easily identify the CO-binding heme. Figure 33

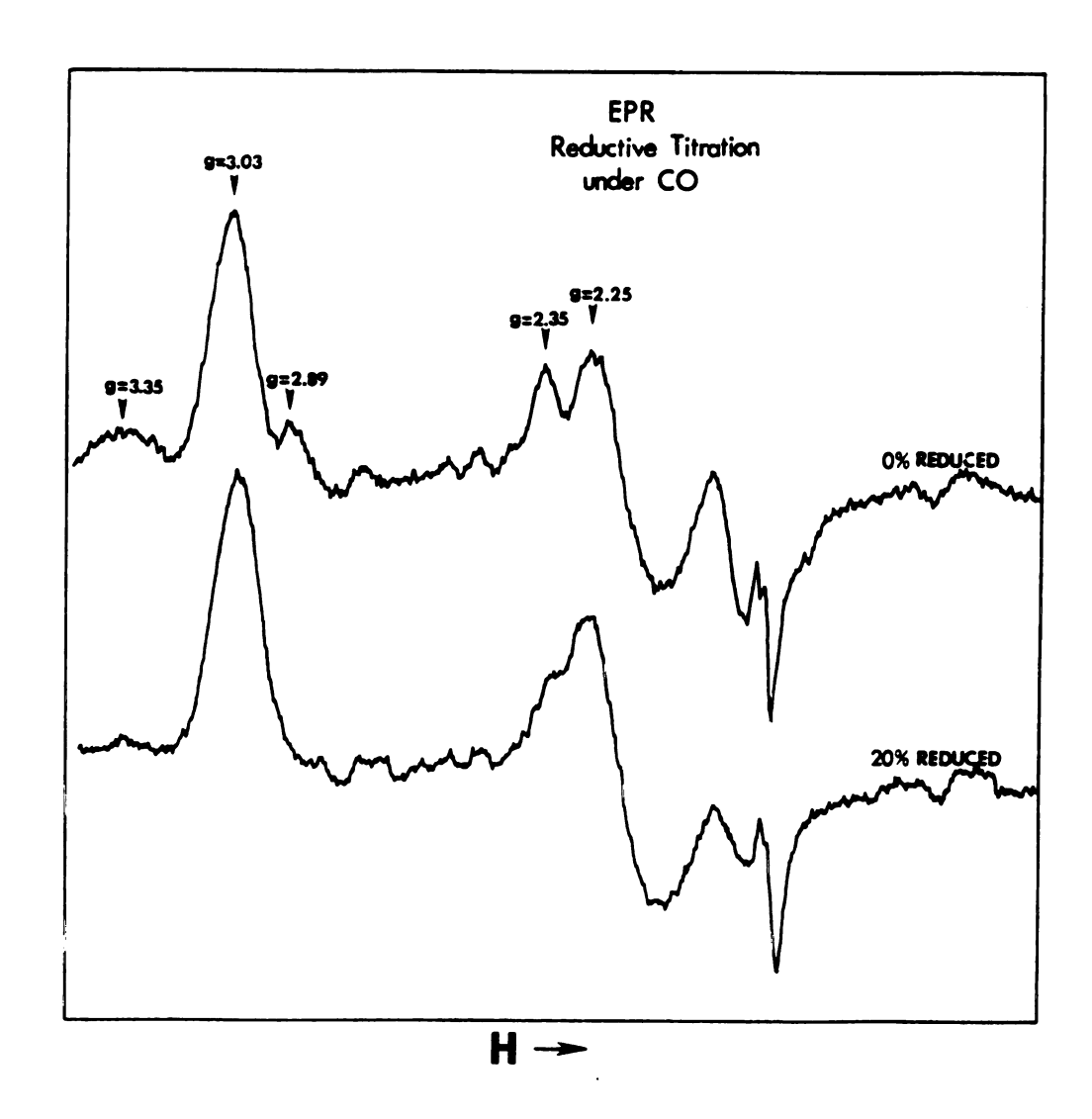


Figure 33. EPR spectra obtained during a reductive titration of  $\sim 100~\mu M \ c_{552}$  under 6 psi of carbon monoxide. Temperature and instrumental parameters are the same as Figure 27.

illustrates the effect of CO-binding on the  $\underline{c}_{552}$  EPR spectrum. Clearly, the pH-labile heme now titrates with a higher potential than the pH-stable heme as the resonance at  $g_z$  = 2.89 is almost completely removed by the addition of 0.8 e-/molecule. CO binding in  $\underline{c}_{552}$  thus necessarily involves a ligand displacement at the pH-labile heme and further substantiates the mutability of its protein environment. The pH-stable heme, on the other hand, does not undergo ligand displacement (<u>i.e.</u>, bind CO) until the protein has begun to denature at high pH (pH = 11.0).

As indicated in the absorption studies discussed earlier, the effects of CN are more pervasive than simple flavin-CN adduct formation. Strekas interpreted the reduction of the  $g_z = 2.89$  resonance in the  $c_{552}$  EPR spectrum that results from the addition of CN to the sample as arising from an alteration of the pH-labile heme's environment. However, he found no effect upon  $c_{203} = c_{303} = c_{3$ 

In an attempt to elucidate the effects of CN upon the hemes in  $c_{552}$ , CN was added to a sample of low flavin:heme  $c_{552}$  at neutral pH. Under these conditions, no effect on the absorbance at 475 nm was noted. Nonetheless, the EPR spectrum taken from a sample frozen 1/2 hour after CN addition displayed the bleaching of the

resonances at g = 2.89 and 2.35 seen by Strekas. For a sample frozen 1.2 hours after CN addition, the EPR spectrum begins to display alteration of the g = 3.35 and the g = 3.02, 2.25 resonances as well. Figure 34 displays the EPR spectra of a sample that had been treated with 5 mM Initially cyanide affects only by the pH-labile It is apparent that histidine/histidine ligation at the pH-labile heme is significantly disrupted independent of flavin CN adduct formation. The incorporation of CN as a heme axial ligand results in a broad  $g_z \approx 3.45$ resonance accompanied by a marked decrease in rhombicity in myoglobin derivatives (79). Some alteration of the g = 3.5 region is seen in the  $c_{552}$  CN spectra, but it is too broad to quantify. On a longer time scale disruption of the methione/histidine axial ligation of the pH-stable heme is evidenced by a decrease in intensity of both its  $g_z$  = 3.02 and  $g_v$  = 2.25 components. This parallels the observed decrease in the 695 nm optical absorption band as a function of CN binding.

chrome  $\underline{c}$  has been characterized by Dyer  $\underline{et}$  al. (80) who found that  $CN^-$  bound in a ligand displacement reaction to the native protein and a variety of cytochrome  $\underline{c}$  derivatives. Their mechanism postulated a protein conformation step which opened the heme crevice as the rate determining step. Activation energies as large as 17 kcal and

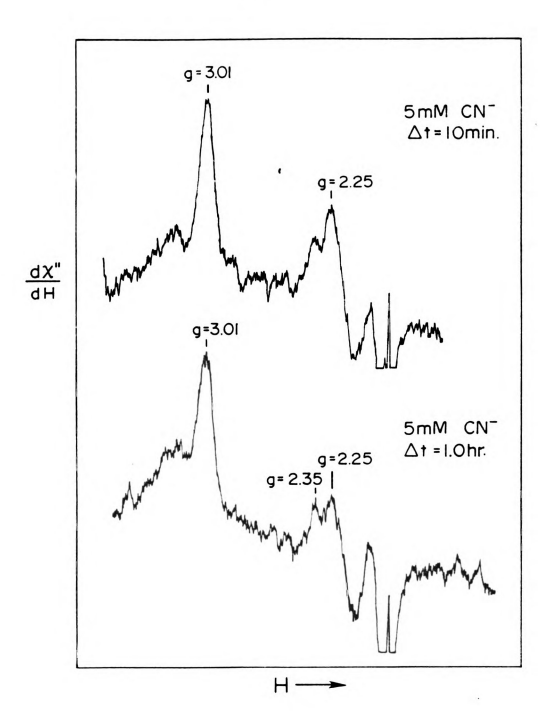


Figure 34. EPR spectra of  $\sim\!100~\mu M~\underline{c}_{552}$  with flavin:heme ratio  $\sim\!1.0$  in 0.1 M Tris, pH 7.5, after the addition of 5 mM CN  $^-$  .

reaction rate constants as slow as  $6.0 \times 10^{-2} \text{ sec}^{-1}$  were found for the cytochrome c derivatives. Those findings correlate well with the observed behavior of  $\underline{c}_{552}$  upon exposure to CN-. The cyanide apparently attacks the pHlabile heme particularly when it has two histidines as axial This is another indication of the mutability of the environment about this heme. The effects of CN on the pH-stable heme could arise from two sources. protein environment presents CN with too large an activation barrier to allow reaction at all, then the disruption of methionine-heme interaction would have to occur via a protein conformational change induced by attack upon the pH-labile heme. Alternatively, the activation barrier might simply be high enough to force the ligand displacement to proceed very slowly. The data obtained to date do not allow us to differentiate between those possibilities.

The changes in heme environments resulting from cyanide-heme interactions may explain the observation by Vorkink (30) that CN binding to  $c_{552}$  resulted in a loss of the derivative shape in the heme Soret CD spectrum whereas  $c_{3}^{2}$  and  $c_{2}^{2}$  binding had no such effect. This was interpreted by Vorkink as evidence of heme-flavin interaction, but more likely arises from the direct alteration of the heme environment by the cyanide.

#### CHAPTER 5

# RESONANCE RAMAN SPECTROSCOPY OF FLAVOCYTOCHROME <u>c</u>552

Resonance Raman spectroscopy has been shown to be a powerful tool for the elucidation of the structure and function of biological molecules, in particular those proteins which contain a heme moiety (41). The information obtained in a resonant scattering experiment is specific to the vibrations of the heme active site, and thus can be used to characterize both radical changes in iron redox and spin states as well as the more subtle perturbations due to alterations of the protein environment surrounding the active site. For example, the vibrations of porphyrin ring substituents can be observed directly (81,82), insight into the planarity of the porphyrin ring can be obtained (83), and porphyrin metalaxial ligand properties can be determined independent of the magnetic state of the metal (84). The technique should be particularly sensitive to vibrational manifestations of chromophore interactions. In the experiments described in this chapter no evidence of direct heme/ flavin or heme/heme interactions through either the heme

axial positions or periphery was found. The resonance Raman spectra of  $\frac{c}{-552}$  can be interpreted in terms of indirect, protein-mediated heme/flavin interactions.

# A. Raman Theory

The total intensity of radiation scattered into a solid angle of  $4\pi$  due to a Raman transition in a molecular system is (85):

$$I_{\text{Scattered}}^{\text{Total}} = (2^{7}\pi^{5}/a)I_{\text{o}}v_{\text{s}}^{4} \sum_{\rho,\sigma} |(\alpha_{\rho\sigma})_{\text{GF}}|^{2}$$
 (5.1)

where  $I_{0}$  and  $V_{0}$  the incident radiation intensity and frequency respectively and  $v_{s}$  represents the frequency of the scattered radiation (i.e.,  $v_{s} = v_{0} \pm v_{GF}$ , where the minus sign refers to Stokes and the plus sign anti-Stokes scattering)  $(\alpha_{\rho\sigma})_{GF}$  is the  $\rho\sigma$  component of the polarizability tensor connecting the initial and final molecular eigenstates defined by the relationship:

$$\begin{pmatrix} P_{x} \\ P_{y} \\ P_{z} \end{pmatrix} = \begin{pmatrix} \alpha_{xx} & \alpha_{xy} & \alpha_{xz} \\ \alpha_{yx} & \alpha_{yy} & \alpha\alpha_{yz} \\ \alpha_{zx} & \alpha_{zy} & \alpha_{zz} \end{pmatrix} \begin{pmatrix} E_{x} \\ E_{y} \\ E_{z} \end{pmatrix}$$

and can be evaluated via a second order perturbation approach originally developed by Kramers and Heisenburg by analogy with classical dispersion theory.

$$(\alpha_{\rho\sigma}) = \frac{1}{c} \sum_{E} \left[ \frac{\langle F | \mu_{\rho} | E \rangle \langle E | \mu_{\sigma} | G \rangle}{h \nu_{GE} - h \nu_{O} + i \Gamma_{E}} + \frac{\langle F | \mu_{\sigma} | E \rangle \langle E | \mu_{\rho} | G \rangle}{h \nu_{FE} + h \nu_{O} + i \Gamma_{E}} \right]$$
(5.2)

where  $\mu_{\rho}$ ,  $\mu_{\sigma}$  are the electric-dipole moment operators in the directions  $\sigma$  and  $\rho$  (e.g.,  $\mu_{\rho}$  =  $\Sigma e(r_K)_{\rho}$ ) and  $(r_K)_{\rho}$  is the  $\rho$ -th component of the  $K^{th}$  electron's position vector.  $\Gamma_E$  is the natural half-width of the state  $|E\rangle$ . The summation runs over all intermediate states,  $|E\rangle$ , exclusive of  $|G\rangle$  and  $|F\rangle$ . A schematic representation of the relative energy levels of the states involved in a resonance Raman experiment is shown in Figure (35). Far from the resonance  $h\nu_{gE} - h\nu_{o} >> 0$  and both terms in Equation (2) contribute to the scattered intensity. As resonance is approached the energy denominator of one vibronic manifold becomes much smaller than the rest and it dominates the summation over states. The remainder of this section will confine itself to the resonance case.

The evaluation of the interaction between the electricdipole operator and the eigenstates of the molecular system in question lies at the heart of Raman theory. The symmetry and intensity of these interactions are directly manifested

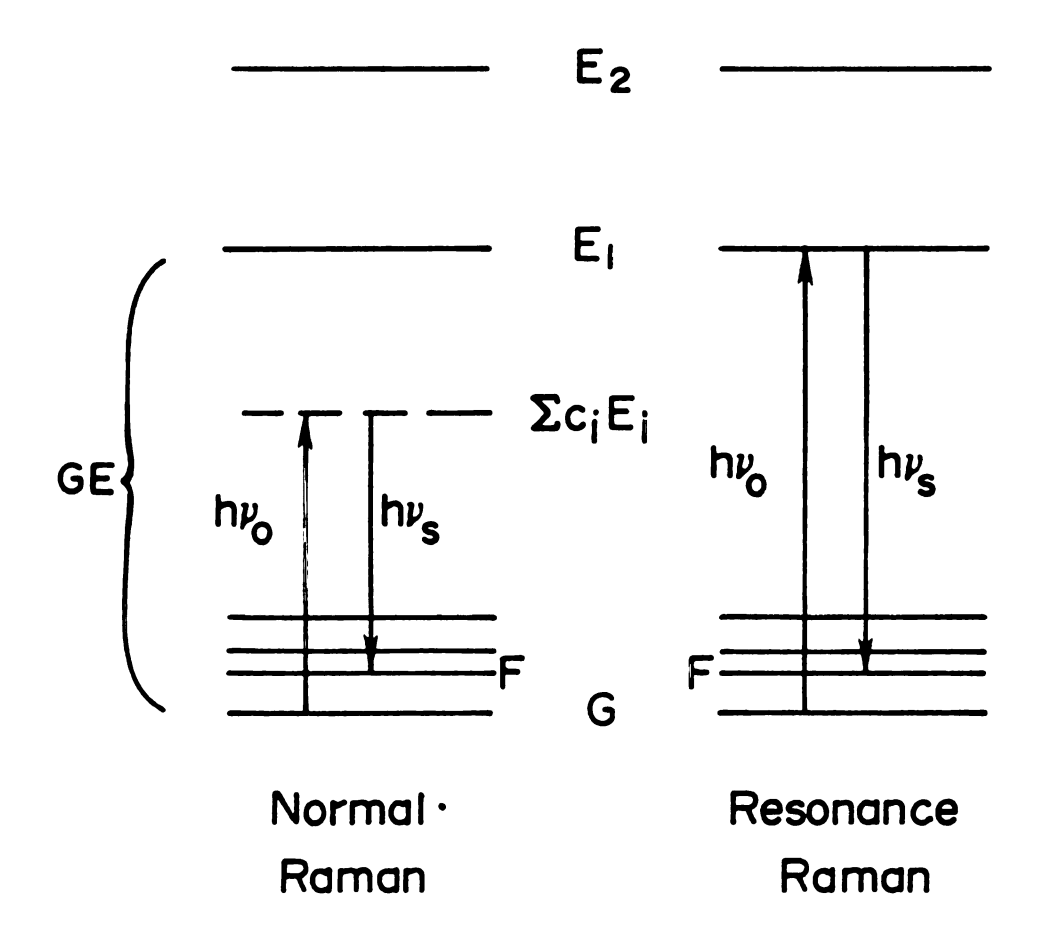


Figure 35. Raman scattering processes

in the polarizability tensor, and hence the scattered radiation. Several methodologies exist for such evaluation. One of the most useful from a spectroscopic standpoint is the vibronic coupling model first advanced by Albrecht (86) and subsequently expanded upon and applied to porphyrin systems by others (87,88,89). It is summarized as follows: The terms  $|G\rangle$ ,  $|F\rangle$ , and  $|E\rangle$  in Equation (5.2) represent the wavefunctions associated with the total (vibrational and electronic) Hamiltonian of the system. The adiabatic Born-Oppenheimer approximation is employed in which the vibronic states are constructed as products of pure vibrational states,  $|n(R_\xi)\rangle$ , and pure electronic states,  $|g(R_\xi,r)\rangle$ . Thus

$$|G\rangle = |g(R_{\xi}, r)\rangle n (R_{\xi})\rangle$$
 (5.3)

where  $R_{\xi}$  and r are the vibrational normal coordinates and the electronic coordinates of the molecule, respectively, and:

$$n(Q_{\xi}) = \pi \phi_{\xi}$$
  $\phi_{\xi}$  = harmonic oscillator wavefunctions

Substituting the above Born-Oppenheimer states into Equation (5.2) one obtains:

$$(\alpha_{\rho\sigma})_{gm\rightarrow gn} = \frac{1}{c} \sum_{e} \sum_{v} \frac{\langle n | \sigma_{ge} | v \rangle \langle v | \rho_{ge} | m \rangle}{h v_{gm,gn} - h v_{o} + i \Gamma_{ev}}$$
(5.4)

for the resonance case. Here  $\sigma_{ge} = \int g(Q_{\xi,r}) \mu_{\sigma} \ e(Q_{\xi}r)^{dr}$  and represents the electronic transition dipole between the electronic states  $|g\rangle$  and  $|e\rangle$ . In order to perform the remaining integration over nuclear coordinates, the parametic dependence of  $\sigma,\rho$  on nuclear coordinates must be removed. To that end, it is necessary to expand the matrix elements  $\sigma$  and  $\rho$  in a Taylor series about the equilibrium nuclear coordinates

$$\sigma(Q_{\xi}) = \sigma(Q_{\xi} = 0) + (\frac{\partial \sigma}{\partial Q_{\xi}})_{Q_{\xi} = 0} Q_{\xi} + \dots = \sigma + \sigma'Q_{\xi} + \dots$$

Truncating the series after the second term and substituting into Equation (5.4) yields

$$(\alpha_{\rho\sigma})_{gm+gn} = \sum_{e} \sum_{v} \sum_{\xi} (hv_{gm,pv} - hv_{o} + i\Gamma_{ev})^{-1}$$

$$x \left[\sigma_{ge} \rho_{eg} < n | v > < v | m > \right]$$

$$+ \sigma'_{ge} \rho_{eg} < n | Q_{\xi} v > < v | m > \right]$$

$$+ \sigma_{ge} \rho'_{eg} < n | v > < v | Q_{\xi} | m$$

$$+ \sigma'_{ge} \rho'_{eg} < n | Q_{\xi} | v > < v | Q_{\xi} | m > 0$$

$$+ \sigma'_{ge} \rho'_{eg} < n | Q_{\xi} | v > < v | Q_{\xi} | m > 0$$

$$(5.5)$$

The fourth term in this expression is small relative to the others and may be neglected. Assuming a vibronic coupling of states,  $\sigma'_{ge}$  and  $\rho'_{ge}$  can be evaluated via perturbation theory. This is referred to as the Herzberg-Teller expansion of the state  $|e\rangle$ 

$$\sigma_{eg}^{\prime} = \sum_{\xi} \sum_{s \neq e} \sigma_{sg} \cdot \frac{\langle s | \frac{\partial H}{\partial R_{\xi}} | e \rangle}{E_{e} - E_{s}}$$
 (5.6)

The extent to which the vibronic coupling operator  $\frac{\partial H}{\partial R_{\xi}}$ , serves to mix the other molecular eigenstates, |s>, with |e> depends upon the relative magnitudes of the coupling matrix element,  $\langle s | \frac{\partial H}{\partial R_{\xi}} | e \rangle$ , and the energy separation between the states. The expression for the polarizability tensor now becomes

$$(\alpha_{\rho\sigma})_{gm\rightarrow gn} = \frac{1}{c} \sum_{e} \sum_{v} \frac{\rho_{ge} \sigma_{eg} \langle n | v \rangle \langle v | m \rangle}{h \nu_{gm,ev} - h \nu_{o} + i \Gamma_{ev}}$$

$$+ \sum_{e} \sum_{s \neq e} \sum_{v} \frac{h_{es}^{\xi}}{h \nu_{e,s} \langle h \nu_{gm,ev} - h \nu_{o} + i \Gamma_{ev} \rangle}$$

$$\times \left[\sigma_{ge} \rho_{sg} \langle n | v \rangle \langle v | Q_{\xi} | m \rangle\right]$$

$$+ \rho_{ge} \sigma_{sg} \langle n | Q_{\xi} | v \rangle \langle v | m \rangle$$

$$+ \rho_{ge} \sigma_{sg} \langle n | Q_{\xi} | v \rangle \langle v | m \rangle$$

$$+ \rho_{ge} \sigma_{sg} \langle n | Q_{\xi} | v \rangle \langle v | m \rangle$$

$$+ \rho_{ge} \sigma_{sg} \langle n | Q_{\xi} | v \rangle \langle v | m \rangle$$

$$+ \rho_{ge} \sigma_{sg} \langle n | Q_{\xi} | v \rangle \langle v | m \rangle$$

$$+ \rho_{ge} \sigma_{sg} \langle n | Q_{\xi} | v \rangle \langle v | m \rangle$$

$$+ \rho_{ge} \sigma_{sg} \langle n | Q_{\xi} | v \rangle \langle v | m \rangle$$

$$+ \rho_{ge} \sigma_{sg} \langle n | Q_{\xi} | v \rangle \langle v | m \rangle$$

$$+ \rho_{ge} \sigma_{sg} \langle n | Q_{\xi} | v \rangle \langle v | m \rangle$$

$$+ \rho_{ge} \sigma_{sg} \langle n | Q_{\xi} | v \rangle \langle v | m \rangle$$

$$+ \rho_{ge} \sigma_{sg} \langle n | Q_{\xi} | v \rangle \langle v | m \rangle$$

$$+ \rho_{ge} \sigma_{sg} \langle n | Q_{\xi} | v \rangle \langle v | m \rangle$$

$$+ \rho_{ge} \sigma_{sg} \langle n | Q_{\xi} | v \rangle \langle v | m \rangle$$

$$+ \rho_{ge} \sigma_{sg} \langle n | Q_{\xi} | v \rangle \langle v | m \rangle$$

The first term in Equation (5.7) involves no vibronic coupling between electronic manifolds and is known as the Albrecht A-term. Since the vibrational integrals in A-term scattering are simple overlap integrals it is sometimes referred to as Franck-Condon (F-C) scattering. Far from resonance, closure may be applied to the F-C vibrational integrals:

$$\frac{1}{c} \sum_{v} \frac{\langle n | v \rangle \langle v | m \rangle}{h v_{gm,er} - h v_{o} + i \Gamma_{ev}} \alpha \langle n | m \rangle = \delta_{m,n}$$

and the A-term contributes only to Rayleigh scattering. As the resonance denominator becomes sensitive to vibronic energy spacings, closure is no longer valid and totally symmetric modes become active via F-C scattering if a small displacement in nuclear equilibrium positions exists between the molecular ground and excited states (90).

The second and third terms in Equation (5.7) combine to yield Albrect B-term or Herzberg-Teller (H-T) scattering. Scattering via this mechanism takes place through coupled vibronic states. The degree to which a given vibration couples the electronic states involved dictates the magnitude of  $h_{es}^{\xi}$  and consequently its resonance Raman intensity.

The application of the preceding theory to heme resonance Raman spectra is surprisingly straightforward considering the molecule's complexity. Only the two dominant

heme electronic transitions need be considered. Resonance with, for example, the Soret (B) transition yields:

$$(\alpha_{\rho\sigma})_{gm\rightarrow gn} = \frac{1}{c} \sum_{v} [h_{vgm,Br} - h_{o} + i\Gamma_{Br}]^{-1} \rho_{gB} \sigma_{gB} \langle n | v \rangle \langle v | m \rangle$$

$$+ \frac{1}{c} \sum_{v} \sum_{\xi} h_{BQ}^{\xi} [(h_{v_{B,Q}})(h_{v_{gm,Br}} - h_{v_{o}} + ir_{Br})]^{-1}$$

$$x \left[\sigma_{gB}\rho_{Qg} < n \mid v > < v \mid R_{\xi} \mid m > \right]$$

+ 
$$\rho_{gB}\sigma_{Qg} < n \mid R_{\xi} \mid v > < v \mid m >$$
 (5.8)

with an analogous expression for visible (Q) resonance. Since  $\rho_{gB}$ ,  $\sigma_{gB}$  >>  $\sigma_{Qg}$ ,  $\rho_{Qg}$ , F-C scattering dominates the R.R. spectrum obtained with Soret excitation and only  $A_{lg}$  modes are enhanced. On the other hand, excitation in resonance with the heme Q transition leads to scattering via the H-T terms since  $\rho_{gQ}$   $\sigma_{gQ}$  <<  $\rho_{gQ}$   $\sigma_{Bg}$   $h_{BQ}^{\xi}$  for vibrational modes that efficiently couple the B and Q states. In order for  $h_{BQ}^{\xi}$  to be non-zero, the symmetry of the vibrational normal coordinate must be contained in the direct product of the coupled electronic states. Both B and Q transitions possess  $E_u$  symmetry and  $E_u$  x  $E_u$  =  $A_{lg}$  +  $B_{lg}$  +  $B_{2g}$  +  $A_{2g}$ . Thus, modes of these symmetries are the only

ones enhanced by H-T scattering. Modes of  $A_{lg}$  symmetry have been shown to be ineffective in vibronic mixing for the cyclic polyene model (91). Heme vibrational modes of the allowed symmetries correspond to in-plane deformations of the porphyrin macrocycle.

The relationship between polarizations of the exciting and scattered radiation is expressed as the depolarization ratio for the band in question. It is defined as

 $I_{\perp}$  = intensity of scattered radiation with polarization  $\perp$  to that of the incident radiation.

= intensity of scattered radiation with polarization
|| to that of the incident radiation.

This ratio is a function of the symmetry of the polarizability tensor of the scattering state. Symmetry patterns for vibrations in the  $D_{4h}$  symmetry group have been determined (92) and are given in Figure (36).

The depolarization ratio can be redefined in terms of invariants of the preceding tensors

$$\rho_{\ell} = 3g^{S} + S_{g}A/10_{g}o + 4g^{S}$$

for 90° scattering geometry. The tensor invariants are:

$$A_{lg} = \begin{pmatrix} 1 & 0 & 0 \\ 0 & 1 & 0 \\ 0 & 0 & 0 \end{pmatrix} \qquad A_{2g} = \begin{pmatrix} 0 & 1 & 0 \\ -1 & 0 & 0 \\ 0 & 0 & 0 \end{pmatrix}$$

$$B_{lg} = \begin{pmatrix} 1 & 0 & 0 \\ 0 & -1 & 0 \\ 0 & 0 & 0 \end{pmatrix} \qquad B_{2g} = \begin{pmatrix} 0 & 1 & 0 \\ 1 & 0 & 0 \\ 0 & 0 & 0 \end{pmatrix}$$

Figure 36. Tensor symmetries for the resonance Raman active vibrational groups of hemes  $\underline{c}$ .

the isotropic invariant  $g^{\circ} = Tr(S^{\circ}S^{\circ+})$ the symmetric invariant  $g^{\circ} = Tr(S^{\circ}S^{\circ+})$ the antisymmetric invariant  $g^{\circ} = -Tr(AA^{+})$ 

where

$$S_{ij}^{o} = \frac{1}{3} \sigma_{ij} (\alpha_{xx} + \alpha_{xy} + \alpha_{zz})$$

$$S_{ij}^{s} = \frac{1}{2} (\alpha_{ij} + \alpha_{ji}) - S_{ij}$$

$$A_{ij} = \frac{1}{2} (\alpha_{ij} - \alpha_{ji}) .$$

Evaluation of the tensor invariants for the resonance Raman active heme modes results in:

$$\rho$$
 = 3/4 for  $B_{lg}$ ,  $B_{2g}$  modes  
= 1/8 for  $A_{lg}$  modes  
=  $\infty$  for  $A_{2g}$  modes

Thus, the experimental determination of  $\rho_{\ell}$  can be used to assign the vibrational symmetries of specific modes. Some care must be exercised if only a single excitation frequency is used to determine  $\rho_{\ell}$  as reduction of heme symmetry (from  $D_{4h}$ ) and/or interference effects from a splitting of molecular x,y degeneracy can lead to dispersion in  $\rho$  (93). Nonetheless, for  $\underline{c}$  type heme proteins the

assignment of heme vibrational symmetries provides a valuable means of systematizing their behavior.

## B. Raman Results and Discussion

As described above, the intensity and character of resonance Raman scattering from heme molecules is quite sensitive to the wavelength of the exciting radiation. Raman spectroscopy employing excitation in resonance with the heme Soret transition yields enhancement of polarized heme vibrational modes, corresponding to Franck-Condon scattering. Excitation in resonance with heme visible absorption bands admits scattering for vibronicallycoupled as well as isolated states. Scattering from coupled states corresponds to a Herzberg-Teller scattering mechanism (90), which allows enhancement of depolarized ( $\rho = 3/4$ ) modes of  $B_{lg}$  and  $B_{2g}$  symmetry and anomalously polarized  $(\rho > 3/4)$  modes of  $A_{2g}$  symmetry in  $D_{4h}$  hemes. Spectra of flavocytochrome  $c_{552}$  have been obtained in both of the abovementioned scattering regimes with 441.6 nm and 514.5 nm excitation. Fluorescence is a much stronger process than resonance Raman scattering. Thus, flavin fluorescence, despite the fact that it is extensively quenched, posed a significant obstacle to these resonance Raman studies and manifests itself as rising baseline in the spectra presented here.

The high and low frequency regions of resonance Raman spectra obtained with 441.6 nm excitation are shown in Figure (37). Scattering from the polarized heme modes of the ferric and ferrous forms of the protein are typical of other <u>c</u>-type cytochromes investigated at this wavelength (94).

The low signal-to-noise ratio displayed by most the F-C active modes in  $c_{552}$  is to be expected since 441.6 nm excitation lies in the pre-resonance enhancement region of the protein's absorption spectrum. Resonance enhancement via simple F-C scattering is proportional to the ratio of the electronic matrix elements and the resonance denominator of Equation (5.7) (95) although this is recognized as only a first approximation (96).

$$R = \varepsilon^2/(hv_{gm,ev} - hv_o)^2 + \Gamma^2$$
 (5.9)

where  $\varepsilon^2$  = extinction coefficient of the resonant absorption band.  $h_{Vgm,eV}$ ,  $h_{Vo}$  are the energies of absorption peak and exciting light, respectively, and  $\Gamma$  is the natural absorption linewidth. For  $c_{552}$   $h_{Vgm,eV}$  = 24390 cm<sup>-1</sup> and  $\Gamma$  = 1200 cm<sup>-1</sup>. Thus, the enhancement at 441.6 nm is approximately 1/3 that at 410.0 nm. This situation is compounded by the fact that for  $h_{Vo} \leq 24390$  cm<sup>-1</sup> the vibrational overlap integrals arising from F-C scattering should exhibit a destructive interference between scattering

Figure 37. Resonance Raman spectra of flavocytochrome  $\underline{c}_{552}$  obtained with 441.6 nm excitation. The power was 10 mW and the  $\underline{c}_{552}$  concentration was 75  $\mu$ M in 0.1 M Tris, pH 7.5.

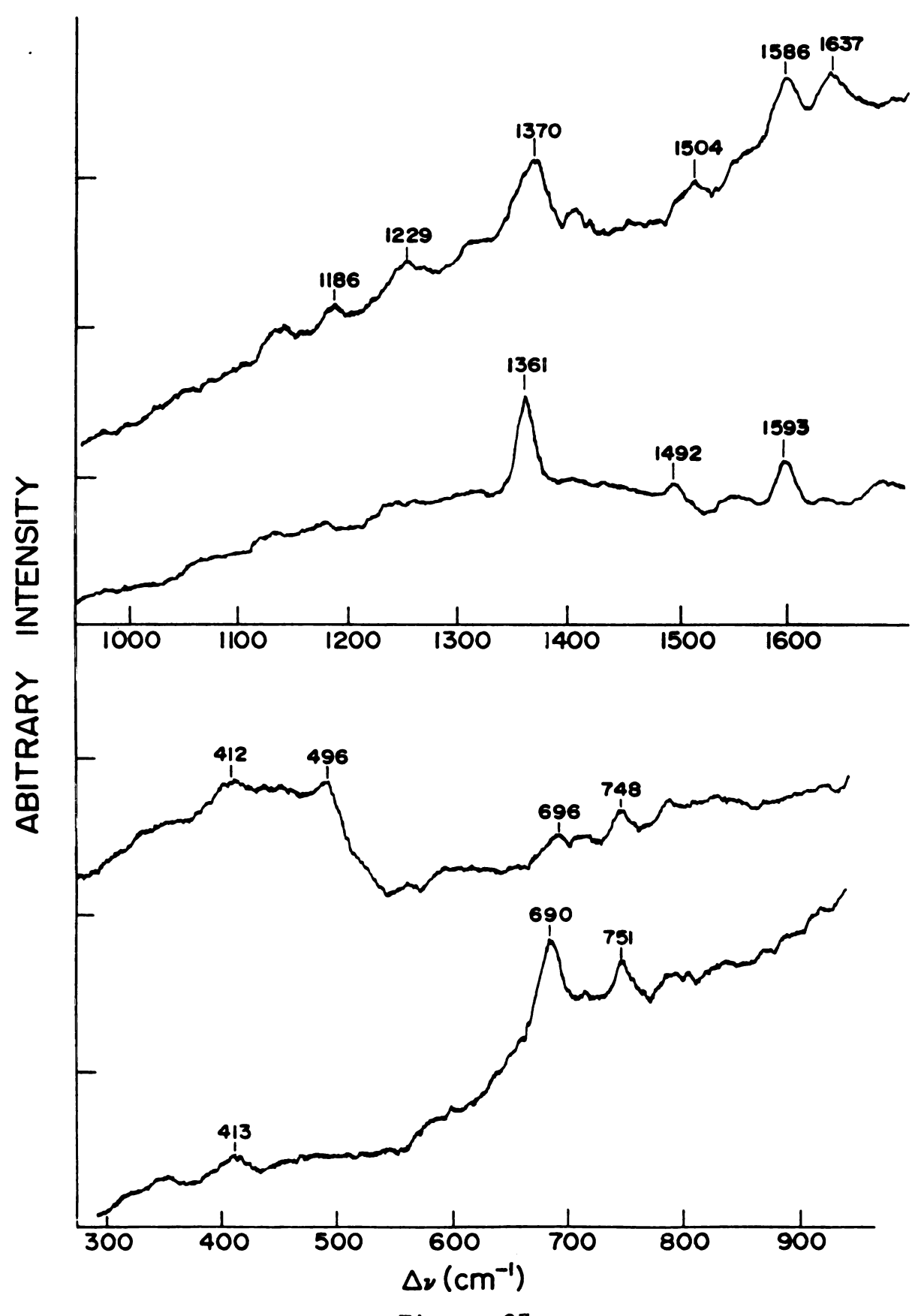


Figure 37

from the vibronic components of the Soret band of  $c_{552}$ (97) further diminishing their intensity. The spectrum of reduced  $c_{552}$  displays a selective enhancement of the  $690 \text{ cm}^{-1}$  and  $1360 \text{ cm}^{-1}$  modes over the other  $A_{lg}$  vibrations. This behavior has been observed in other heme proteins (98). Vibrational modes active in F-C scattering gain intensity from the simple overlap integrals of Equation (5.8), i.e.,  $\langle n | v \rangle \langle v | m \rangle$ , and, therefore, their intensity is dictated by the distortion in their equilibrium positions between excited and ground electronic states. selective enhancement of 690 cm<sup>-1</sup> and 1360 cm<sup>-1</sup> modes indicates that the excited state of the heme Soret band experiences a porphyrin macrocycle expansion in the direction of those modes' normal coordinates. These coordinates, particularly for the 1360 cm<sup>-1</sup> band, have been shown to originate primarily from in-phase  $C_{\alpha}N$  symmetric stretching in metallooctaethyl porphyrins (99). For oxidized  $c_{552}$  the relative enhancement of both the 696 cm<sup>-1</sup> and 1360 cm<sup>-1</sup> modes is diminished, presumably reflecting a smaller distortion of C\_N stretch in the Soret excited state due to the increased central ion charge. Even at the extremely low laser power used (~10 mW) a small amount of heme photoreduction is evident as a low energy shoulder on the 1370 cm<sup>-1</sup> band of the oxidized protein. has been used as an indication of heme redox state (100) and photoreduction (101,36) although some ambiguity exists

Table 4. Raman Modes for Flavocytochrome  $\underline{c}_{552}$  Obtained With 441.6 nm Excitation.

Feri	ic	Ferrous	
412	(w)	413 (w)	
496	(m)		
696	(w)	690 (s)	
748	(m)	751 (m)	
1186	(w)		
1229	(w)		
1370	(s)	1361 (s)	
1504	(w)	1492 (w)	
1586	(m)	1593 (m)	
1637	(m)		

All frequencies in units of  ${\rm cm}^{-1}$ 

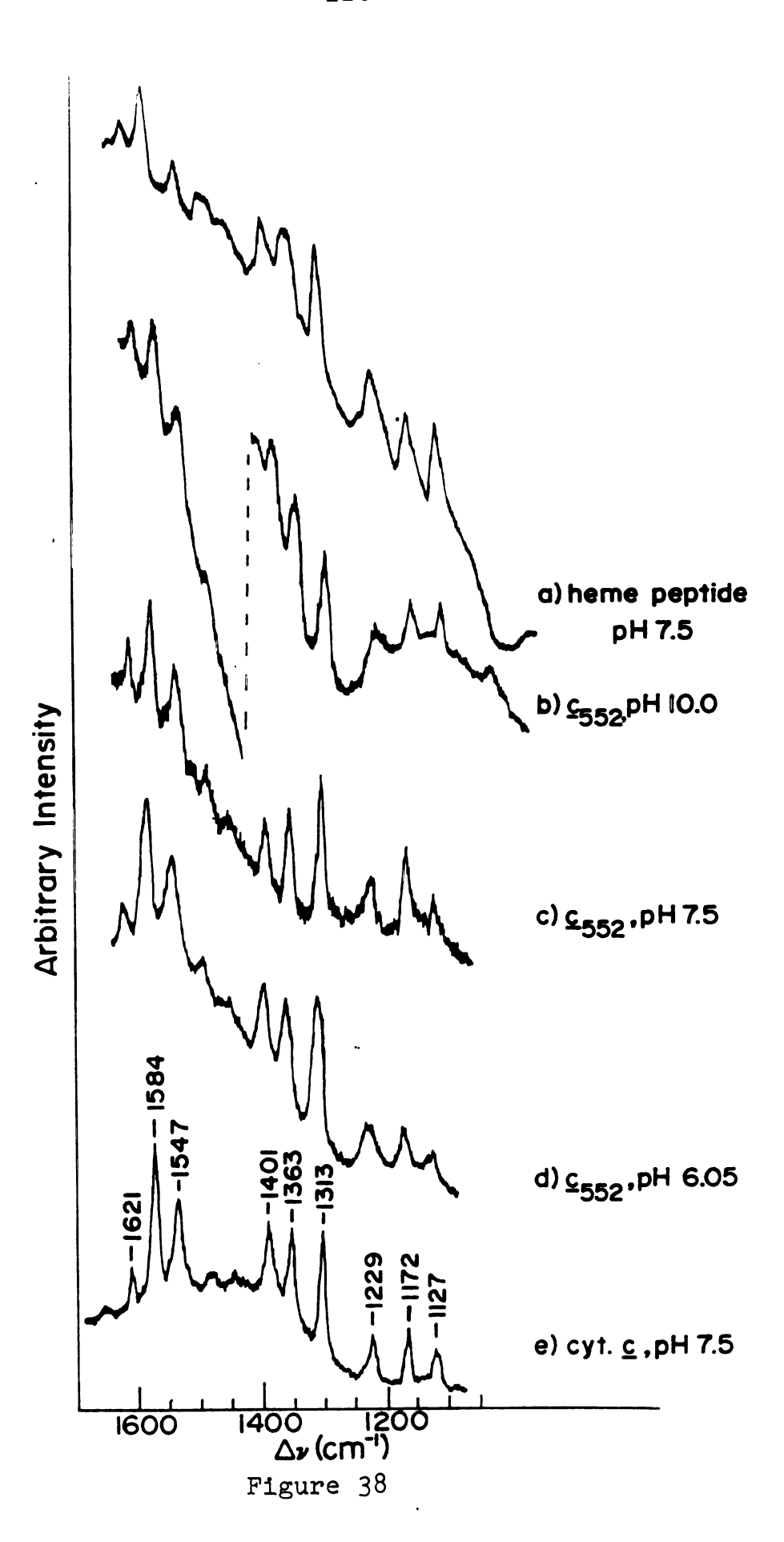
w - weak = medium = s - strong.

in interpretations based on its position since the mode is also sensitive to the basicity of heme axial ligands (81). No evidence of resonance enhancement of flavin vibrational modes is observed.

Resonance Raman spectra of reduced  $c_{552}$  and its diheme subunit, obtained with 514.5 nm excitation and shown in Figure (38), display the variety of mode symmetries expected for heme visible band resonance scattering. resonance Raman spectrum of reduced horse heart cytochrome c is included for ease of comparison. Vibrational symmetries have been assigned (See Table 5) on the basis of the depolarization ratios obtained from the reduced protein under the assumption of  $D_{\mu_h}$  heme symmetry. the holoprotein and heme peptide spectra are quite similar to those of horse heart cytochrome c and other small molecular weight monoheme c proteins (100,102) the only substantial difference being the flavin fluorescence background. anomalously polarized (ap) band at 1586  $cm^{-1}$  and the depolarized (dp) band at 1621 cm<sup>-1</sup>, which are sensitive to heme spin state (83), appear at frequencies consistent with low spin heme c. This confirms the assignment made from previous magnetic studies (33). The position of the polarized oxidation state marker at 1363 cm<sup>-1</sup> offers no evidence of anomalous heme axial ligation such as that seen with the P-450 cytochromes (103).

Figure (39) displays spectra of the ferric forms of  $c_{552}$ ,

Figure 38. Resonance Raman spectra obtained with 514.5 nm excitation of (a) 70 µM ferrous flavocytochrome  $\underline{c}_{552}$  diheme peptide in 0.1 M Tris pH 7.5 with 350 mW of laser power; (b) 100  $\mu M$  ferrous flavocytochrome  $c_{552}$  in 0.1 M CAPS, pH 10.0 with 180 mW of laser power; (c) 80  $\mu M$  ferrous flavocytochrome  $\underline{c}_{552}$  in 0.1 M Tris, pH 7.5 with 250 mW of laser power; (d) 100  $\mu\text{M}$  ferrous flavocytochrome  $\underline{c}_{552}$  in 0.1 M MES, pH 6.05 with 250 mW of laser power: (e) 200 uM ferrous horse heart cytochrome c in 0.1 M Tris, pH 7.5 with laser power equal to 250 mW. Frequency positions of the principal bands are given in Table 5. fluorescence background of the diheme peptide spectrum arises from a small amount of residual flavin peptide which could not be separated from the sample.



High Frequency Raman Modes for Flavocytochrome  $c_{552}$  Species Obtained with 514.5 nm Excitation. Table 5.

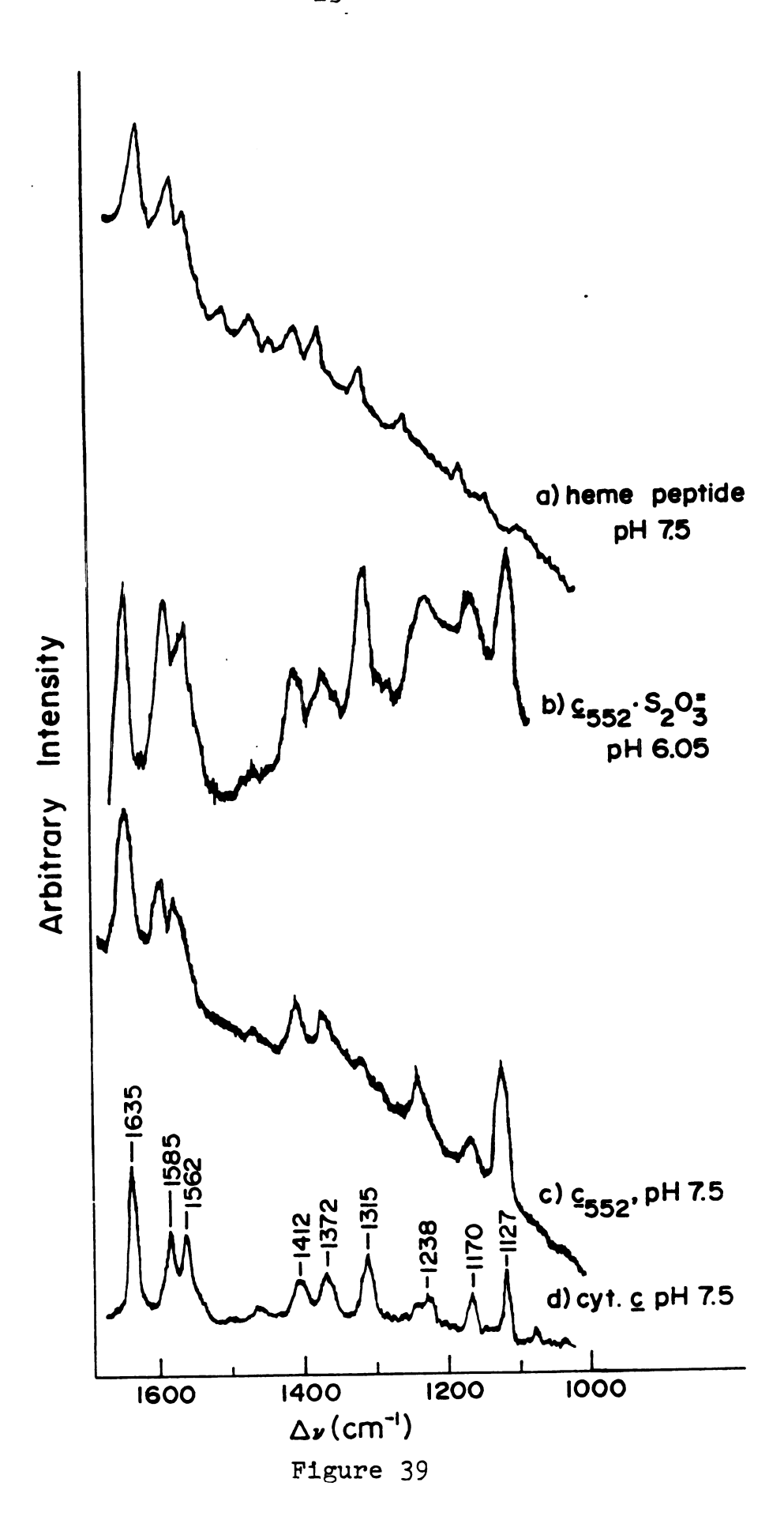
		Ferrous			
Mode Symmetry	Cyt. <u>c</u> (pH 7.5)	Heme Peptide (pH 7.5)	Cyt <u>e</u> 552 (pH 7.5)	Cyt. <u>c</u> 552 (pH 6.05)	Cyt. <u>e</u> 552 (pH 10.0)
B <sub>1g</sub> (.75)	1621 (m) <sup>a</sup>	1622 (m)	1621 (m)	1621 (m)	1621 (m)
A <sub>2g</sub> (3.18)	1584 (vs)	1585 (s)	1586 (vs)	1585 (vs)	1586 (s)
B <sub>1g</sub> (.74)	1547 (s)	1541 (m)	1544 (s)	1542 (s)	1548 (m)
B <sub>lg</sub> (.83)	1401 (s)	1401 (m)	1402 (s)	1399 (s)	1402 (m)
Alg (.29)	1363 (s)	1362 (m)	1363 (vs)	1362 (s)	1363 (s)
$A_{2g}$ (1.93)	1313 (vs)	1310 (vs)	1311 (vs)	1312 (vs)	1311 (vs)
B <sub>lg</sub> (.60)	1229 (m)	1228 (s)	1230 (m)	1229 (m)	1230 (m)
B <sub>2g</sub> (.70)	1172 (m)	1173 (s)	1172 (m)	1174 (m)	1173 (m)
A <sub>2g</sub> (1.10)	1127 (m)	1126 (s)	1127 (m)	1126 (m)	1124 (m)

Table 5. Continued.

		Ferric			Cyt <u>e552</u>
Mode Symmetry	Cyt. <u>c</u> (pH 7.5)	Heme Peptide (pH 7.5)	Cyt. c552 (pH 7.5)	Cyt. c <sub>552</sub> (pH 6.05)	S <sub>2</sub> 0 <sup>=</sup> (pH 10.0)
В 1,8	1635 (vs)	1642 (vs)	1640 (vs)	1642 (vs)	1643 (vs)
A2g	1585 (s)	1587 (s)	1586 (s)	1588 (s)	1589 (vs)
$_{ m Jg}$	1562 (s)	1567 (m)	1571 (s)	1565 (s)	1567 (s)
$_{ m B_{1g}}$	1412 (m)	1409 (m)	1407 (m)	1407 (m)	1408 (m)
$^{ m A}_{ m 1g}$	1372 (m) '	1373 (m)	1372 (m)	1370 (m)	1372 (m)
A2g	1315 (s)	1315 (m)	1315 (w)	; 1314 (s)	1315 (vs)
$_{ m Jg}$	1238 (m),1250 (m)	1248 (w)	1244 (m)	1246 (m)	1243 (s)
B <sub>2g</sub>	1170 (s)	1172 (m)	1169 (m)	1173 (m)	1172 (m)
A <sub>2g</sub>	1127 (s)	~1122 (vw)	1126 (s)	1 1 1	1128 (s)

s = strong, vs = very strong,  $^{\rm a}$ Vibrational frequencies are in units of cm  $^{\rm -1}$ .  $^{\rm m}$  = medium,  $^{\rm w}$  = weak,  $^{\rm w}$  = very weak.

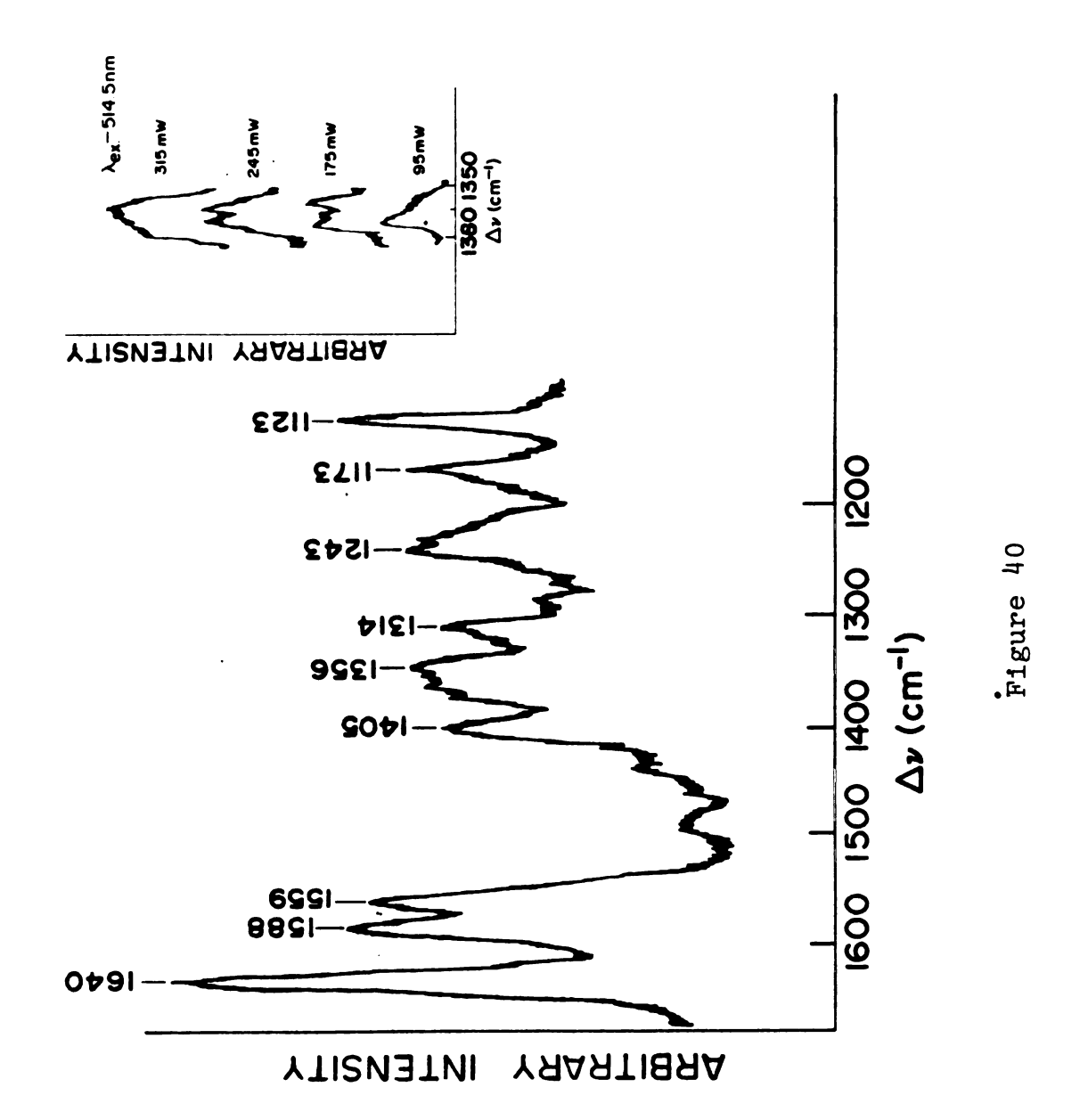
Figure 39. Resonance Raman spectra obtained with 514.5 nm excitation of (a) 70  $\mu$ M ferric  $c_{552}$  diheme peptide in 0.1 M Tris, pH 7.5 with 250 mW of laser power; (b) 100  $\mu$ M ferric flavocytochrome  $c_{552}$  in 0.1 M MES, pH 6.05 2 mM Na $_2$ S $_2$ O $_3$  with 200 mW of laser power; (c) 80  $\mu$ M ferric flavocytochrome  $c_{552}$  in 0.1 M Tris, pH 7.5 with 95 mW of laser power; (d) 200  $\mu$ M ferric horse heart cytochrome  $c_{552}$  in 0.1 M Tris, pH 7.5 with 250 mW of laser power. Frequency positions of the principal bands are given in Table 5.



its diheme peptide and horse heart cytochrome c, in the high frequency region, obtained with 514.5 nm excitation. As with the ferrous spectra, the positions and intensities of the Raman bands of the holo- and apo-protein are generally typical of monohemes c. Two major departures from this "typical" behavior are evident. The first is a small but consistent deviation in the positions of the high frequency modes with  $B_{1g}$  symmetry, as may be noted from Table (5). These bands are characterized by depolarization ratios equal to 3/4 and occur at 1635, 1562, 1412, and 1250 cm<sup>-1</sup> in horse heart cytochrome  $\underline{c}$ . In ferric  $\underline{c}_{552}$ these modes, and only these modes, show wavenumber shifts relative to horse heart cytochrome c. The shifts range from +9 cm<sup>-1</sup> (for the 1571 cm<sup>-1</sup> band) to -5 cm<sup>-1</sup> (for the 1407 cm<sup>-1</sup> band). The observation that the positions of only a specific symmetry class of resonance Raman active heme vibrations are anomalous is suggestive of some specific perturbation of the heme environment in  $c_{552}$ . Moreover, this perturbation of the  $B_{1\sigma}$  modes is not observed in the ferrous form of the protein (See Table 5).

The second case of anomalous behavior lies in the relative ease with which the heme in the holoprotein is photoreduced in the laser beam. The small amount of photoreduction observed with Soret excitation increases dramatically with the higher laser powers used for visible excitation. Figure (40) shows a spectrum of

Tris, pH 7.5 obtained with 315 mW of 514.5 nm laser light incident upon the state marker band in ferric  $\frac{c}{552}$  as a function of 514.5 nm intensity upon sample. Insert: The position and intensity dependence of the oxidation Resonance Raman spectrum of 80  $\mu M$  ferric flavocytochrome  $c_{552}$  in 0.1 M the sample. Figure 40.



resting  $c_{552}$  at 315 mW incident laser power, plus an inset displaying spectra in the oxidation state marker band region as a function of incident laser power. It is apparent that at high laser intensity this band shifts from 1370 cm<sup>-1</sup> to 1356 cm<sup>-1</sup>, a position indicative of ferrous iron (100). At intermediate powers a double peak is clearly visible. Neither horse heart cytochrome c nor the heme peptide displays this behavior; indeed, spectra of the ferric forms of these proteins were routinely obtained with 200 mW of laser power.

The binding of thiosulfate and cyanide to the oxidized protein resulted in an initial lowering of flavin fluorescence. However, CN binding was found to be short-lived. Subsequent to cyanide binding, the ratio  $A_{475}/A_{525}$  returned to its initial value and flavin fluorescence increased greatly. Thiosulfate, on the other hand, remained bound and continued to quench flavin fluorescence. Relative fluorescence levels of these species are contrasted in Figure (21). The instability of the  $\underline{c}_{552}\cdot\text{CN}$  complex precluded observation of its resonance Raman spectrum. The spectrum obtained with 514.5 nm excitation of  $\underline{c}_{552}\cdot S_{203}$  is included in Figure 39. It differs from the unbound holoprotein only in the substantial increase in intensity exhibited by the 1315 cm<sup>-1</sup> and 1589 cm<sup>-1</sup> anomalously polarized modes.

The pH dependence of the holoprotein Raman spectra

was also investigated. Fluorescence levels increased markedly at both the high pH ( $\sim$ 10.0) and  $1 \sim$  pH ( $\sim$ 6.0) limits of  $c_{552}$  stability. This resulted in a deterioration of Raman spectral quality and a spectrum of the ferric protein at high pH could not be obtained. As with other cytochromes,  $\underline{c}_{552}$  band positions display some pH dependence. In particular the band which appears at  $1544 \text{ cm}^{-1}$  and 1571 ${
m cm}^{-1}$  in the ferrous and ferric holoprotein, respectively (at pH 7.5) was sensitive to pH changes. Figure 38 exhibits the pH dependence of scattering from ferrous  $c_{552}$ and attests to the dramatic rise in background fluorescence as the high pH limit of heme:flavin subunit binding stability is reached. A summary of band positions, intensities and depolarization ratios obtained for the various forms of flavocytochrome  $c_{552}$  with 514.5 nm excitation is given in Table 5.

The general features of the resonance Raman spectra of flavocytochrome  $\underline{c}_{552}$  presented here conform well to the classification methodology developed for monoheme proteins by Spiro and Strekas (100). Upon closer examination, however, several distinguishing aspects of the  $\underline{c}_{552}$  spectra become apparent. These can be divided into two categories: general effects involving the flavin moiety of the protein and specific perturbations of heme vibrational modes. The former have the more obvious impact on the spectra, whereas the interpretation of the latter

provides insight into the multicomponent nature of flavo-cytochrome  $c_{552}$ .

# Flavin Effects

The most salient of the flavin effects is the broad fluorescence background it produces in the resonance Raman spectra of  $\underline{c}_{552}$ . This is unusual not because of its existence, but rather because it is weak enough to permit the observation of resonance Raman scattering. The factors leading to the quenching of flavin fluorescence have been discussed in detail in Chapter 3 and need not be reiterated here. However, the presence of the protein's flavin moiety has other effects upon the heme resonance Raman spectra of  $\underline{c}_{552}$ .

An indication of heme/flavin communication is apparent in the heme photoreduction at high incident laser power. The shift in the "oxidation state marker" frequency from  $1370~{\rm cm}^{-1}$  to  $1360~{\rm cm}^{-1}$  has been used as an indication of increased electron density located on the heme iron (104). Such a shift occurs in flavocytochrome  $\underline{c}_{552}$  spectra at moderate laser powers, but it is absent in the heme peptide and horse heart cytochrome  $\underline{c}$  spectra even at high power. Photoreduction has been observed in other heme proteins, most notably cytochrome oxidase, and was attributed to a flavin contamination which was postulated to be the initial site of photoreduction (101). In the case of  $\underline{c}_{552}$ 

the flavin is an integral part of the functional protein. The flavin excited state is extensively delocalized by interactions with protein aromatic residues (as indicated by fluorescence quenching) and thus could be expected to provide an efficient pathway for heme photoreduction. Under aerobic conditions the photoeffects described here are most evident for the 1372 cm<sup>-1</sup> (dp) band. highest laser power used, two of the  $B_{lg}$  heme modes (at 1571 and 1407 cm<sup>-1</sup>) begin to decrease in frequency; however, the systematic lowering of heme vibrational frequencies known to result from chemical reduction is largely absent despite the fact that the oxidation state marker appears at 1356 cm<sup>-1</sup> in the "photoreduced" protein (7 cm<sup>-1</sup> lower in wavenumber than in chemically reduced  $c_{552}$ ). In particular, the  $1640 \text{ cm}^{-1}$  (dp) mode which undergoes large changes in both position and intensity depending on the iron redox state clearly retains its oxidized character. indicates that the lability of the "oxidation state marker" is predicated, at least in part, upon factors independent of the formal iron redox state. Anomalous oxidation state marker behavior has also been observed in carbon monoxy and oxyhemoglobin and myoglobin resonance Raman spectra (81).

The resonance Raman spectra obtained with Soret excitation are noteworthy for the absence of any bands attributable to flavin scattering despite the fact that the 441.6 nm

exciting radiation is in resonance with the flavin absorption at 450 nm in  $c_{552}$ . This absorption arises from an in-plane flavin  $\pi + \pi^*$  transition (105). Thus, resonance enhancement of in-plane isoalloxazine vibrational modes would be expected to result in several peaks in the 1000-1600 cm<sup>-1</sup> region of the resonance Raman spectrum. modes have recently been observed in resonance Raman spectra of protein-bound FAD (106) and in CARS spectra of FAD and glucose oxidase (107). The absence of flavin bands in our spectra can be readily explained by the fact that at 441.6 nm heme scattering dominates the spectrum because of its greater extinction, leaving the flavin modes unobservable at the laser power used. Resonance enhancement via simple Franck-Condon scattering is proportional to the quantity R given in Equation (5.9). For the following conditions:  $v = 22,645 \text{ cm}^{-1} (441.6 \text{ nm}), v_0(\text{flavin}) = 22,422 \text{ cm}^{-1}$  $(446 \text{ nm}), v_0(\text{heme}) = 24,390 \text{ cm}^{-1} (410 \text{ nm}), \Gamma (\text{flavin})$  $\sim$  1500 cm<sup>-1</sup>,  $\Gamma$  (heme)  $\sim$  1200 cm<sup>-1</sup>,  $\varepsilon_{\rm m}$ (heme) = 125 mM<sup>-1</sup> cm<sup>-1</sup> and  $\varepsilon_{m}(\text{flavin}) = 10 \text{ mM}^{-1} \text{ cm}^{-1}$ , the ratio R(heme)/R(flavin) is calculated to be more than one hundred. Thus any flavin bands would be at least an order of magnitude less intense than the  $c_{552}$  heme bands, and undetectable with a conventional spectrometer.

#### Heme Vibrational Bands

All the features found in the resonance Raman spectra of  $c_{552}$  can be readily interpreted as monoheme scattering coupled with the flavin effects discussed above. plicability of previous classification schemes (100) to the heme scattering of  $c_{552}$  is obvious and confirms their assignment as low-spin heme c. This is particularly striking in the spectra of reduced  $\underline{c}_{552}$  and its heme peptide under visible excitation. For both the holo- and apoprotein all bands are within ±2 cm<sup>-1</sup> of their horse heart cytochrome  $\underline{c}$  values, except the depolarized band at  $\sim$ 1545  ${
m cm}^{-1}$  which displays a pH-dependent position. Investigations of <u>Desulfovibrio</u> <u>vulgaris</u> cytochrome <u>c</u> by Kitagawa <u>et al</u>. (102) indicate that this band is sensitive to the nature of heme axial ligands. In fact, they used its position to monitor a pH-dependent heme ligand change: a shift in frequency from 1541  $cm^{-1}$  to 1536  $cm^{-1}$  was interpreted as resulting from the replacement of histidine by lysine in the protein at high pH.

The existence of an analogous pH dependence in the heme axial ligation of ferric  $\underline{c}_{552}$  has been indicated in a previous EPR study of the protein by Strekas (33). The situation is somewhat more complicated in  $\underline{c}_{552}$  than in cytochrome  $\underline{c}_3$  because only one of the protein's two hemes displays pH-dependent behavior. The EPR spectra of ferric

c552 obtained by Strekas (33) and reproduced in our laboratory can be interpreted to arise from a heme axial ligation scheme involving one pH-stable heme with methionine/histidine ligands and one pH-labile heme favoring lysine/histidine ligands at low pH and histidine ligands at high The pH-dependent behavior of the 1545 cm<sup>-1</sup> Raman band in ferrous  $c_{552}$  indicates that a similar axial ligation scheme obtains for the reduced protein. If this is the case, the resonance Raman spectra of ferrous  $c_{552}$  at neutral pH should, in principle, exhibit three peaks for the ligand-sensitive band at  $1545 \text{ cm}^{-1}$ : one at  $1547 \text{ cm}^{-1}$ , another at 1541 cm<sup>-1</sup> and a third at 1536 cm<sup>-1</sup>, corresponding to methionine/histidine (as in ferrous horse heart cytochrome c), histidine/histidine, and lysine/histidine ligation, respectively. In practice, a single asymmetric peak appears in this region: at 1542 cm<sup>-1</sup> in the holoprotein at pH 6.05, 1544  $cm^{-1}$  at pH 7.50 and 1548  $cm^{-1}$ at pH 10.0, suggesting that the pH-dependent ligand shift is also operative for the reduced protein. For the ferrous heme peptide at pH 7.5 the band is observed at 1541  $\rm cm^{-1}$ , indicating a preference for the low pH ligand (lysine) in the apoprotein.

The spectra of ferric  $\underline{c}_{552}$  holo- and apo-proteins, while retaining the general characteristics of monoheme  $\underline{c}$  spectra, display a larger deviation from horse heart cytochrome  $\underline{c}$  behavior than do the ferrous spectra. Two

effects are most likely responsible for this behavior: ligand effects seen in both  $\underline{c}_{552}$  and the heme peptide, and a general perturbation of heme modes of  $B_{lg}$  symmetry observed only in the oxidized holoprotein. The ligand effects which were limited to a single mode in reduced  $\underline{c}_{552}$  are more widespread in the ferric spectra.

The ligand effects seen here can be interpreted as reflecting a change in the heme iron electronegativity as a function of axial ligand electron donating capabilities. A recent study by Kitagawa, et al. (108) utilizing metalloporphyrins with a variety of central metal ions indicates that the position of several high frequency Raman bands and the  $Q_{0,0}$  optical absorption maximum are directly correlated to the electronegativity of the central metal ion. Increased metal electronegativity allows for better conjugation of the metal  $rp_z$  orbital with the porphyrin  $a_{2u}$  orbital, shifting the  $Q_{00}$  transition to higher energy and giving rise to a stronger  $\pi$ -bonding system in the porphyrin macrocycle. Stronger  $\pi$  bonding results in higher frequencies for the affected vibrations. results can be extrapolated to heme proteins with the realization that while the central metal ion does not change, its apparent electronegativity is a direct result of the electron donor power of the axial ligands. frequencies of the ligand sensitive Raman bands should

increase in the order of methionine to histidine to lysine based the electron donating capabilities of those ligands. This expectation has been shown to be true for several high frequency heme c Raman bands. Kitagawa et al. (102) have found that the bands at 1635, 1562, and 1372 cm<sup>-1</sup> are pH (ligand) dependent in ferric horse heart cytochrome c, changing to 1641, 1568 and 1375 cm<sup>-1</sup> upon replacement of the axial methionine by lysine at high pH. The Raman data presented here confirm that this situation also applies to flavocytochrome  $c_{552}$ . The heme peptide frequencies parallel the high pH values of horse heart cytochrome c (i.e., lysine/histidine ligands), indicating the effect of the pH labile heme. For the ferric holoprotein, however, the positions of all of the high frequency  $B_{lg}$  modes are shifted (relative to horse heart cytochrome c). Particularly evident is the 9  $cm^{-1}$  change in the position of the 1562 cm<sup>-1</sup> band. The band positions of the ferric heme peptide  $B_{lg}$  modes are, with the exception of the 1642 cm<sup>-1</sup> band, intermediate between the values for horse heart cytochrome  $\underline{c}$  and holo-cytochrome  $\underline{c}_{552}$ . On the basis of axial ligation it would be expected that the situation would be reversed; the holoprotein with its mixture of lysine and histidine ligands would have band positions closer to horse heart cytochrome c than to the heme peptide. The expected situation holds for the low pH holoprotein, but is not the case at pH 7.5. Thus, relative wavenumber shifts in the

spectra cannot be explained as arising solely from axial ligand changes; the changes in frequency of the  $B_{lg}$  modes must also be diagnostic of some other protein influence.

Normal coordinate calculations (99) have indicated that  $B_{lg}$  modes in general and the  $\sim 1565$  cm<sup>-1</sup> mode in particular involve out-of-phase stretching of atoms at the porphyrin periphery (either  $C_{\beta}$  -  $C_{\beta}$  or  $C_{m}$ -H stretches), whereas the  $1372 \text{ cm}^{-1}$  mode is closely associated with C-N symmetric stretching. In fact, studies of metalloetioporphyrins by Spaulding et al. (83) have stressed the importance of contributions from the core expansion of the inner 16-membered ring to both the oxidation state  $(A_{1g})$ and spin state (A2g) marker bands. The depolarized modes appearing at  $\sim 1565 \text{ cm}^{-1}$  and  $1250 \text{ cm}^{-1}$  in ferric hemes have been shown to be particularly sensitive to substituent effects. The former shifts from 1547 cm<sup>-1</sup> in ferrous cytochrome c to 1538 cm<sup>-1</sup> in protoheme reconstituted ferrous cytochrome  $\underline{b}_5$ , indicating the presence of the two peripheral vinyl groups in the protoheme. A similar effect was noted in ferric heme a by Kitagawa et al. (109), who observed that the 1564 cm<sup>-1</sup> mode in a bis-imidazole iron-protoporphyrin complex shifted to 1555  $cm^{-1}$  in the heme <u>a</u> bisimidazole complex, reflecting the contribution of the heme  $\underline{a}$  peripheral carbonyl group. The 1250 cm<sup>-1</sup> mode has been shown to be sensitive to deuteration of the methine hydrogens in ferrous mesoporphyrin IX dimethyl ester

complexes (110). These observations indicate that the depolarized modes of the heme are more sensitive to peripheral influences on the porphyrin than are the high frequency  $A_{2g}$  or  $A_{1g}$  modes. In flavocytochrome  $c_{552}$  these  $B_{1g}$  modes all experience frequency shifts (with respect to horse heart cytochrome c) in the oxidized protein that are absent in the reduced protein. The effect is obscured by the axial ligand dependence of the 1640 cm<sup>-1</sup> and 1571 cm<sup>-1</sup> bands, but is clearly independent of it since the 1407 cm<sup>-1</sup> band shows no axial ligand effect in reduced or oxidized  $c_{552}$  or in any of the ferric bacterial cytochromes c studied by Kitagawa c al. (102).

The binding of  $S_2O_3^{-}$  to the low pH form of the oxidized protein produces no appreciable change in the heme Raman frequencies, implying that there is very little perturbation of the local heme vibrational environment upon substrate binding. Thus, in its low pH form, the heme environment is already in a conformation amenable to substrate binding. However, the intensity of Herzberg-Teller active heme modes is dependent upon the extent to which they couple the porphyrin Q and B states. The large increase in the relative intensities of the two anomalously polarized bands (at  $\sim 1315$  cm<sup>-1</sup> and  $\sim 1589$  cm<sup>-1</sup>) in going from  $c_{-552}$  at pH 7.5 to the thiosulfate-bound protein may be indicative of an alteration in the electronic environment of the heme.

It is apparent that the redox state of the protein (and by implication the flavin) has a noticeable effect on the peripheral environment of at least one of the heme moieties. The effect is small. No extra bands occur in the heme spectra, nor are there any dramatic changes in electron density at the heme iron (as evidenced by the position of the 1370 cm<sup>-1</sup> band). This suggests that there is no direct heme/flavin interaction through either electronic resonance or the axial heme positions, and if heme/flavin interaction occurs it does so via a protein-mediated heme/flavin communication through the heme periphery. The heme vibrational mode frequencies are consistent with an interpretation which considers both heme axial ligation and an indirect protein mediated heme/flavin interaction.

#### CHAPTER 6

#### CONCLUSION

The results obtained from the application of a variety of spectroscopic techniques to flavocytochrome  $\underline{c}_{552}$  have been described in the preceding chapters. Individually these techniques provide insight into a number of specific properties of the protein, but their true utility lies in a synthesis of these specific results which leads to the elucidation of general relationships between the protein's structural and functional aspects. These relationships can be divided into three general categories:

- 1) chromophore : chromophore interactions;
- 2) chromophore : protein interactions;
- 3) chromophore interactions with exogenous ligands

This chapter serves to summarize the nature and extent of these interactions in an effort to arrive at a consistent description of flavocytochrome  $\underline{c}_{552}$  and the general class of multicomponent enzymes it represents.

## A. Heme/Heme Interactions

Communication between redox centers in a multicomponent enzyme such as  $\underline{c}_{552}$  is a necessary prerequisite for the proper function of the protein in electron transport. Perhaps the most straight forward mechanism for such communication lies in the direct coupling of the action centers by electronic, magnetic or chemical means. No evidence for direct heme/heme interaction in flavocytochrome  $c_{552}$  can be found with any of the spectroscopic techniques used in this study. The EPR and absorption spectra of the protein are completely consistent with isolated low spin heme  $\underline{c}$ . MCD and EPR spectroscopies would be particularly sensitive to heme/heme magnetic interactions within  $c_{552}$ , yet both yield spectra of  $\underline{c}_{552}$  that are typical of isolated hemes. No magnetic coupling such as spin-spin or dipole-dipole interactions are evident using either of these techniques. These findings preclude the possibility of heme: heme stacking or even the sharing of a common axial ligand (e.g., histidine) between the two hemes, as either of these would lead to a significant distortion of heme magnetic properties such as that found in bacterial c'cytochromes (111) or mitochondrial cytochrome c oxidase (112).

Heme/heme interaction in  $\underline{c}_{552}$  was originally postulated as an explanation for the protein's derivative shaped Soret CD spectrum. Exciton coupling does lead to derivative shaped bands, however, it is not a necessary condition

for such CD behavior. Derivative Soret CD spectra have been observed in monoheme proteins such as cytochrome  $\underline{c}$ from Candida lerusei (113) and horse heart cytochrome c, where no possibility of heme/heme interactions exist. The global properties of the protein molecule must be considered in an interpretation of heme c CD spectra (114) Myer (115) interpreted the negative peak of horse heart ferricytochrome c as resulting from heme-protein interactions which reflected the conformational integrity of the heme crevice. Considering the lack of corraborative evidence for heme/heme magnetic interaction, the CD characteristics of the Soret region of  $c_{552}$  must be ascribed to a similar heme-protein interaction. ruption of this interaction by CN is not surprising considering the extensive effect CN has on the environment of the pH-labile heme.

# B. Heme/Flavin Interactions

The interaction between the dissimilar redox centers in  $\underline{c}_{552}$ , while more in evidence than heme/heme interactions, is indirect in nature. The most obvious manifestation of heme/flavin communication is found in the ease with which the heme moieties of ferric  $\underline{c}_{552}$  are photoreduced during the course of resonance Raman spectroscopy. This photoreduction is dependent upon the flavin group (it is absent

in the diheme peptide of  $\underline{c}_{552}$ ) and is indicative of the existence of a pathway for electron transport between flavin and heme. Heme vibrational modes of  $B_{lg}$  symmetry display a dependence upon the oxidation state of the protein (and by implication the flavin). This can be interpreted as resulting from a perturbation of the peripheral environment of at least one of the hemes.

The resonance Raman data cited above establish that some form of indirect contact between flavin and heme in  $\underline{c}_{552}$  exists, however there is no datum available at this time that requires direct heme/flavin coupling for its explanation. Flavin fluorescence is significantly quenched in  $\underline{c}_{552}$ , but the extensive quenching exhibited by hemefree, flavin-containing, peptide fragments of the protein leaves any possible further effects due to flavin-heme Forster coupling undetectable. The alteration of the protein's EPR spectrum upon CNT binding is most easily explained as resulting from a direct CNT attack upon the pH-labile heme rather than a flavin/heme interaction.

The absence of evidence for direct coupling between chromophores requires that the mechanism of electron flow in  $\underline{c}_{552}$  actively involve the polypeptide matrix. Thus, the protein environment of the redox centers in  $\underline{c}_{552}$  becomes critical to their proper function. A partial definition of chromophore environments within  $\underline{c}_{552}$  is possible from the spectroscopic data and is summarized below.

# C. Flavin Environment

The flavin in  $\underline{c}_{552}$  displays no magnetic or Raman spectra and, therefore, is less "visible" than the protein's heme Nonetheless, it is possible to infer a number of characteristics of its protein environment from absorption and fluorescence data. The ability of the flavin to form adducts with exogenous ligands dictates that the portion of the group containing the N-5 position is accessible from the external solution. However, the nearly complete quenching of flavin fluorescence and the CD spectra of the flavin-containing peptides argues that it is closely associated with aromatic (tyrosine) residues in the protein matrix. This is corroborated by the increased reduction potential ( $E_0 = 0 \text{ mV}$ ) of the flavin in  $\underline{c}_{552}$  relative to free flavins ( $E_0 = -200 \text{ mV}$ ), which indicates a highly hydrophobic flavin environment. The hydrophobicity of the flavin environment could also inhibit the formation of the charged semiquinone species and favor a concerted, two electron transfer at the flavin. A flavin configuration that exposes only the central edge of the isoalloxazine ring system to the solution while maintaining the rest of the flavin in a crevice of hydrophobic residues is consistent with the above observations.

#### D. Heme Environments

The two hemes in  $c_{552}$  exist in distinctly different protein environments. Optical and MCD data confirm that both hemes are low-spin six-coordinate heme c. However, the EPR spectra of  $c_{552}$  clearly indicate that the axial ligands of two hemes are different. One heme has a pHinvariant axial ligation of methionine and histidine whereas the other possesses either histidine/histidine or lysine/histidine ligands, favoring the former at high pH and the latter at low pH. Resonance Raman spectra of the protein are consistent with this picture and further suggest that at least one of the hemes (presumably the pHlabile one) experiences a perturbation of its peripheral environment due to the redox state of the flavin moiety. The reduction potentials of the two hemes are approximately equal, a result unexpected in light of their differing axial This strongly implies that the degree of hydroligands. phobicity of the two heme environments is markedly dissimilar or that a high degree of positive cooperativity exists between them. The spectra of low pH (6.05)  $c_{552}$ and  $\underline{c}_{552} \cdot S_2 O_3^{=}$  are nearly identical, suggesting that the protein configuration inducing low pH (histidine/lysine) form of the pH-labile heme is more amenable to substrate binding by the flavin.

# E. Exogenous Ligand Binding

The behavior of the hemes in  $c_{552}$  toward exogenous ligands serves to emphasize the differences in their pro-The pH-labile heme is quite accessible tein environments. to CO and CN . EPR data unequivocally establishes it as the CO binding site in the protein at physiological pH and also indicate that its axial ligation is greatly disrupted by CN . Binding of both CO and CN can be expected to proceed via a ligand displacement reaction. indicates that the native protein heme ligands are relatively loosely held and their displacement represents only a small kinetic barrier to the binding reaction. held pH-labile heme is also the probable source of the small high spin heme signal observed in both absorption and EPR spectra of  $c_{552}$ . The high spin signal can be postulated to arise from some protein conformation where neither lysine nor histidine occupies the 6th ligand position of the pHlabile heme. The observation that  $N_3$  does not quench this high spin signal whereas CN does indicates that the heme is not exposed to the solvent, but occupies some internal, largely hydrophobic pocket in the protein that can discriminate against the azide molecule. The pH-stable heme, on the other hand, displays much less of a propensity to bind exogenous ligands. It binds CO only when the pH of the protein environment is high enough to induce significant

changes in the tertiary structure of  $\underline{c}_{552}$ . CN binding to the pH-stable heme, as evidenced by the disappearance of the 695 nm absorption band in  $\underline{c}_{552}$ , proceeds very slowly suggesting that its native axial ligands are tightly-held and/or are not accessible to the solution. Thus, the pH-stable heme apparently exists in a tightly-bound, largely hydrophilic environment within the protein that allows at most limited access to its axial positions. Thiosulfate, sulfite, and cyanide ions apparently bind to the flavin moiety in  $\underline{c}_{552}$  by a simple adduct formation reaction which bleaches the visible absorption of the flavin. The interaction of CN with the heme groups in  $\underline{c}_{552}$  subsequently leads to a partial restoration of flavin absorption possibly by inducing protein conformational changes that reduce the flavin affinity for cyanide.

# F. Protein Mediated Communication Between Redox Centers

The description of the mechanism of electron transport in multicenter enzymes is indeed a formidable problem with no unique solution. Perhaps the most simplistic concept of multicenter enzymes is to consider the polypeptide portion of the protein as a passive matrix which holds the redox centers in the correct juxtaposition for efficient coupling between them. This concept is quite useful from a synthetic standpoint, requiring only that the correct positioning of redox centers be mimicked in order to

reproduce the functional aspects of the protein. However, this simplified notion finds little applicability to flavo-cytochrome  $\mathbf{c}_{552}$ . This multicenter enzyme is obviously dependent upon its polypeptide component in order to function. The protein environment affects the redox potential, binding characteristics and spectral properties of redox centers in the protein. Moreover, there is no apparent coupling of the centers themselves, necessitating a protein-mediated communication between them. Clearly,  $\mathbf{c}_{552}$  is an example of a multicenter enzyme where non-coupled redox centers exist in an active polypeptide matrix.

Polypeptide activity could take the form of direct participation of amino acid residues in electron transfer between redox centers or of introduction of conformation changes during the course of oxidation and reduction that bring the previously uncoupled redox centers into direct contact. The second possibility seems unlikely in light of the data obtained during reductive titrations of the protein that show no evidence of chromophore coupling in the MCD, EPR or absorption properties of  $c_{552}$  at any point in the titration. The direct participation of amino acid residues in electron transport has been postulated as a vehicle for oxidation and reduction in c-type cytochromes (116,117). There is currently no evidence for any axial ligand exchange accompanying electron transfer in cytochromes c (110) suggesting that such reactions proceed via

either an outer-sphere charge transfer or a tunneling Charge transfer interactions require the exmechanism. tensive electronic interaction of donor and acceptor centers resulting in a splitting of product and reactant potential surfaces (117). Electron transfer then occurs adiabatically along the lower energy surface. Tunneling processes require only minimal interaction between redox centers (119,118). Thus, a significant barrier to electron transfer exists and transfer occurs via quantum mechanical tunneling. tunneling is an intrinsically weak process with an exponential distance dependence, small changes in the orientation and separation of the redox centers can profoundly affect transfer rates. In the absence of direct electronic interactions between redox centers, either mechanism would be strongly dependent upon interactions between the polypeptide chain and the electron transfer prosthetic groups. Electronic and conformational interactions could induce a significant lowering of the tunneling barrier height and a coupling of chromophore and amino acid residue electronic states would be necessary for charge-transfer processes to occur. Both charge-transfer and tunneling have been suggested as mechanisms for electron transfer in monoheme c proteins. Tunneling has been implicated in the oxidation kinetics of low potential cytochromes in Rhodopseudomonas (120) and Chromatium (121) and several theoretical treatments of the data from these systems exist (122,123).

One mechanism for mammalian cytochrome  $\underline{c}$  reduction envisions a series of electron transfer hops from the reductase via a charge-transfer channel of aromatic amino acid residues to the porphyrin edge of the heme center in the protein (117).

The application of such an electron transfer schemes to flavocytochrome  $c_{552}$  is intriguing. Without crystallographic data, the relative positions of the redox centers and amino acid residues in  $\underline{c}_{552}$  is uncertain. This makes definitive assignment of electron transfer pathways and mechanisms in the molecule impossible. Nonetheless, the spectroscopic data gathered from the protein provides many indications that such pathways may well exist. Hemes and flavins are well suited to function as electron transfer centers. Both have rather unstable electrons in their reduced states and extended molecular orbital  $\pi$ -systems which are highly polarizable. Moreover, their reduction potentials in  $\underline{c}_{552}$  are nearly equivalent and electron transfer (via either charge-transfer or tunneling) is most rapid between species where donor and acceptor potentials are closely matched (117). Thus, the hydrophobic protein environment of the pH-labile heme in  $\underline{c}_{552}$  serves to modify its redox potential in a manner that would make it more amenable to electron transfer from the flavin. Aromatic residues (specifically two tyrosines) in  $c_{552}$  also significantly modify the excited state of the flavin moiety,

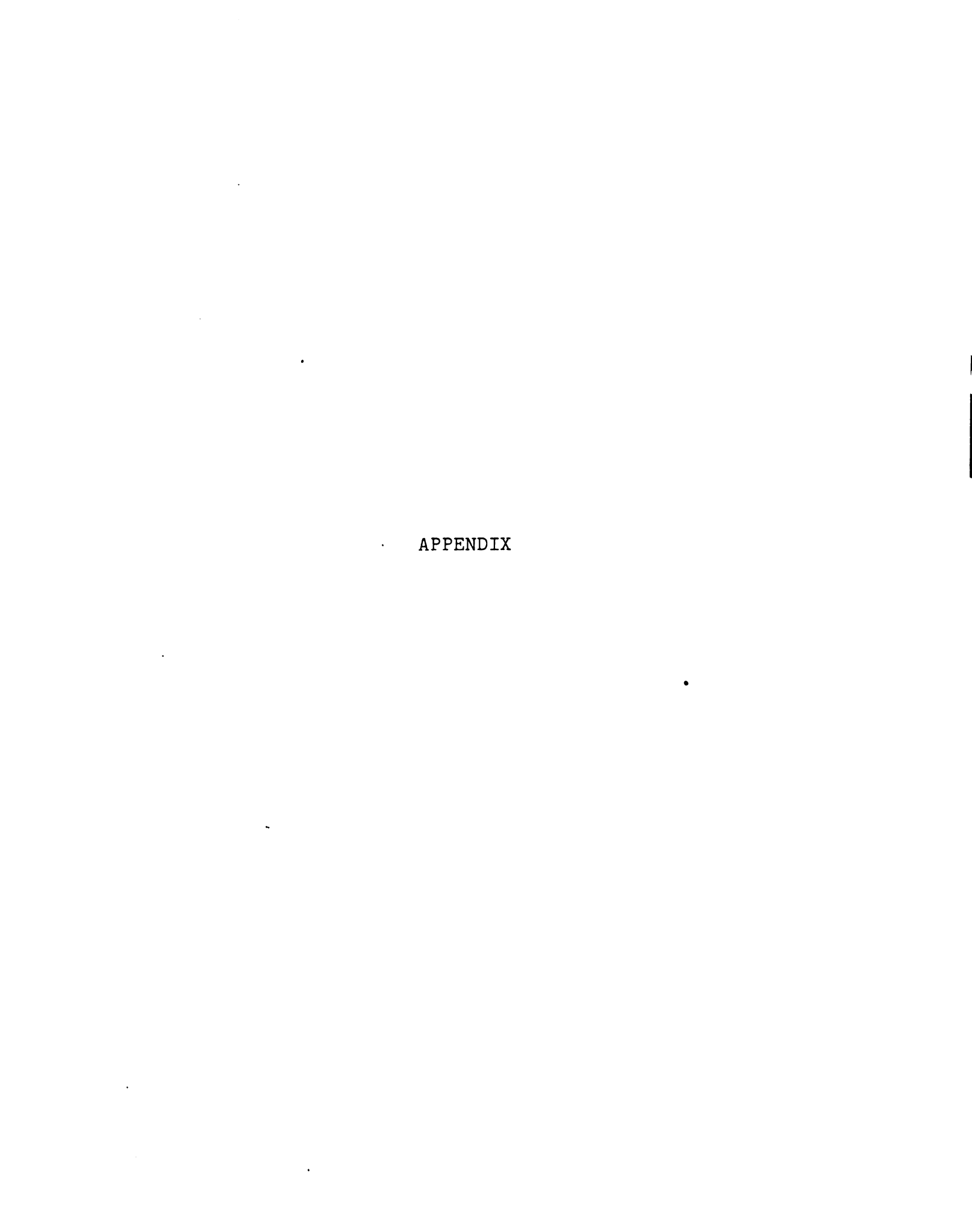
delocalizing it and presumably providing a pathway for radiationless energy transfer.

It has been demonstrated that flavins can form charge transfer complexes with tyrosine, tryptophan and phenols under inorganic conditions (124,125), and in view of their intimate contact with protein tyrosine residues, it is reasonable to assume that such an interaction occurs in  $c_{552}$ . The observation that photo-excitation of the flavin in  $c_{552}$ results in the photoreduction of at least one of the protein's hemes indicates that the delocalized flavin excited state is communicated to the heme(s) in question. The pH-labile heme is the most likely candidate for interaction with the flavin. That its hydrophobic environment contains the aromatic amino acid residues intimately associated with the flavin is a matter of speculation. However, the variability of its environment makes it the obvious choice as the source of the peripheral perturbation evident in the heme resonance Raman spectra. instructive to note that studies of the oxidation potentials of mesotetraphenyl-porphyrins by Giravdeau et al. (126) have suggested the existence of two sites for electron transfer in metalloporphyrins - the pyrrolic nitrogens (which are sensitive to iron-axial ligand electron density) in oxidation and the peripheral  $\pi$ -electron system in reduction. If these results extrapolate to  $c_{552}$ , the alteration of the heme peripheral environment in the oxidized protein may be

indicative of an electron transfer pathway via peripheral aromatic residues that is altered upon reduction of the protein. The electron transfer pathway between hemes in  $\underline{c}_{552}$  is even more obscure but presumably would entail a protein mediated communication between the loosely held axial position of the pH-labile heme and the  $\pi$ -system of the pH-stable heme.

The picture that emerges for flavocytochrome  $\underline{c}_{552}$  is one in which electron transfer is initiated by formation of a flavin-substrate adduct. The disparity in redox potential between  $S^{\pm}$  and the protein's flavin moiety results in reduction of the flavin. The excess electrons in the isoalloxazine  $\pi$ -system are delocalized through tyrosine amino acid residues near the flavin and are transferred to the hemes which act as a two-electron acceptor at a slightly higher potential than the flavin. The transfer can be postulated to occur via the periphery of the pH-labile heme. Reduced substrate could again bind to the flavin, filling the system to its 4 electron capacity.

The pH-stable heme presumably could then communicate with a higher potential cytochrome (possibly  $\underline{c}_{555}$ ) in either the organism's light-driven photosynthetic chain or its ATP-coupled dark reactions.



#### APPENDIX

If the three redox centers in  $\frac{c}{552}$  are assumed to behave as independent redox couples then the following system of equations must be solved:

$$E = E_F^{\circ} + \frac{.059}{2} \log [F]_{ox}/[F]_{red}$$
 (A1)

$$E = E_{H(1)}^{\circ} + \frac{.059}{1} \log [H(1)]_{ox}/[H(1)]_{red}$$
 (A2)

$$E = E_{H(2)}^{\circ} + \frac{.059}{1} \log [H(2]_{ox}/[H(2)]_{red}]$$
 (A3)

where  $E_{H(1)}^{o}$ ;  $E_{H(2)}^{o}$  are the midpoint potentials of the individual hemes.

Dividing Equations (2) and (3) by 2 and subtracting from Equation (1) yields:

$$0 = (E_{F}^{\circ} - \overline{E}_{H}^{\circ}) + \frac{.059}{2} \log \frac{[F]_{ox}[H(1)]_{red}[H(2)]_{red}}{[F]_{red}[H(1)]_{ox}[H(2)]_{ox}}$$

Where 
$$\overline{E}_{H}^{\circ} = E_{H(1)}^{\circ} + E_{H(2)}^{\circ}/2$$

Thus,

$$\Delta E = \overline{E}_{H}^{\circ} - E_{F}^{\circ} = \frac{.059}{2} \log \frac{[F]_{ox}[H(1)]_{red}[H(2)]_{red}}{[F]_{red}[H(1)]_{ox}[H(2)]_{ox}}$$
(A4)

In order to evaluate  $\Delta E$  from Equation (4) the concentrations of the oxidized and reduced species of each of the two hemes must be determined from the average value obtained from a reductive titration. The extent to which each heme contributes to the amount of heme reduction measured is governed by the relative midpoint potentials of the two hemes. Three different cases need to be considered:

(1) If 
$$E_{H(1)}^{\circ} = E_{H(2)}^{\circ}$$
, then
$$\Delta E = \frac{.059}{2} \log \frac{[F]_{ox} \cdot [H]_{red}^{2}}{[F]_{red} \cdot [H]_{ox}^{2}}$$

Where  $[H]_{red}$ ,  $[H]_{ox}$  = average concentration of reduced and oxidized hemes.

(2) If  $E_{H(1)}^{\circ} > E_{H(2)}^{\circ}$  then Equation (4) holds and  $[H(1)]_{red}$ ,  $[H(2)]_{red}$  can be determined from the relative midpoint potentials of heme (1) and heme (2).

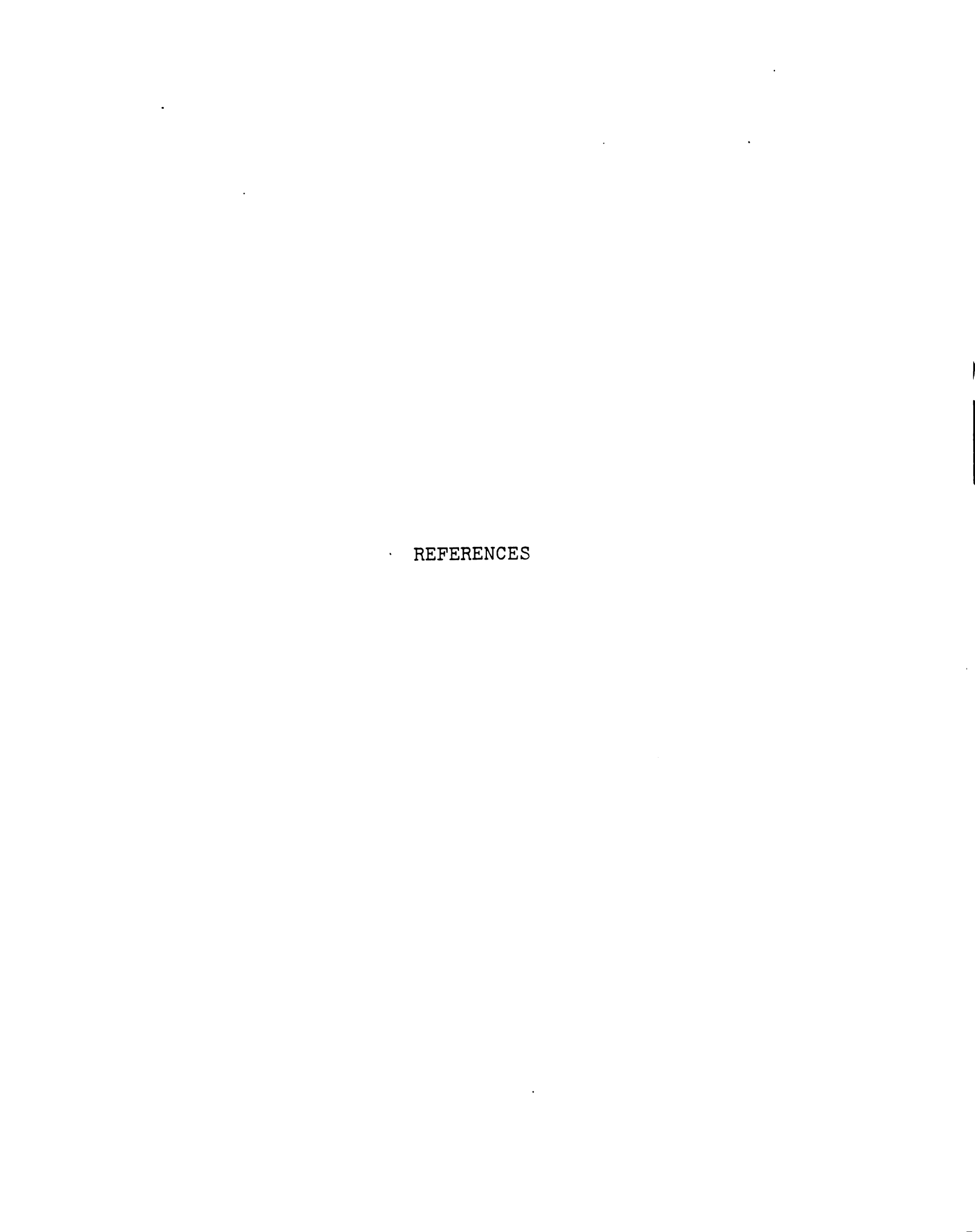
(3) If  $E_{H(1)}^{\circ} >> E_{H(2)}^{\circ}$ , then heme (1) is completely reduced before either heme (2) or the flavin begin to accept electrons and only a two center equilibrium need be considered. Thus,

$$\Delta E = E_{H(2)}^{\circ} - E_{F}^{\circ} = \frac{.059}{2} \log \frac{[F]_{ox}^{1/2} \cdot [H(2)]_{red}}{[F]_{red}^{1/2} \cdot [H(2)]_{ox}}$$

All three of the above situations lead to a systematic variation of the "constant" E over the course of the titration (See Table 1) and thus are not consistent with the data.

Table A1. Calculated Values of AE From a  $c_{552}$  Reductive Titration.

		ΔE (1n	ΔE (1n mV) for		
Average % Heme Reduced	% Flavin Reduced	Hemes As 2e <sup>-</sup> Couple	E''(1)=E''(2)	EH(1)=EH(2) + 30 mV	EH(1)=EH(2) + 100 mV
49.2	0.9	35.4	35.0	34.9	
59.7	0.9	40.9	46.1	51.0	0.3
68.5	0.6	38.7	48.9	59.7	15.9
4.77	12.0	42.0	57.9	9.69	30.1
83.1	22.0	37.2	58.0	72.2	33.8
89.5	26.0	41.5	69.5	87.9	48.2
96.2	48.0	41.0	85.2		58.7



## REFERENCES

- 1. Govindjee and Govindjee, R., Scientific American, 231, 68-82 (1976).
- 2. White, A., Flandler, P., and Smith, E., "Principles of Biochemistry", McGraw-Hill, New York (1973).
- 3. Boyer, P. R., Chance, B., Ernster, L., Mitchell, P. Racker, E., and Slater, E. C., Ann. Rev. of Biochem., 46, 955-1026 (1977).
- 4. Dickerson, R. E., and Timkovich, R. in "The Enzymes", Vol. XI (Boyer, P. D., ed), 397-550 (1975).
- 5. Marks, G. S., "Heme and Chlorophyll", VanNostrand, London, London (1969).
- 6. Moore, G. R., and Williams, R. J. P., Coord. Chem. Rev., 18, 125-197 (1976).
- 7. Creutz, C., and Sutin, N., Proceed. Natl. Acad. Sci., USA, 70, 1701-1703 (1973).
- 8. Ambler, R. P., Meyer, T. E., and Kamen, M. D., <u>Proceed. Natl. Acad. Sci., USA</u>, <u>73</u>, 472-475 (1976).
- 9. Cookson, D. J., Moore, G. R., Pitt, R. C., Williams, R. J. P., Campbell, I. D., Ambler, R. P. Buschi, M., and LeGall, Jr., Eur. J. Biochem., 83, 261-275 (1978).
- 10. Takano, T., Trus, B. L., Mandel, N. Mardel, G., Kallan, U. B., Swanson, R., and Dickenson, R. F., J. Biol. Chem., 252, 776-785 (1977).
- 11. Salemme, F. R., Freer, S. T., Nguyen, H. X., Alden, R. A., and Kraut, J., J. Biol. Chem., 248, 3910-3921 (1973).
- 12. Timkovich, R., and Dickerson, R. E., J. Biol. Chem., 251, 4033-4046 (1976).
- 13. Mayhew, S. G. and Ludwig, M. L. in "The Enzymes", Vol. XII, (Boyer, P.D. ed) 57-120, Academic Press, New York (1975).

- 14. Palmer, G., Muller, F., and Massey, V., in "Flavins and Flavoproteins", 3rd Intntl. Symp. (Kamin, M. ed.) pp. 123-140 (1970), Elsevier.
- 15. Palmer, G., and Massey, V. in "Biol. Oxidations" (Singer, T. P. ed), pp. 263-299 (1968) John Wiley & Sons.
- 16. Lehninger, A. L., in "Biochemistry" Worth Publishers, New York (1970).
- 17. Singer, T. P., Edmondson, D. E., and Kenney, W. C. in "Flavins and Flavoprotein" (Singer, T. P. ed) (1976) Elsevier.
- 18. Capeillere-Blandin, C. Brey, R. C., Iwasubo, M., and Labeyrie, F., Eur. J. Biochem. 54, 549-566 (1975).
- 19. Bastsch, R. G. and Kamen, M. D., <u>J. Biol. Chem.</u>, <u>235</u>, 825-831 (1960).
- 20. Bartsch, R. G., Meyer, T. E., and Robinson, A. B. in "Structure and Function of Cytochromes" (Okunuki, K., Kamen, M. D. and Sekuzv, I. eds.) pp. 443-451 Univ. of Tokyo Press (1968).
- 21. Walker, W. H., Kenney, W. C., Edmondson, D. F., and Singer, T. P., <u>Eur. J. Biochem.</u>, <u>48</u>, 449-453 (1974).
- 22. Kennel, J. R. and Kamen, M. D., <u>Biochim. Biophys.</u> <u>Acta</u>, <u>234</u>, 458-467 (1971).
- 23. Fukumori, Y., and Yamanaka, T., <u>J. Biochem</u>. (Tokyo), 85, 1405-1414 (1975).
- 24. Probst, I., Wolf, B., and Schlegel, H., <u>Biochim</u>. <u>Biophys. Acta.</u> <u>576</u>, 471-478 (1979).
- 25. Hopper, D. J., and Taylor, D. G., <u>Biochem J.</u>, <u>167</u>, 155-162 (1977).
- 26. Siebert, M. and DeVault, D., <u>Biochim. Biophys. Acta</u>, <u>205</u>, 220-231 (1970).
- 27. VanGrondelle, R., Duysens L., Vanderwel, J. and VanderWel, H., <u>Biochim. Biophys. Acta</u>, <u>461</u>, 188-201 (1977).
- 28. Romijn, J. C. and Amesz, J., <u>Biochim. Biophys. Acta</u>, 461, 327-338 (1977).

- 29. Case, O., and Parson, W., <u>Biochim. Biophys. Acta</u>, <u>292</u>, 677-684 (1973).
- 30. Vorkink, W., Ph.D. Thesis, University of Arizona.
- 31. Yong, F. C. and King, T. E., <u>J. Biol. Chem.</u>, <u>245</u>, 1331-1338 (1970).
- 32. Moss, T. H., Bearden, A. J., Bartsch, R. G., and Cusanovich, M. A., Biochemistry, 7, 1583-1590 (1968).
- 33. Strekas, T. C., <u>Biochim. Biophys. Acta</u>, <u>446</u>, 179-191 (1976).
- 34. Edmondson, D. E. and Singer, T. P., <u>J. Biol. Chem.</u>, <u>248</u>, 8144-8149 (1973).
- 35. Cusanuvich, M. A., Ph.D. Thesis, University of California, San Diego, CA.
- 36. Salmeen, I., Rimai, L. and Babcock, G. T., <u>Biochemistry</u>, <u>16</u>, 800-806 (1970).
- 37. Sutherland, J. C., Vickery, L. E., and Klien, M. P., Rev. Sci. Instrum., 45, 1089-1094 (1974).
- 38. Gouterman, M. in "The Porphyrins", Vol. III, (Dolphin, D. ed), pp. 1-165 (1978), Academic Press.
- 39. Simpson, W. T., <u>J. Chem. Phys.</u>, <u>17</u>, 1218-1221 (1949).
- 40. Gouterman, M., <u>J. Chem. Phys.</u> <u>30</u>, 1139-1161 (1959).
- 41. Felton, R. H. and Yu, N. T. in "The Porphyrins", Vol. III (Dolphin, P. ed.), pp. 347-393 (1978), Academic Press, New York.
- 42. Zerner, M., Gouterman, M., and Kobayushi, H., Theoret. Chim. Acta (Berlin), 6, 363-400 (1966).
- 43. Smith, D. W., and Williams, R. J. P., in "Structure and Bonding", Vol. 7, pp. 1-45, (1970), Springer Verlay, Berlin.
- 44. Adar, F., in "The Porphyrins", Vol. III, (Dolphin, D. ed), pp. 167-209 (1978), Academic Press, New York.
- 45. Drew, H. R., Dickenson, R. E., J. Biol. Chem., 253, 8420-8427 (1978).
- 46. Lambeth, D., Campbell, K., Zand, R., and Palmer, G., J. Biol. Chem., 248, 8130-8136 (1973).

- 47. Meyer, T. E., and Bartsch, R. G. in "Flavins and Flavo-proteins", (Singer, T. P. ed.), pp. 312-317 (1976) Elsevier.
- 48. Muller, F. and Massey, V., <u>Jour. Biolg. Chem.</u>, <u>244</u>, pp. 4007-4012 (1969).
- 49. Beetlestune, J., and George, P., Biochemistry, 3, 707-714 (1964).
- 50. Kotaki, A., and Yagi, K., <u>J. Biochem.</u>, <u>68</u>, 509-56 (1970).
- 51. Chance, B., Erecinska, M., Lee, C. P., Oshino, R., Ohnishi, T. and Prig, M., in "Flavins and Flavoproteins" (Kamin, H. ed) pp. 669-680 (1971) Elsevier.
- 52. Kenney, W. C., Edmondson, D., Seng, R., and Singer, T. P., Biochem. Biophys. Res. Communs., 52, 434-439 (1973).
- 53. Edmondson, D. and Toller, G., <u>Biochemistry</u>, <u>10</u>, 113-122 (1971).
- 54. Förster, Th., Disc. Faraday Soc., 27, 7-17 (1959).
- 55. Hatano, M. and Nozawa, T., Advs. in Biophys., 11, 95-149 (1978).
- 56. Stephens, P. J., <u>Ann. Rev. Phys. Chem.</u>, <u>25</u>, 201-232 (1974).
- 57. Vickery, L., Nozawa, T., and Saver, K., <u>J. Amer. Chem.</u> Soc., <u>98</u>, 343-350 (1976).
- 58. Briat, B., Berger, D. and Leliboux, M., <u>J. Chem. Phys.</u> <u>57</u>, 5606-5607 (1972).
- 59. Vickery, L., Mtds. in Enzymology, 41, 64-82, (1977).
- 60. Vickery, L., Nozawa, T. and Sauer, K., J. Amer. Chem. Soc., 98, 351-359 (1976).
- 61. Templeton, D. M., Hollebone, B. R., and Tsai, C. S., submitted to <u>Biochemistry</u> (1980).
- 62. Palmer, G., to be published in "The Porphyrins", Vol. IV, (Dolphin, D., ed.), Academic Press, NY (1980).
- 63. Griffith, J. S., Nature, 180, 30-31 (1957).

- 64. Kotani, M., <u>Prog. Theoret. Phys. Suppl.</u>, <u>17</u>, 4-13 (1961).
- 65. Weisbluth, M., in "Hemoglobin: Cooperativity and Electronic Processes", Springer-Verlay (1973).
- 66. Mun, S. K., Chang, J. C., and Das, T. P., <u>J. Amer.</u> Chem. Soc., <u>101</u>, 5562-5569 (1979).
- 67. Peisach, J., Blumberg, W. E., and Adler, A., Am. N. Y. Acad. Sci., 206, 310-327 (1973).
- 68. Taylor, C. P. S., Biochemices et Biophysica Acta., 191, 137-149 (1977).
- 69. Brautigan, D. L., Feinberg, B. A., Hoffman, B. M., Margoliash, E., Peisach, J., and Blumberg, W. E., J. Biological Chem., 252, 574-582 (1977).
- 70. Moore, G. R., and Williams, R. J. P., <u>FEBS Lett.</u>, 79, 229-232 (1977).
- 71. Mashiko, T., Marchon, J. C., Musser, P. T., Reed, C. A., Kastner, M. E., and Scheidt, W. R., <u>J. Amer.</u> Chem. Soc., 101, 3653-3654 (1979).
- 72. Lemberg, R. and Barrett, J. in "The Cytochromes", Academic Press, New York (1975).
- 73. Siedow, D. W., Vickery, L. E. and Palmer, G., submitted to J. Biol. Chem. (1980).
- 74. Kassner, R. J., <u>J. Amer. Chem. Soc.</u>, <u>95</u>, 2674-2677 (1973).
- 75. Pettigrew, G. W., Bartsch, R. G., Meyer, T. E. and Kamen, M. D., Biochemica et Biophysica Acta, 503, 509-523 (1978).
- 76. Palmer, G. and Massey, V., in "Biological Oxidations" (Singer, T. P. ed), pp. 263-299 (1968), Wiley.
- 77. Wellner, D., and Meister, A., <u>J. Biol. Chem.</u>, <u>236</u>, 2357-2362 (1961).
- 78. Palmer, G., Muller, F., and Massey, V. in "Flavins and Flavoproteins", (Kamin, H. ed.), pp. 123-140 (1970).
- 79. Hori, H., <u>Biochemica et Biophysica Acta</u>, <u>251</u>, 227-235 (1971).

- 80. Dyer, C., Schubert, A., Timkovich, R. and Feinberg, B., Biochemica et Biophysica Acta, 579, 253-268 (1979).
- 81. Salmeen, I., Rimai, L., Gill, D., Yamamoto, T., Palmer, G., Hartzell, C. R., and Beinert, H., Biochem. Biophys. Res. Communs., 52, 1100-1107 (1973).
- 82. Lutz, M., Biochimica et Biophysica Acta, 460, 408-430 (1977).
- 83. Spaulding, L. D., Chang, C. C., Yu, N. T. and Felton, R. H., J. Amer. Chem. Soc., 97, 2517-2524 (1975).
- 84. Burke, J. M., Kincaid, J. R., and Spiro, T. G., J. Amer. Chem. Soc., 100, 6077-6083 (1978).
- 85. Tang, J., and Albrecht, A. C., in "Raman Spectroscopy", Vol. 2 (Szymanski, H. A., ed), pp. 33-69, (1970) Plenum Press.
- 86. Albrecht, A. C., J. Chem. Phys., 33, 156-171 (1960).
- 87. Nafie, L. A., Pezolet, M. and Peticolas, W. L., <u>Chem. Phys. Lett.</u>, <u>20</u>, 563-568 (1973).
- 88. Friedman, J. M. and Hochstrasser, R. M., <u>J. Amer.</u> Chem. Soc., <u>98</u>, 4043-4048 (1976).
- 89. Shelnutt, J. A., O'Shea, D. C., Yu, N. T., Cheng, L. D. and Felton, R. H., <u>J. Chem. Phys.</u>, <u>64</u>, 1156-1165 (1976).
- 90. Clark, R. J. H., and Stewart, B., <u>Structure and Bond-ing</u>, 36, 1-80 (1979).
- 91. Perrin, M. H., Gouterman, M., and Perrin, C. L., <u>J</u>. <u>Chem. Phys.</u>, <u>50</u>, 4137-4150 (1969).
- 92. McClain, W. M., <u>J. Chem. Phys.</u> <u>55</u>, 2789-2795 (1971).
- 93. Collins, D. W., Fitcher, D. B., and Lewis, A., J. Chem. Phys., 59, 5714-5719 (1973).
- 94. Yamamoto, T., Ph.D. Thesis, University of Michigan (1974).
- 95. Albrecht, A. C. and Hutley, M. C., <u>J. Chem. Phys.</u>, <u>55</u>, 4438-4443 (1971).
- 96. Champion, P. M., and Albrecht, A. C., <u>J. Chem. Phys.</u> <u>71</u>, 1110-1121 (1979).

- 97. Friedman, J. M. and Hochstrasser, R. M., <u>Chemical Physics</u>, 1, 457-467 (1973).
- 98. Remba, R. D., Champion, P. M., Fitchen, D. B., Chiang, R., and Hager, L. P., <u>Biochemistry</u>, <u>18</u>, 2280-2290 (1979).
- 99. Kitagawa, T., Abe, M., and Ogushi, H., <u>J. Chem. Phys.</u> 69, 4516-4523 (1978).
- 100. Spiro, T. G. and Strekas, T. C., <u>J. Amer. Chem. Soc.</u>, <u>96</u>, 338-345 (1974).
- 101. Adar, F., and Yonetani, T., <u>Biochimica et Biophysica</u> Acta, 502, 80-86 (1978).
- 102. Kitagawa, T., Ozaki, Y., Teraoka, J., Kyogoku, Y., and Yamanaka, T., Biochimica et Biophysica Acta, 494, 100-114 (1977).
- 103. Ozaki, Y., Kitagawa, T., Kyogoku, Y., Shimada, T., Iizuka, T., and Ishimura, Y., <u>J. Biochem</u>. (Tokyo), 80, 1447-1451 (1978).
- 104. Kitagawa, T., Kyogoku, Y., Iizuka, T., and Saito, M. I., J. Amer. Chem. Soc., 98, 5169-5173 (1976).
- 105. Sun, M., Moore, T. A., and Song, P. S., <u>J. Amer. Chem.</u> Soc., <u>94</u>, 1730-1740 (1972).
- 106. Kitagawa, T., Nishiru, Y. Kyogoku, Y., Yamano, T., Ohishi, W., Takai-Suzuki, A., and Gahi, K., Biochem-istry, 18, 1804-1808 (1979).
- 107. Dutta, P., Nestor, J., and Spiro, T., Proceed. Natl. Acad. Sci. (USA), 74, 4146-4149 (1977).
- 108. Kitagawa, T., Ozaki, Y., and Kyogoku, Y., Advs. Bio-Phys., 11, 153-196 (1978).
- 109. Kitagawa, T., Kyogoku, Y., and Orii, Y., <u>Arch. Biochem.</u> Biophys., 181, 228-235 (1977).
- 110. Spiro, T. G., and Burke, J. M., <u>J. Amer. Chem. Soc.</u>, <u>98</u>, 5482-5488 (1976).
- 111. Maltempo, M. M., Moss, T. H., and Casanovich, M. A., Biochimica et Biophysica Acta, 342, 290-305 (1974).
- 112. Babcock, G. T., Vickery, L. E. and Palmer, G., J. Biol. Chem., 251, 7907-7919 (1976).

- 113. Hamaguchi, K., Ikada, K., and Narita, N., in "Structure and Function of Cytochromes", (Okunuki, K., Kamen, M. D., and Sekuzu, I., eds), pp. 328-334, Univ. Park Press, Baltimore, MD (1968).
- 114. Hsu, M.-C., and Woody, R. W., <u>J. Amer. Chem. Soc.</u>, <u>93</u>, 3515-3525 (1971).
- 115. Meyer, Y. P., Biochemistry, 7, 765-772 (1968).
- 116. Salemme, F. R., Kraut, J., and Kamen, M. D.,  $\underline{J}$ . Biol. Chem., 246, 7701-7716 (1973).
- 117. Moore, G. R. and Williams, R. J. P., Coord. Chem. Rev., 18, 125-197 (1976).
- 118. Salemme, F. R., Ann. Rev. Biochem., 46, 299-329 (1977).
- 119. Blankenship, R. E., and Passor, W. W., to be published in "Topics in Photosynthesis", Vol. III, (Barber, J., ed), Elsevier, Amsterdam.
- 120. Kihara, J. F., and McCray, J. A., Biochimica et Biophysica Acta, 292, 297-309 (1973).
- 121. Devaut, D., Parks, J., and Chang, B., <u>Nature</u>, <u>215</u>, 642-644 (1967).
- 122. Itopfield, J. J., <u>Biophys. J.</u>, <u>18</u>, 311-321 (1977).
- 123. Jortner, J., <u>J. Chem. Phys.</u>, <u>64</u>, 4860-4867 (1976).
- 124. Harbury, H. A. and Foley, K. A., <u>Proceed. Natl. Acad.</u> <u>Sci. (USA)</u>, <u>44</u>, 662-666 (1958).
- 125. Fleishman, D. E., and Tollen, G., <u>Biochimica et Biophysica Acta</u>, <u>94</u>, 255-270 (1965).
- 126. Giravdeau, A., Callot, H. J., and Gross, M., <u>Inorganic</u> Chemistry, 18, 201-206 (1979).